Validated Sentinel fields for the set of met-ocean variables considered

Rulent, Julia; Badger, Merete; Ahsbahs, Tobias; Martin, Adrien C. H.; Shaw, Andy ; Boye Hansen, Lars; Abdalla, Saleh; Bidlot, Jean ; Bonaldo, Davide ; Cavaleri, Luigi; Espino, Manuel; Wiesse, Anne; Staneva, Joanna

COPERNICUS EVOLUTION AND APPLICATIONS WITH SENTINEL ENHANCEMENTS AND LAND EFFLUENTS FOR SHORES AND SEAS

Published: 01/03/2018

COPERNICUS EVOLUTION AND APPLICATIONS WITH SENTINEL ENHANCEMENTS AND LAND EFFLUENTS FOR SHORES AND SEAS

Date: March 2018

Deliverable Number: 2.1

Due date for deliverable: March 2018

Actual submission date: March 2018

Leader: Technical University of Denmark

Document Dissemination Level: Public

Co-ordinator: Universitat Politècnica de Catalunya (UPC)
Project Contract No: H2020-EO-2016-730030- CEASELESS
Project website: https://ceaseless.barcelonatech-upc.eu

DOCUMENT INFORMATION

Title	Validated Sentinel fields for the set of met-ocean variables considered
Lead Author	Merete Badger
Contributors	Tobias Ahsbahs, Adrien Martin, Andy Shaw, Julia Rulent, Lars Boye Hansen, Saleh Abdalla, Jean Bidlot, Davide Bonaldo, Luigi Cavaleri, Manuel Espino, Anne Wiesse, Joanna Staneva
Distribution	Public
Document Reference	

DOCUMENT HISTORY

Date	Version	Prepared by	Organisation	Approved by	Notes
March 5, 2019	0.0	Merete Badger	DTU		First version, Template
March 22, 2019	0.1	Merete Badger	DTU		Draft version with contributions from DTU, ECMWF, NOC, CNR, UPC
March 29, 2019	0.2	Merete Badger	DTU		Draft version with contributions from DTU, ECMWF, NOC, CNR, UPC, HZG, DHI GRAS
March 31, 2019	1.0	Merete Badger	DTU		Final Version

ACKNOWLEDGEMENT

This project has received funding from the European Union's H2020 Programme for Research, Technological Development and Demonstration under Grant Agreement No: H2020-EO-2016-730030- CEASELESS.

DISCLAIMER

CONTENT

DOCUMENT INFORMATION 3
DOCUMENT HISTORY 3
ACKNOWLEDGEMENT 3
DISCLAIMER 3
CONTENT 4
Executive Summary 5
1. Introduction 7
2. Sentinel-1 8
2.1. Overview 8
2.2. Validation of ocean wind retrievals from Level-1 products 8
2.2.1. Comparisons against buoy wind speeds in the North Sea and Irish Sea 8
2.2.2. Comparisons against wind lidars on the North Sea coast 11
2.2.3. Comparisons against wind turbine production data in the Danish Seas 13
2.3. Validation of Level-2 OWI roducts 16
2.4. Validation of Sentinel 1 Level 2 Radial Velocity (RVL) against HF radar 18
3. Sentinel-2 23
3.1. Overview 23
3.2. Validation of water quality 24
3.3. Validation of satellite-derived bathymetry 29
3.4. Validation of coastal dynamics 31
4. Sentinel-3 34
4.1. Overview 34
4.2. Validation of Sentinel-3 SRAL 34
4.2.1. Global validation of Sentinel-3 SRAL wind and wave products 34
4.2.2 Comparison of wind, wave and sea level products against Jason-3 at cross-over points in the four case studies area 60
4.2.3. Comparison against a coupled wave-ocean numerical model: Total Water Level 64
4.2.4. Comparison of wind and wave products over the North Sea-Baltic Sea 70
4.2.5. Comparison of wind and wave products over the Mediterranean Sea 75
4.2.6. Comparison of wave products over the Catalan Coast 80
5. References 85

EXECUTIVE SUMMARY

This document is Deliverable 1.2 of Task 1.2 "Multi-variable scientific validation (set of metocean fields & applications)" of Work Package 1 "Multimission data provision, improvement and validation" of the the CEASELESS (Copernicus Evolution and Applications with Sentinel Enhancements and Land Effluents for Shores and Seas) project.

We provide an overview of validation efforts in the context of the Copernicus Sentinel mission data used in the CEASELESS project. The validation results are structured according to sensor type i.e. from the Copernicus Sentinel-1, 2 and 3 missions, respectively. Information about the different sensors and how to obtain data is given in a previous report with the title "Collection of Sentinel-1/2/3 and in-situ data for the considered study cases".

Key results of the validation efforts include:

- Wind speeds retrieved from Sentinel-1 A/B Level-1 agree well with in situ observations if Sentinel-1A scenes acquired before November 2015 are disregarded due to a calibration issue. Inter-calibration is necessary before Sentinel-1 A/B scenes can be used to extend the data series delivered by the previous mission Envisat.
- Wind speeds from the Sentinel-1 A/B Level-2 OWI product are comparable in accuracy to those retrieved from Level-1 data if the wind directions used as input to wind speed retrievals are of the same quality.
- Sentinel-1 Level-2 RVL products suffer from uncorrected instrument effects that presently prevent exploitation of the data.
- Sentinel-1 Level-2 RVL adjusted using land and after correction of the wind-wave bias using ECMWF winds shows a small bias (-7cm/s) and root-mean-square difference of 0.4m/s against HF radar.
- Sentinel-2 based water quality show promising results for retrieval of sediment concentrations in high spatial and temporal detail. Match-up analysis is a challenge due to both the dynamic nature of the study areas and the high spatial resolution of the S-2 products so evaluation needs to made on a qualitative approach.
- Sentinel-2 based satellite-derived bathymetry can add detailed high resolution information about shallow water bathymetri. Comaprisons with best possible freely available data (EMODnet 2018) show big increase in the level of detail while at the same time being fully up-to-date. Interpolation artefacts from EMODnet was shown to be corrected in a blended bathymetry layer.
- Sentinel-2 is highly suited for analyses of coastal dynamics. The high temporal and spatial coverage allows for frequent and detailed assessments of coastal erosion and accretion.
- Global validation shows that surface wind speed and significant wave height, which are part of Seninel-3 Surface Topography Mission Level 2 Marine Ocean and Sea Ice Areas (SRAL-L2MA) from Sentinel-3A have been very good since the start of the mission if the reprocessed data set produced in December 2017 is considered.

- The characteristics of Sentinel-3B wind and wave data are similar to those of Sentinel-3A after the implementation of Sentinel-3B PB 1.13 on 6 December 2018, which eliminated the backscatter bias that degraded the wind speed products.
- Regional comparisons in the Mediterranean Sea shows that different altimeter datasets have consistent performances as far as wind speed is concerned, but with significant differences in terms of estimated wave heights. Sentinel-3 SRAL captures wave peaks in the Catalan Sea.

1. INTRODUCTION

This document was created in the framework of Work Package 1 (WP1) "Multimission data provision, improvement and validation" of the CEASELESS (Copernicus Evolution and Applications with Sentinel Enhancements and Land Effluents for Shores and Seas) project.

The main objective of this work package is the procurement and collation of products from the Sentinel-1, 2 and 3 missions for dissemination to all partners in the project. The increasing quantity, diversity and quality of observations provided by Copernicus Sentinel satellites offer new possibilities to monitor complex meteorological and oceanographic conditions in coastal regions with unprecedented level of detail. Improvements in spatial resolution, temporal coverage and the benefits of combining observations from multiple sensors in the Sentinel family are bringing enhanced capability that is of direct relevance to scientific and operations applications that seek to better understand, model and forecast marine weather conditions in coastal regions. The aim of this task is to support end users to promote wider exploitation of these new Sentinel satellite data in coastal areas that are subject to complex atmospheric, sea state and ocean circulation processes and are characterised by high levels of man-made pressure and economic activities.

The work in WP1 is composed of four complementary tasks:

- Task 1.1 Sentinel data for coastal scales (provision and verification)
- Task 1.2 Multi-variable scientific validation (set of metocean fields & applications).
- Task 1.3 Synergies between different missions and applications (multi variable/process validation).
- Task 1.4 New and improved Sentinel products for the coastal zone (added value for users and CMEMS).

This document relates to Task 1.2 and focuses on the validation of Sentinel-1/2/3 data and derived products with relevance for metoean applications. The document presents in successive order the validation efforts carried out for Sentinel-1, Sentinel-2 and Sentinel-3. For each mission, the report gives an overview of the variables considered and their quality with respect to other data sets that are available to the CEASELESS partners. The objective is to provide assessments of the quality of Sentinel data and derived metocean variables, which can be used as a reference by other CEASELESS partners and in the broader metocean community.

2. SENTINEL-1

2.1. OVERVIEW

The Sentinel-1 mission delivers all-weather observations with global coverage from active microwave Synthetic Aperture Radar (SAR) instruments operating at C-band.

The Sentinel-1 mission consists of a minimum of two units flying simultaneously. Sentinel-1A was launched on April 3, 2014 and Sentinel-1B on April 25, 2016. Both satellites are currently operational.

The SAR instruments on Sentinel-1 offer four scanning modes characterised by different spatial resolutions and image sizes. The four modes provide the following capability:

- Strip Map Mode: 80 km Swath, 5 x 5 m spatial resolution
- Interferometric Wide Swath: 250 km Swath, 5x20 m spatial resolution
- Extra-Wide Swath Mode: 400 km Swath, 25 x 100 m spatial resolution
- Wave-Mode: 20 km x 20 km, 5 x 20 m spatial resolution

Further information about the Sentinel-1 A/B payload is available at
https://sentinel.esa.int/web/sentinel/missions/sentinel-1/instrument-payload

2.2. VALIDATION OF OCEAN WIND RETRIEVALS FROM LEVEL-1 PRODUCTS

This section shows validation efforts related to wind fields at the height 10 m retrieved from Level-1 SAR products. The analyses are mainly based on the SAR wind archive from the Technical University of Denmark (DTU) that is publically available at https://satwinds.windenergy.dtu.dk/. The archive mainly consists of Envisat and Sentinel-1 scenes but also some data from TerraSAR-X and Radarsat-1. Wind retrievals are performed consistently using the Geophysical Model Function called CMOD.5N (Hersbach, 2009) to retrieve wind speeds from the Normalized Radar Cross Section (NRCS) with a pixel size of 500 m.

2.2.1. Comparisons against buoy wind speeds in the North Sea and Irish Sea

In the following, we investigate the consistency of wind retrievals from Envisat and Sentinel-1 SAR through comparison with in situ observations. For wind speed validation, it would be ideal to compare with data from meteorological masts equipped with sonic anemometers at several heights (as presented in CEASELESS Deliverable 4.3), but such data is not available in large quantities. Instead data from ocean buoys is used. Buoy data is initially collected from CMEMS service (located at ftp://myocean.bsh.de/Core/ at the time of access but now moved to ftp://my.cmems-du.eu). Data quality from this service is deemed not sufficient as initial quality control reveals obvious flaws, e.g. units are inconsistently in m/s and knots. Most importantly for this study, meta data of the measurements are missing, most notably the measurement height. Measurement heights need to be accurate as the mean wind speed increases with height. Instead of using data from the CMEMS service, buoy data from BSH, Met Eirinn, and the MetOffice have been acquired directly, including the necessary meta data. Data is quality controlled to remove obvious issues, e.g. long periods of 0 m/s wind speed or spikes in the wind speed of more than 15m/s between two consecutive measurements. In total, 16 buoys are used for this study.

Buoy winds and SAR winds are compared by choosing samples that are not longer than 30 minutes apart and by averaging the SAR winds on a rectangular box of 10 km around the buoy location. Buoy winds are extrapolated to 10 m using a simple logarithmic wind profile with fixed roughness length. Data pairs where either the SAR or the buoy wind speed is below 0.5 m/s are filtered out because they are considered highly uncertain. Buoy to SAR wind comparison are done for Envisat, Sentinel-1A and Sentinel-1B. Sentinel-1A has undergone a significant recalibration that is applied after 2015-11-25 (Miranda, 2016). The period before is denoted as "before recalibration" and treated separately.

Figure 1 shows the resulting comparisons as scatterplots with the black line indicating the mean over a 1 m/s bin and the vertical lines indicating one standard deviation. All comparisons show overestimations in SAR wind speeds below 5 m/s and only few samples are available above 20 m/s. Overall, Envisat (a) shows a bias of 0.87 m/s while Sentinel-1A (c) and Sentinel-1B (d) show a bias of 0.1 m/s and 0.17 m/s, respectively. Sentinel-1A before recalibration (b) has a bias of 0.94 m/s, which is similar to that for Envisat. Merging Envisat and Sentinel-1A/B data is problematic due to the offset in bias of approximately 0.7 m/s while differences between Sentinel-1A and B seem neglectable. The Sentinel-1A period before recalibration shows even higher biases and should not be merged with Sentinel-1A/B data.

Several possible reasons for inconsistencies between Envisat and Sentinel-1 have been investigated and are summarized below:

1. Differences in the wind direction input: All data are reprocessed with local wind direction inputs, which generally improves the RMSE but influences the biases below 0.1 m/s.
2. Difference in polarization: Biases vary largely between polarizations, also to the same sensor. Comparing the same polarization does not explain differences in the bias.

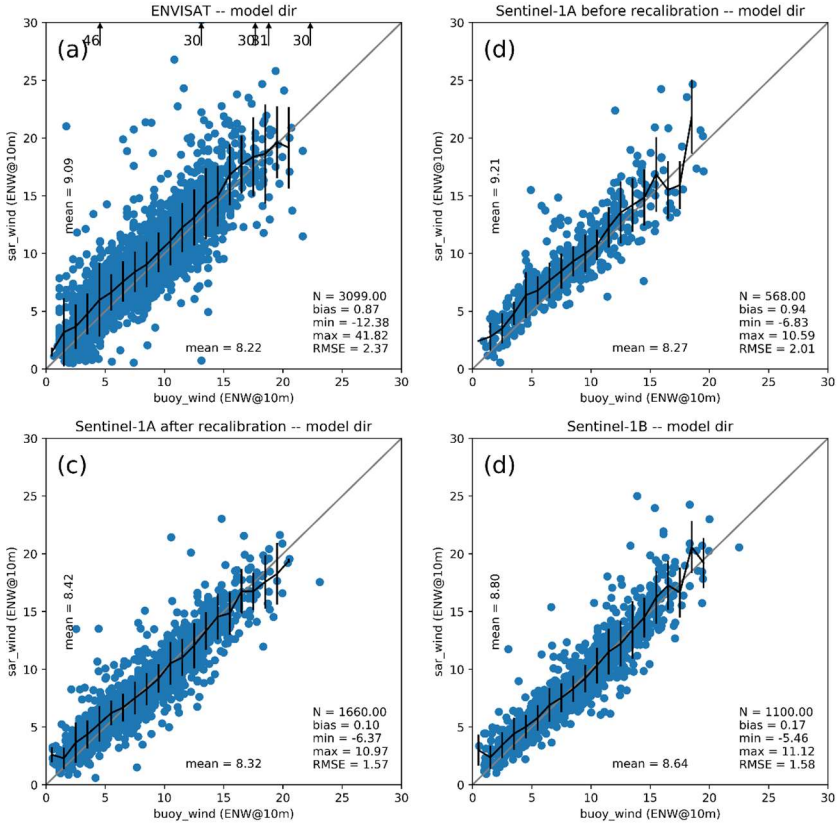

Figure 1. Comparison of SAR and buoy wind speeds for (a) Envisat, (b) Sentinel-1A before recalibration, (c) Sentinel-1A after recalibration, (d) Sentinel-1B.

Inter-calibration of SAR observations

A method to reduce differences in the bias of SAR wind speed retrievals is developed. It is observed that wind speed residuals are incidence angle dependent. Therefore, an incidence angle dependent correction offset on the NRCS is calculated. Corrections are derived from applying CMOD5.N as a forward model from to wind speed and direction from global circulation models. A detailed description can be found in Badger et al. (submitted). This method is found to perform well for incidence angles above 25°. Figure 2 shows the resulting comparisons to the same buoy data set as shown above. The number of samples is reduced by 905 for Envisat due to the incidence angle filtering while only few samples are excluded from Sentinel-1A /B. Biases now range from -0.17 to 0.07 m/s, which is a large improvement. RMSEs between Envisat and Sentinel-1/B are very similar with Sentinel-1A before recalibration having the highest RMSE.

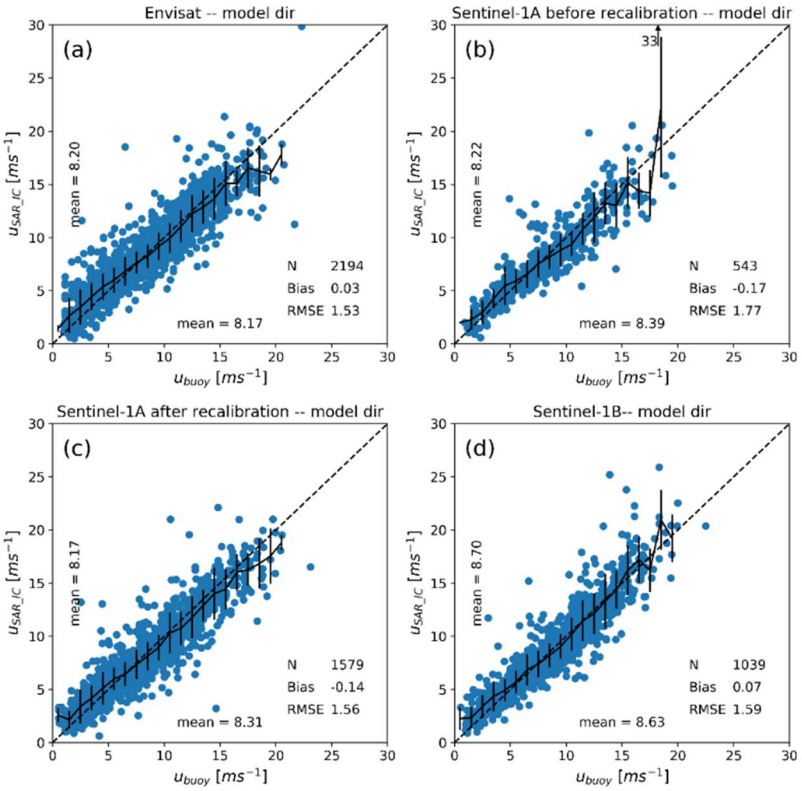

Figure 2 Comparison of inter-calibrated SAR wind speeds and buoy wind speeds for (a) Envisat, (b) Sentinel-1A before recalibration, (c) Sentinel-1A after recalibration, (d) Sentinel-1B.

The presented inter-calibration method for SAR wind speeds greatly improves consistency between sensors. The presented method takes polarization, sensing mode, and temporal changes in the corrections into account. The following additional improvements are found:

1. Biases for Envisat with HH polarization are reduced from 1.43 m/s to 0.03 m/s and RMSE reduced from 2.77 to 1.92 m/s making them comparable to wind retrievals based on VV polarization.
2. Biases in the Envisat data increase between 2006 and 2012. Inter-calibration reduced biases over this period greatly.

2.2.2. Comparisons against wind lidars on the North Sea coast

In addition to the absolute accuracy, it is essential to test the accuracy of the spatial wind speed variability given by SAR near the coastline. Geophysical Model Functions that are used for the SAR wind retrieval processing are tuned to open ocean wind conditions and their accuracy closer to the coastline has been questioned for decades. The RUNE data set can be used to quantify the wind speed gradient from the coatline and further offshore and for comparisons against the SAR wind maps. In the following, we summarize the comparisons of wind speeds from SAR and scanning lidar. Full details of the analyses and results are given in Ahsbahs et al. (2017).

A total of 15 colocated Sentinel-1 scenes were acquired during the RUNE measurement campaign using scanning lidars on the Danish North Sea coast. The scanning lidars were operated in two configurations: Dual Doppler scans performed with an inclination of the lidar beam and sector scans with a uniform scanning height of 50 m. In both cases, extrapolation of the lidar wind speeds had to be performed in order to match the 10-m wind speeds from SAR. A neutral atmosperic stability had to be assumed since no temperature observations were available for calculation of a stability correction. Observations from the coastal mast at Høvsøre were used to classify the cases according to stability.

Figure 3 shows the average of SAR and scanning LiDARs wind speeds taken over transects going from 1 km off the coastline to the maximum range available. This results in a single averaged wind speed over the transect for both the SAR and LiDAR measurements. The RMSE is 1.31 m/s for the dual Doppler and 1.42 m/s for the sector scan. The averaged wind speeds are between 4 m/s and 10 m/s for most cases and only one case has wind speeds as high as 16 m/s. Cases with neutral atmospheric conditions and wind directions from the North Sea towards the land show the best agreement.

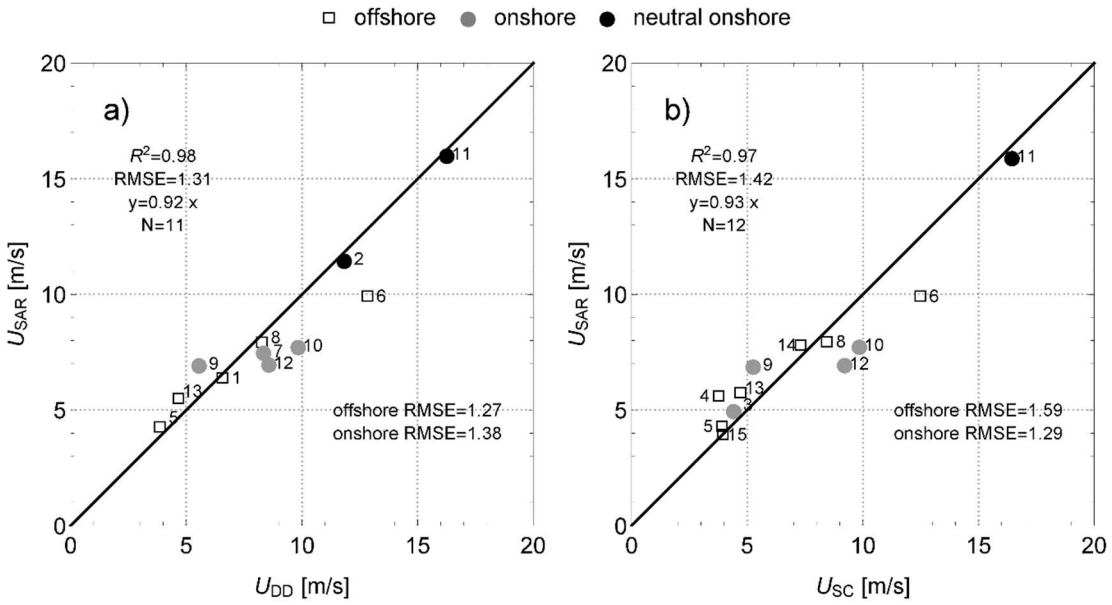

Figure 3. Comparisons of mean wind speeds retrieved from SAR and scanning lidar; a) dual Doppler lidar; b) sector scans.

In order to get a qualitative estimate of how SAR and LiDARs measure the horizontal wind speed gradient, wind speeds are plotted as a function of distance from the coastline. We consider distances up to 3 km offshore because all lidars deliver observations here. Wind speeds are nondimensionalized through division of all values with the wind speed at 3 km. The nondimensional dual Doppler wind speed in Figure 4a shows a lower gradient than the SAR wind. The nondimensional wind speed in Figure 4 (b) is very close for sector scan and SAR winds, and both systems similarly estimate a relative reduction of the wind speed when approaching the coast.

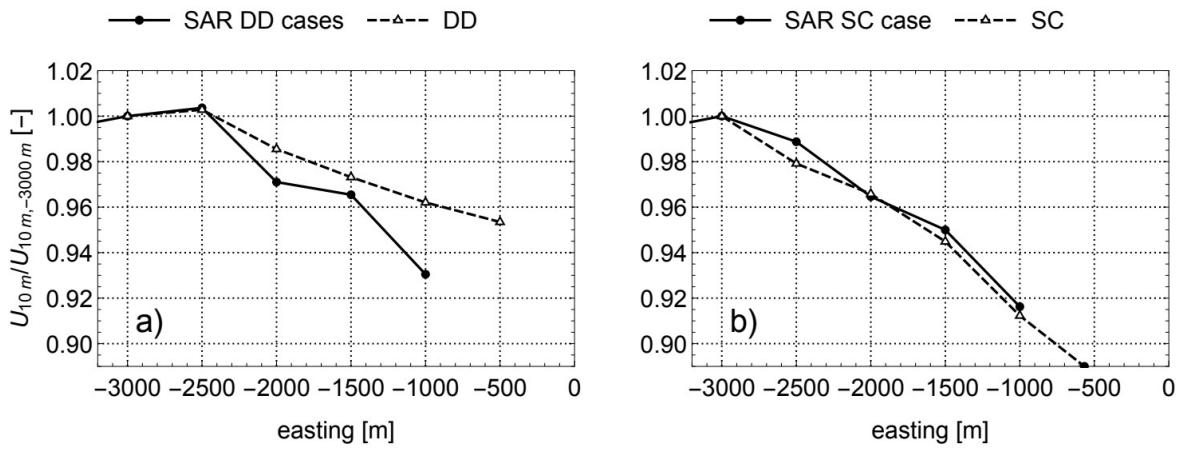

Figure 4. Relative wind speeds retrieved from SAR and LiDAR and nondimensionalized with the wind speed 3 km from the coastline; a) dual Doppler lidar; b) sector scans. From Ahsbahs et al. (2017)

2.2.3. Comparisons against wind turbine production data in the Danish Seas

SAR wind retrievals have been compared to wind turbine production data at the Anholt Offshore Wind Farm located in the Kattegat Strait of Denmark in the waters between Djursland and the island of Anholt (Figure 5). The Anholt Offshore Wind Farm is approximately 20 km long and up to 8 km wide. The shortest distance to Djursland is 16 km, and there are 21 km to the island of Anholt. The Anholt wind farm consists of 111 Siemens SWT-120-3.6MW wind turbines with a rotor diameter of 120 m with a total capacity of 400 MW and it was constructed during 2012–2013. The following results have been extracted from Ahsbahs *et al.* (2018).

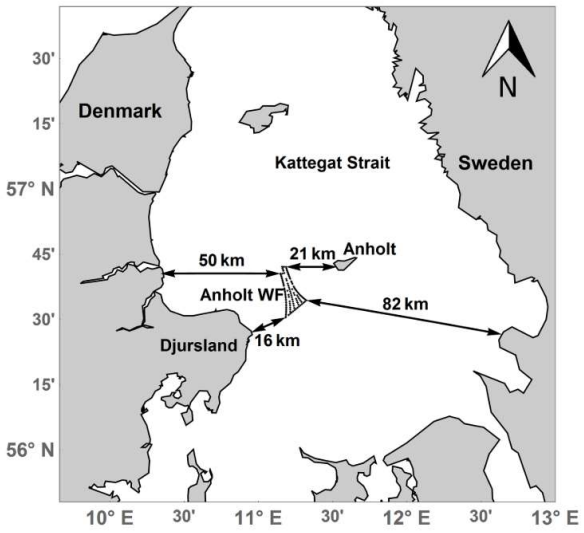

Figure 5 Position of the Anholt wind farm (Anholt WF) and distances to the coast.

Wind turbines produce power from the wind but they can also be seen as large anemometers that measure the wind speed. The Supervisory Control And Data Acquisition (SCADA) system on the turbines monitors and records wind turbine data, e.g. power production or pitch angle. The wind turbine power curve links the free wind speed to a power production. This wind speed (hereafter SCADA wind speed) can be derived from power and pitch combined with the power curve. The resulting wind speed is equivalent to the reference wind speed used to create the power curve and is treated as a measurement at the turbine hub height.

SAR wind speeds are retrieved from Sentinel-1A for the period of 12.2014–06.2015. SCADA wind speeds are roughly representative for the wind turbine hub height at 81.6 m. A logarithmic wind profile is used for extrapolation with a wind speed dependent roughness length using Charnock's relation and the Charnock parameter (Grachev and Fairall, 1996). Wind turbines extract energy from the wind and thus decrease its velocity. The region of reduced velocity is called a wake. Comparisons between SAR wind speeds and SCADA winds are carried out upstream (free-stream conditions) and down-stream (wake conditions) of the wind turbines at Anholt as shown in Figure 6.

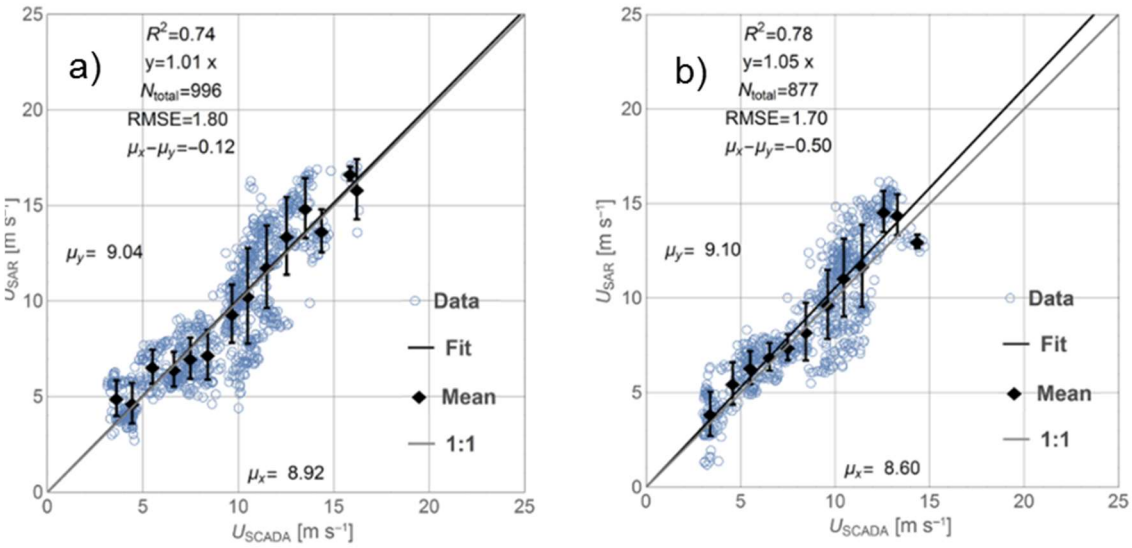

Figure 6 Comparison of SAR and SCADA wind speeds at 10 m height. a) for free stream conditions; b) for waked conditions.

For free stream condition in (a), SCADA wind speeds at hub height range from 4 to 20 m/s covering most of the range of wind turbine operation. Comparisons with SAR wind speeds yield a mean bias of -0.16 m/s (i.e. a tendency of SAR to estimate higher winds in this plot). The correlation coefficient (R^2) of the linear fit through the origin is 0.74, the slope of the fit is close to 1.0, and the RMSE is 1.80 m/s. Downstream in (b), the averaged SCADA wind speed is 9.1 m/s and comparisons to SAR give a bias of −0.50 m/s, again suggesting higher wind speeds from SAR. The correlation coefficient of 0.78 is good for a linear fit with a slope of 1.06, and the RMSE is 1.70 m/s. It is remarkable that wind

speeds derived from SAR and the wind turbine power production are comparable and results are similar to comparisons with in situ measurements at lower heights.

Observations of the past wind conditions are typically used in wind resource assessment to estimate the wind conditions, which a potential wind farm would be exposed to. Satellite SAR observations from Envisat are available 10 years before the wind farm at Anholt was constructed. Our analysis of SAR wind maps is complemented by an analysis of numerical simulations from the Weather Research and Forecasting (WRF), which are also available to a developer prior to the wind farm construction. The Anholt wind farm is located close to shore and experiences strong wind speed gradients between 245 and 275° that have been reported from the mesoscale WRF model and SCADA data (Peña et al., 2018). It is tested weather the variability of the mean wind speed at the site could have been predicted from SAR wind maps prior to the wind farm construction. Only data for the free-stream row of turbines is shown.

The wind speed variability from SAR and WRF is first examined using two different sampling scenarios for the WRF simulations: the full WRF data set (2002 to 2012) and the WRF samples collocated with the SAR scenes, see Figure 7. For both scenarios, the WRF simulations show a smooth and monotonically increasing mean wind speed from south to north along Row A. The maximum deviation of mean wind speeds from the two WRF data sets is below 0.5 %. This suggests that the reduced sampling rate, which corresponds to the sampling of SAR observations, has little effect on the mean wind speed. The wind speed variability from SAR observations is less smooth and shows a local maximum at turbine A23. SAR winds are increasing from south to north until they stay approximately constant from turbine A24 on. The wind speed variability from SAR is in good agreement with the two WRF data sets from turbine A01 until A25 where the SAR wind speeds start to decrease.

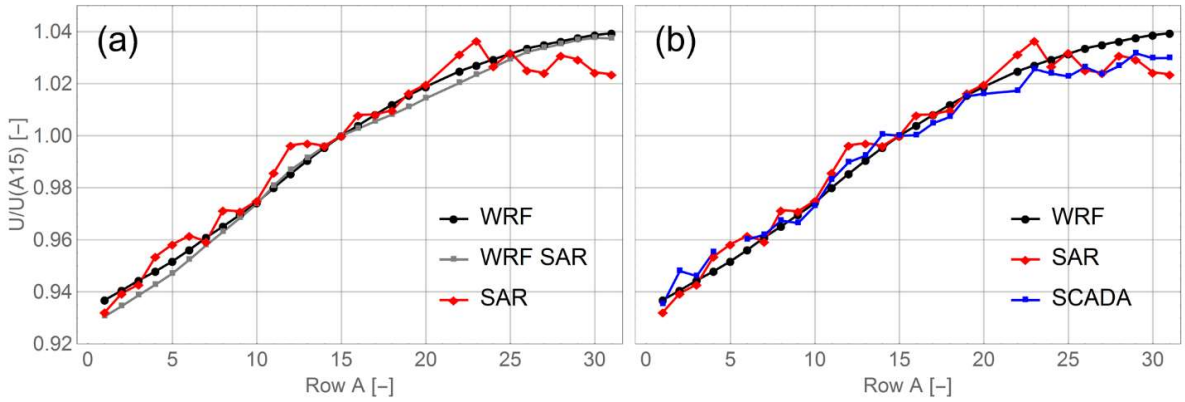

Figure 7. Average wind speed relative to turbine A15 for wind directions between 245 and 275◦. (a) Data from WRF (2002–2012) and SAR (2002–2012). The entire time period is used for "WRF" and WRF data coinciding with SAR images are used in "WRF SAR". (b) Data from full WRF time series, SAR, and SCADA (2013–2015). No turbine was erected at location A21.

All available data including the SCADA wind speed are shown in Figure 7 (b). All available data from both SAR and WRF before wind farm construction are used to best approximate the wind speed climatology from each data set. The SCADA winds, in contrast, cover a shorter period after the wind farm construction. There is a clear increase in the wind speed from turbine A01 until A20 in agreement with both the SAR and the WRF data sets. The wind speed variability along Row A is likely caused by fetch from the coastline to the wind farm varying between 16 and 50 km for the given wind sector.

We have shown that Sentinel-1A SAR winds compare relatively well to wind speeds derived from wind turbine production data. Further, we have tested on the Anholt case if SAR derived winds can be used to estimate variations of mean wind speeds prior to wind farm installation. This is found to be true using archived data from the Envisat mission.

2.3. VALIDATION OF LEVEL-2 OWI RODUCTS

ESA is producing a Level 2 ocean product (OCN) for selected areas and this product includes ocean wind fields (OWI). In this section, a validation study of the ocean winds against observations from ocean buoys is presented. OWI products are retrieved using a new Geophysical Model Function called CMOD-IFR2 NN. The SAR wind inversion is done using statistical Bayesian inference (CLS, 2011). To our knowledge, the performance of the OWI product has not been systematically tested against reference measurements. The aim of this analysis is to investigate the performance of the Level-2 OWI product with respect to the buoy data used above for inter-calibration of SAR winds. To supplement this bouy data set, the ocean buoy network of NOAA from the US East Coast is used as well (https://www.ndbc.noaa.gov/). SAR scenes are collocated with buoy data using the same criteria as above and no inter-calibration of the OWI product is been performed.

Figure 8 shows comparisons of DTU's SAR wind product (a) and the OWI product (b) against buoy wind speeds. The DTU product shows more scattered outliers compared to the OWI product. The RMSE is similar between both with 1.40 m/s for DTU and 1.35 m/s for OWI. A large difference can be found in the bias with DTU SAR winds over-predicting by 0.17 m/s and OWI wind speeds underestimating by -0.58 m/s. DTU's SAR wind product tends to overestimate the wind speed below 7 m/s, as has also been reported in previous studies (Badger et al., submitted).

The more pronounced outliers in the DTU product can be explained by several factors:

1. ECMWF wind directions used by ESA are expected to be more accurate than those from GFS used by DTU and thus the SAR wind retrieval is less prone to errors.
2. The DTU SAR wind product does not include hard target removal. Hard targets cause an increased NRCS causing erroneously high wind speeds in the retrieval process.
3. The Bayesian approach in the OWI product of using both SAR derived and ECMWF wind vectors in the processing likely reduces the influence of e.g. rain contamination.

The first influence is tested by retrieving the SAR wind speed from the DTU product with the ECMWF wind direction used in OWI. Figure 9 shows DTU's SAR wind processing but with ECMWF wind direction as an input. It can be seen that outliers are reduced and that the overall scatter is reduced to 1.31 m/s.

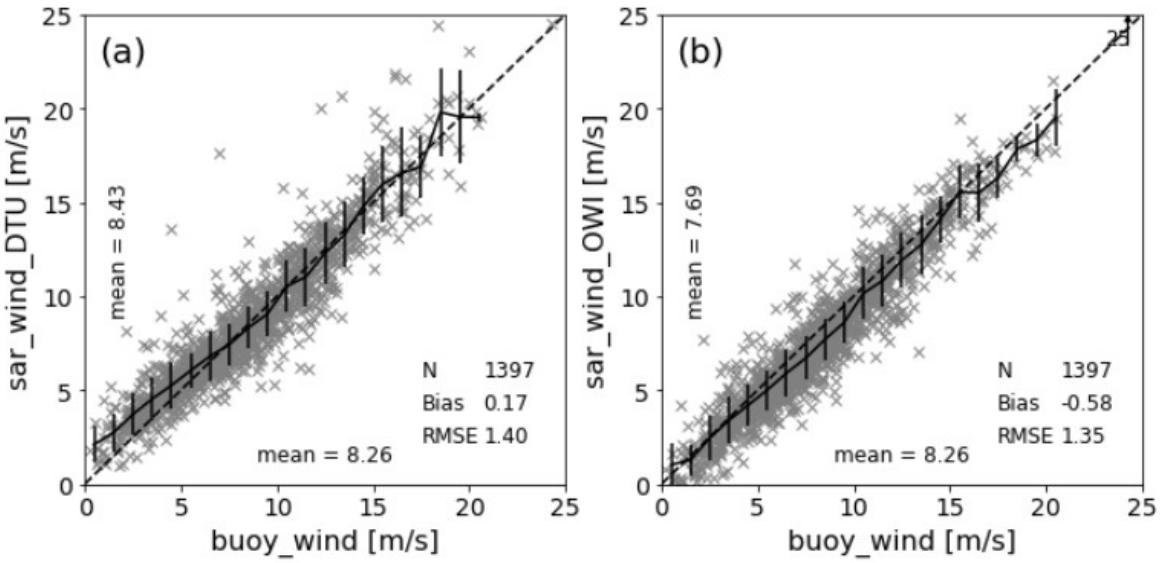

Figure 8 Scatterplot of SAR winds compared to buoy wind measurements for a) SAR winds processed at DTU and b) the Level-2 OWI product from ESA.

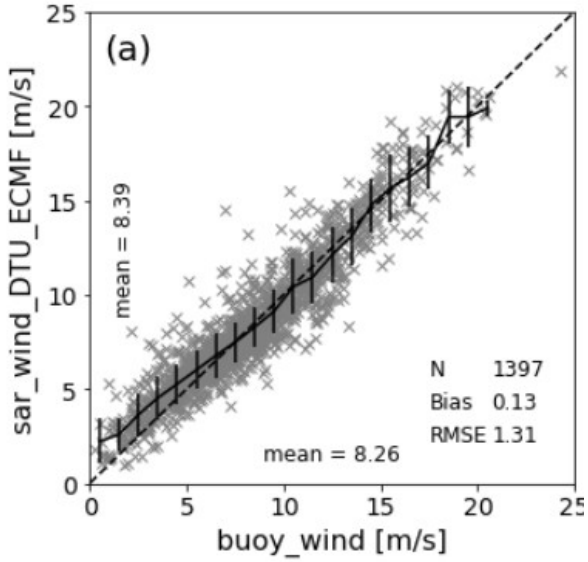

Figure 9. Scatterplot of SAR winds compared to buoy wind measurements for SAR winds processed at DTU using ECMF wind direction from the OWI product.

This validation study shows that the ESA OWI product is only marginally improving the accuracy of SAR wind retrievals compared to a more straightforward and simple processing as done by DTU. Using ECMWF wind directions for wind retrieval of the DTU product actually yields a slightly lower

RMSE than the OWI product and the lowest numerical bias. The OWI product shows lower mean wind speeds than measured from the ocean buoys. It should be noted here that the extrapolation of the ocean buoy data to 10 m is done crudely using a simple logarithmic profile, though it is not expected to fully account for the bias of -0.58 m/s. An improvement in the OWI product is the removed overestimation SAR winds below 7 m/s.

While working with the OCN data, an error has been noticed regarding the naming convention for the SAFE file format (https://sentinel.esa.int/web/sentinel/technical-guides/sentinel-1-sar/products-algorithms/level-2-algorithms/formatting). NetCDF files and their attributes for the measurement time are inconsistent with the measurement time of the SAFE file and the source SLC file. This flaw can be corrected using the time from the name string of the SLC file but an update with correct time stamps would be advisable to guide end users. Additionally, the naming of netCDF files is not unique, causing problems when netCDF files are extracted into a single folder.

2.4. VALIDATION OF SENTINEL 1 LEVEL 2 RADIAL VELOCITY (RVL) AGAINST HF RADAR

As demonstrated in Deliverable D1.1, the current operational Sentinel-1 Level 2 RVL products suffer from uncorrected instrument calibration effects that presently prevent exploitation of the data. New methods have been developed to mitigate these errors in RVL products and evaluate the geophysical information content for a specific acquisition configuration over the HF radar instrumented site of German Bight for Sentinel-1A. Here we will succinctly present the different corrections that have been developed and applied, and evaluate the impact of these corrections by comparing the S1 RVL data against HF radar measurements.

An example over German Bight is shown in Figure 10. The original Sentinel-1 Level 2 ocean radial velocity (L2 OCN RVL) product is represented on Figure 10-top-left for the acquisition on the 18th of January 2018 17h17. We analysed 14 Sentinel-1A snapshots of the exact same geometry. This geometry occurred exactly every 12-days. Data for some dates were missing for reasons unknown.

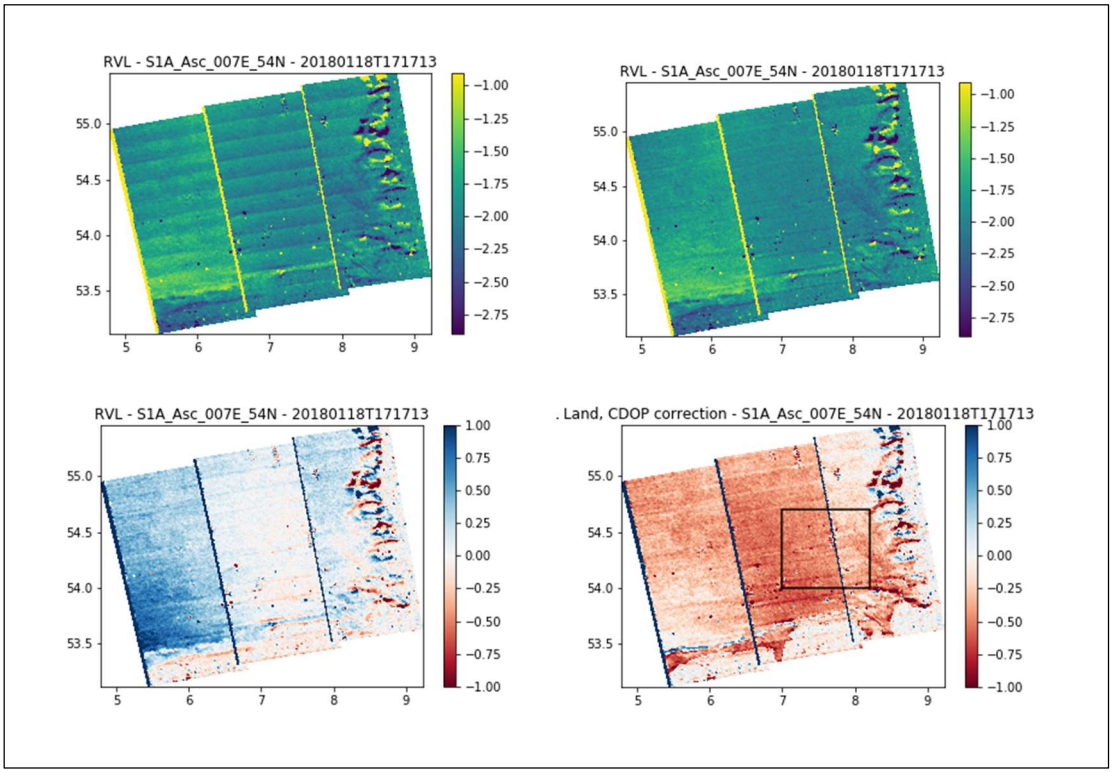

Figure 10. Sentinel-1 Level-2 Radial Velocity over the German Bight on 18 January 2018 (17h17) for (top-left) original operational products, (top-right) after correction for scalloping effects, (bottom-left) after additional correction to set retrieved velocity o over land to zero, and (bottom-right) after additional correction to remove the wind-wave induced Doppler contribution using ECMWF wind vector. The black box represents the area used for comparison between surface current estimated from S1A and HF radar. The colour bar is in m/s.

From Figure 10 top left, we note the repeated wavy patterns in the North-South direction, corresponding to the flight direction of the satellite (known as the azimuth direction). These patterns are known as scalloping and are due to the SAR acquisition technique. A simple correction developed by taking the median value of the 14 S1A snapshots makes it possible to remove most of this scalloping effect. This is shown by the de-scalloped RVL (Figure 10-top-right), where we can see that the average velocity over land (East and South part of the snapshot) has an average value of minus 2 m/s. This is clearly in error since the radial velocity over land is expected to be zero on average. Using this assumption of zero mean velocity over land, a linear bias is estimated and removed for each range in the sub-swaths and for each snapshot. The magnitude of this correction ranges from -0.5 to +2.5m/s and is therefore not negligible. In the case of German Bight, a second correction over land can be estimated and applied in the azimuth direction using exclusively data from the eastern sub-swath, since land is present in the scene for all azimuth positions along-track. This correction presents oscillations around zero in the along-track azimuth direction and can be applied across all ranges in the

swaths. This correction reaches up to a maximum of ±0.15m/s. The impact of applying these two land corrections for the 18/01/2018 scene is shown in Figure 10-bottom-right.

The final correction to be applied is not linked to instrument calibration or acquisition effects but is purely geophysical. Indeed, it is well known that the Doppler velocity measured by SAR is dominated by contributions by wind-waves (e.g. Martin et al., 2014 JGR-O). This artefact velocity, also called wave bias, can reach up to 2 m/s and, to first order, is a function of the relative wind/radar direction, and to the second order, of the incidence angle and wind speed. The amplitude of the wave bias is maximum in the up/downwind directions and is described relatively well by the C-DOP empirical model (Mouche et al., 2012). Here, the wave bias correction is estimated using ECMWF wind vectors as input to the C-DOP model. Once this final correction is applied, the corrected RVL (Figure 10-bottom-right) should represent the best estimates of ocean radial surface current in the radar line-of-sight perpendicular to the satellite track.

The corrected Sentinel-1A RVL were compared against HF radar radial surface currents for each of the 14 snapshots. HF radar data provided by HZG were obtained generally between 17:19 and 17:39 (Figure 11). The median value of the radial surface currents was computed over the black box for the HF radar (Figure 11) and for Sentinel-1A (Figure 10). The sequence of S1A and HF radar matchups of median radial current over the black box for the 14 S-1A overpasses is represented in Figure 12 (left) together with the difference against HF radar measurements (Figure 12-right). Statistics of the residuals between S1A and HF radar data are summarised in Table 1. There was no colocated HF radar measurements for S1A sequence 10. This imply there is 13 (14-1) HF/S1A pairs.

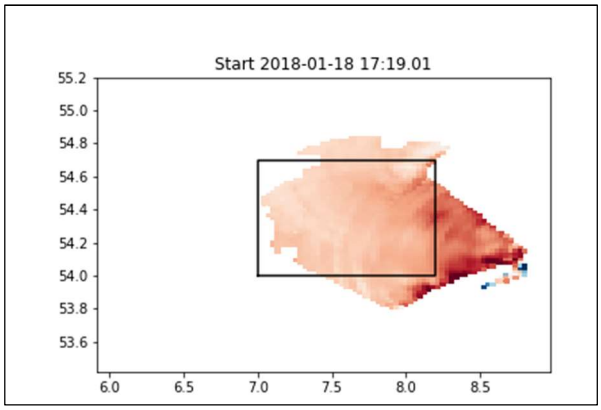

Figure 11. HF radar radial surface current in the direction of the S1A ascending line-of-sight. The colourbar is the same as in Figure 10. The black box represents the area over which the S1A and the HF radar median current are estimated and compared.

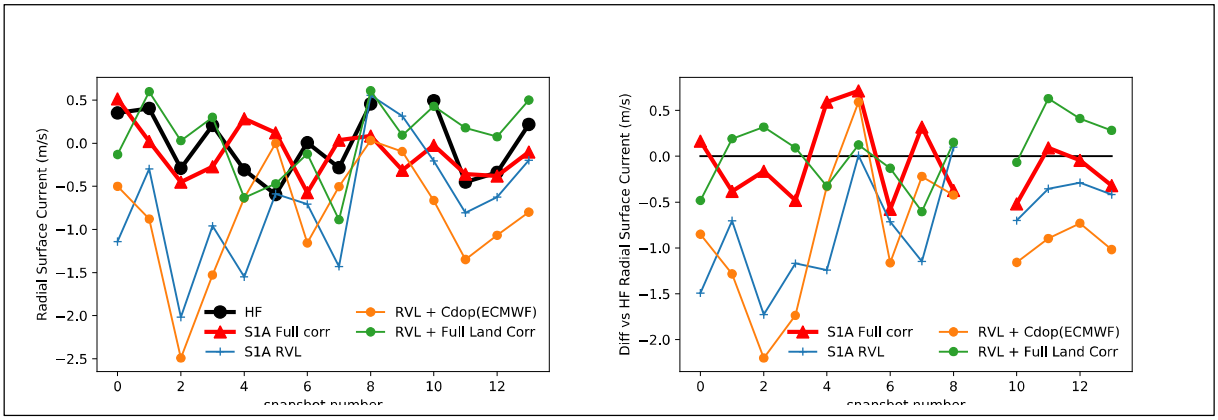

Figure 12: Median radial surface current in m/s in the S1A line-of-sight calculated over the black box for 14 different S1A overpasses for (left) S1A and HF radar radial surface current, (right) the residual current (S1A minus HF radar). The different products and applied corrections are indicated in the legend.

Table 1: Statistics of S1A radial surface current against HF radar for 13 S1A overpasses

	Bias (m/s)	RMSD (m/s)	correlation
S1A RVL Original Operational products	-0.76	0.93	0.5 (p-value 9%)
RVL corrected for wave bias with C-DOP(ECMWF wind)	-0.88	1.10	Not Significant
RVL corrected for biases over land	0.05	0.35	0.67 (p-value 1%)
S1A with full corrections applied	-0.07	0.42	Not Significant

In Figure 12, the thick black lines indicates that the HF radar median radial surface current fluctuates between -0.5 m/s and +0.5 m/s between the different scenes. The S1A RVL operational products (blue line) present much stronger variability, with currents ranging from -2 m/s to 0 m/s and a large mean bias against HF radar of -0.76 m/s and a root-mean-square-difference (RMSD) of nearly 0.93 m/s for the 13 (14-1) pairwise HF/S1A comparisons. The poor performance of the original operational S1A RVL products against HFradar is not surprising as the wind-wave artefact was not removed and is well-known to introduce biases of up to 2 m/s.

If S1A products were perfectly calibrated, only one correction would need to be applied to enable comparisons with HF radar data, and that is the correction for the wind-wave artefact velocity (I.e. the wave bia). This is represented by the orange curve in Figure 12 showing the current for RVL products corrected for wave bias using C-DOP and ECWMF wind vectors. On its own, the wave bias correction does not improve the results against HF radar at all, and in fact, introduces a negative bias against HF radar that is greater than 0.8 m/s and has an RMSD greater than 1 m/s.

In contrast, if the original RVL products are adjusted using the land corrections (green curve), we get much better comparisons with HF radar, with only a small positive bias (5 cm/s), a RMSD of 0.35 m/s and a correlation of 0.67. If we then correct for the wind-wave artefact, the overall statistics are degraded slightly, with a small negative bias (-7 cm/s) and RMSD of 0.4 m/s. This result is unexpected and might point at errors in the ECMWF wind direction. Further work will be necessary to understand the exact origin of this small deterioration, for example by using wind direction from regional numerical weather prediction system or from HF radar estimation of 'wind sea' waves direction.

3. SENTINEL-2

3.1. OVERVIEW

Sentinel-2 is a wide-swath, high-resolution, multi-spectral imaging mission consisting of two operational satellites.

Sentinel-2A was launched on 23 June 2015 and Sentinel-2B was launched on 7 March 2017.

The Sentinel-2 Multispectral Instrument (MSI) samples 13 spectral bands: four bands at 10 metres, six bands at 20 metres and three bands at 60 metres spatial resolution. The spectral bands of Sentinel-2 are illustrated in Figure 13.

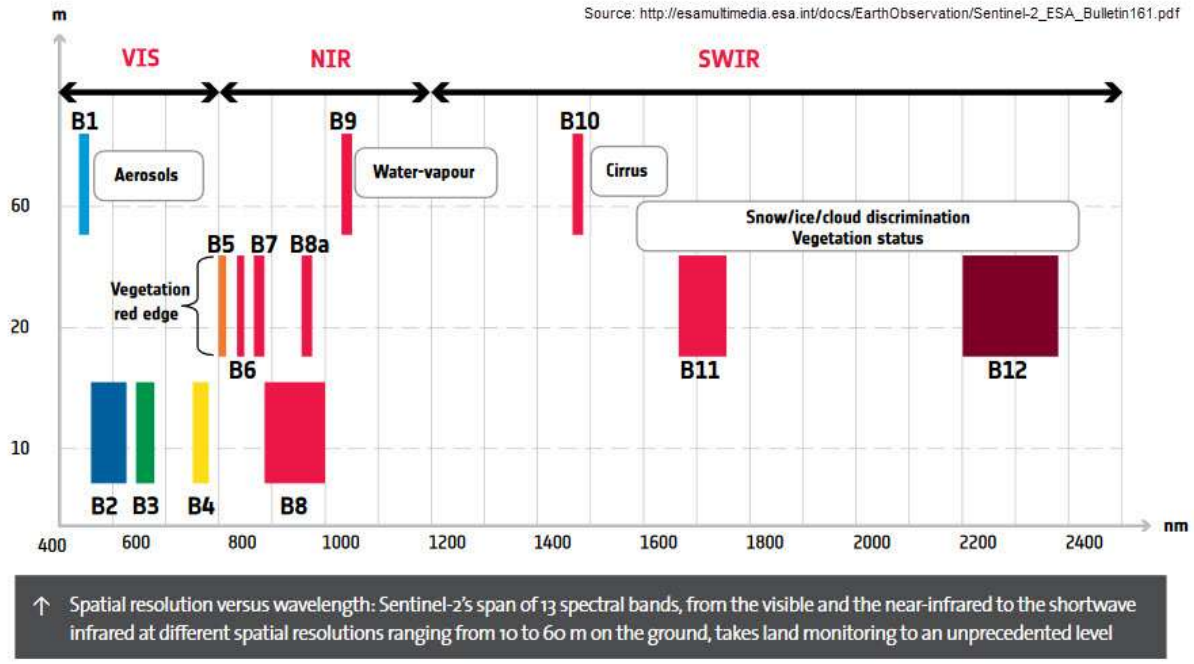

Figure 13: Spectral bands sampled by Sentinel-2 Multispectral Instrument (MSI)

Further information about the Sentinel-2 A/B payload is available at
https://sentinel.esa.int/web/sentinel/missions/sentinel-2/instrument-payload

3.1.1. Sentinel-2 products considered in CEASELESS

Water Quality

Considering the highly varying physical conditions found in the coastal areas included in CEASELESS there are no standard Level-2A products of relevance available to the CEASELESS services. A custom processing of Level-1C from both Sentinel-2A and Sentinel-2B has therefore been adopted. The primary water quality product is total suspended matter concentrations.

Name	High-Level Description	Production & Distribution	Data Volume
Level-1C	Top-Of-Atmosphere reflectances in cartographic geometry	Systematic generation and online distribution	~600 MB (each 100km x 100km²)
Level-2A	Bottom-Of-Atmosphere reflectances in cartographic geometry	Systematic and on-User side (using Sentinel-2 Toolbox)	~800 MB (each 100km x 100km²)

Satellite-derived Bathymetry

Early in the project it was realized that the Ebro Delta is a problematic test case for satellite-derived bathymetry due to primarily a persistent high background turbidity level. For the Adriatic case area turbidity is similarly a challenge and furthermore, the coastal stretch is characterized by a steep profile so optical deep conditions (no bathymetry retrieval possible) are met relatively quite close to the coastline. Focus has therefore been on the Wadden Sea area. The bathymetry in the Wadden Sea area is extremely complex and dynamic and the tidal effect further complicates the depth retrieval.

Coastal Dynamics

Considering the land/water border is an important model boundary it was decided to look in the potential of using Sentinel-2 to analyze and quantify both short-term and long-term changes.

3.2. VALIDATION OF WATER QUALITY

Access to suitable validation data has proven to be very difficult. The high spatial resolution of Sentinel-2 combined with the dynamic nature of the coastal areas results in a very short time window for a proper cal/val match-up definition. Instead, the products have been evaluated based on time series plots where the satellite derived products are aggregated to monthly values and plotted over a full year and the behaviour analysed: do we see the expected seasonality? Do we identify the expected spatial variations with high/low concentrations at the expected places? Two different retrieval schemes have furthermore been included in order to identify differences between the different underlying methodologies.

Figure 14:Defined comparison stations near the Ebro Delta AOI where water quality data has been extracted from the processed Sentinel-2 scenes and evaluated.

Figure 15:Extracted pixel values from two different sediment retrieval methods: C2RCC and ACOLITE. A clear seasonal pattern is found with expected elevated high concentrations during the winter period were the highest wind and precipitation levels are also observed.

Water quality data has been shared with UPC for tests and inclusion in their modelling activities. The sediment data was actively used to confirm model results in a detailed study on the southern part of the Ebro delta (Grifoll et al 2019)

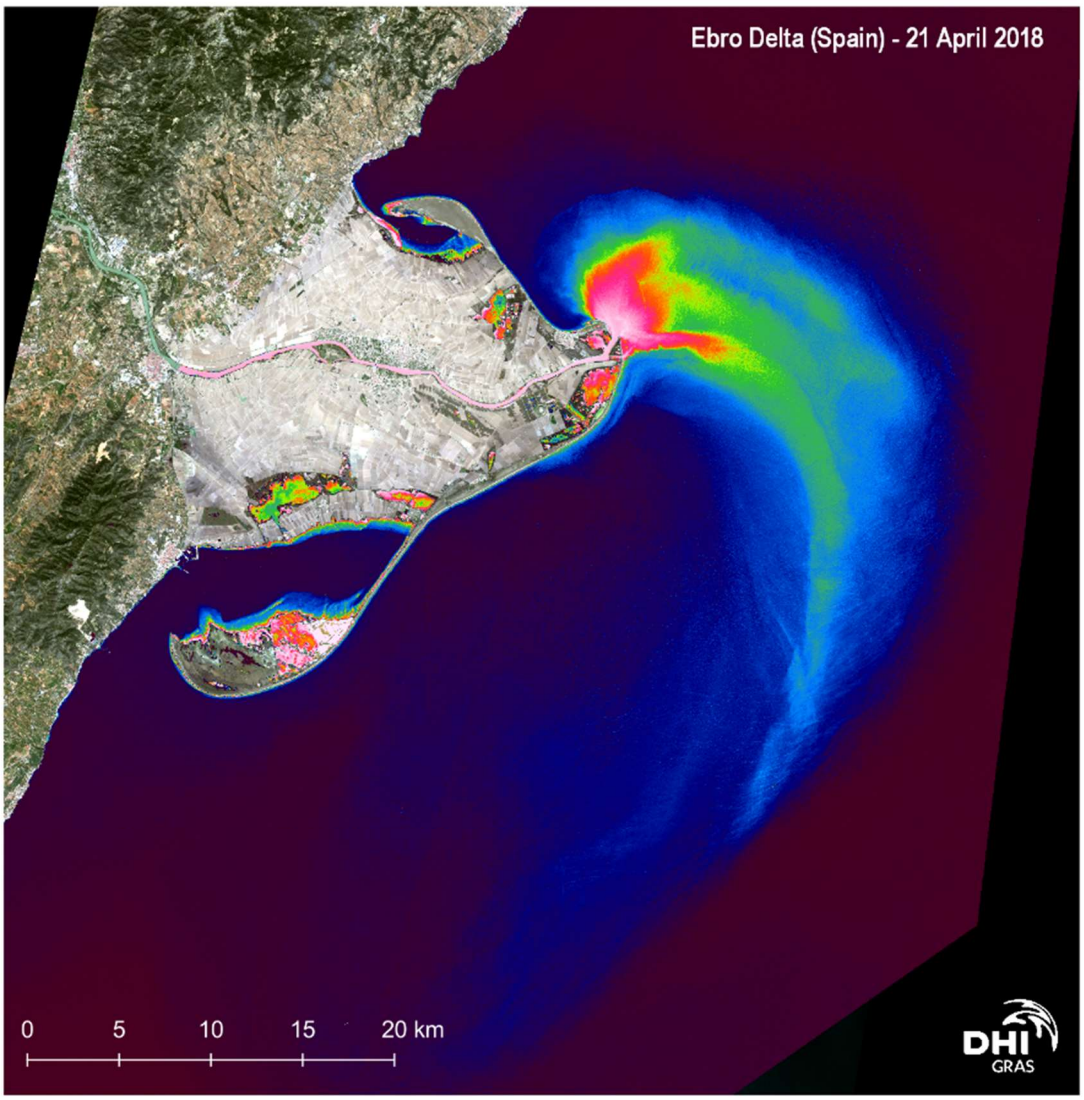

Figure 16: Sentinel-2 based sediment concentration map over the Ebro Delta study area from 21st April, 2018. On this day a significant plume from the river outlet in the central part is clearly visible. The extent of the plume extends more than 20km from the outlet.

The apparent good performance was confirmed in a comparison exercise based on in-situ data from a dedicated field campaign in the northern part of the delta. During 2017 a number of sediment samples were collected by UPC, covering both sheltered locations inside the very shallow parts of the bay and more dynamic areas near the mouth of the Bay.

Figure 17: Sample locations marked with orange dots where sediment samples were collected over a period of time in 2017.

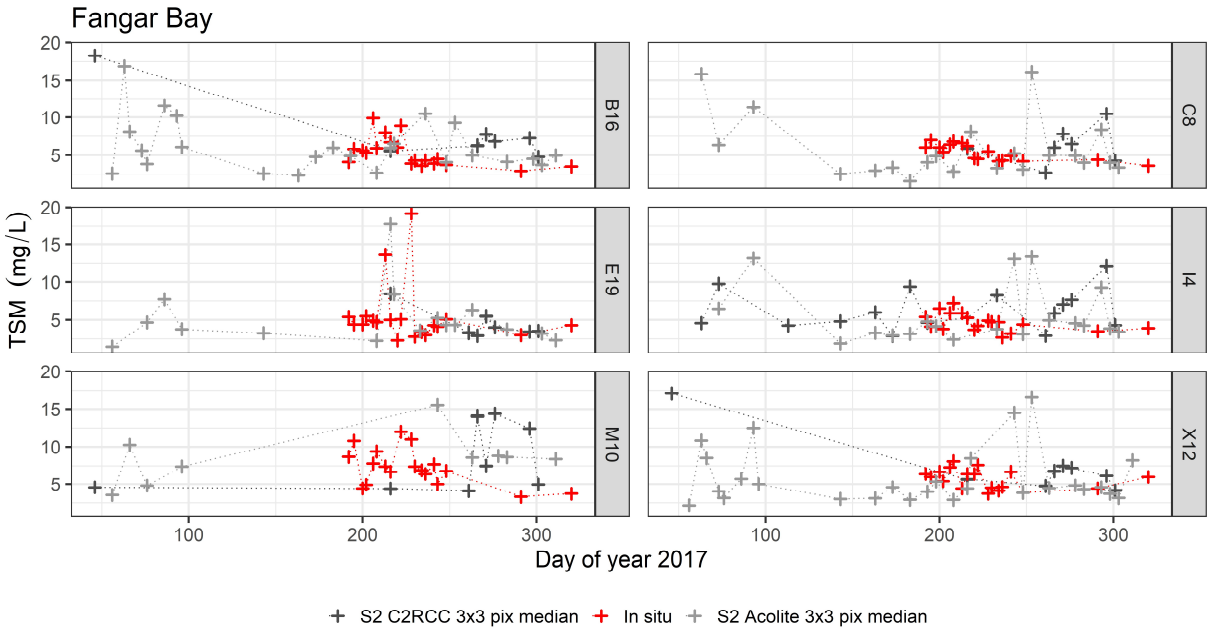

Figure 18: Comparison between measured sediment concentrations (red) and two different Sentinel-2 based sediment retrieval schemes (grey). Station locations are shown in the precious figure.

3.3. VALIDATION OF SATELLITE-DERIVED BATHYMETRY

As mentioned earlier, the focus of the satellite-derived bathymetry activities has been on the German Bight area. The bathymetry in this area is extremely complex due to the dynamic nature of the Wadden sea and the significant tidal effects and re-suspension taking place.

In order to optimize the output coverage, we have established a combined high/low tide bathymetry layer and a complete mapping of the tidal zone has been achieved. This data was integrated into the EMODnet 2018 high resolution bathymetry layer to create a full and complete bathymetry coverage of the HZG model domain. An integrated and full coverage is required for the modelling activities. The major advantages of satellite-derived bathymetry is the high spatial resolution (10m x 10m) and the ability to derive fully up-to-date depth estimations. By integrating the detailed and up-to-date Sentinel-2 bathymetry data into the coarse-scale EMODnet data a complete layer is created with EMODnet coarse-scale in the deeper and more stable areas and sentinel-2 in the shallower and dynamic parts where high spatial resolution is also most important.

Figure 19: Subset of bathymetry around the island of Sylt near the Danish/German border in the Wadden Sea. The combined Sentinel-2/EMODnet bathymetry (left) show much greater level of detail than the original EMODnet data (right). An artefact in EMODnet data (a cut-line in the north-eastern part of the area is corrected in the fused bathymetry layer. The orange lines relates to the transects shown in Figure 20 and Figure 21.

No recent bathymetry survey data is available for the area but a qualitative evaluation of the Sentinel-2 product show good agreement with the general EMODnet data (EMODnet data has been used as the reference depth). The Sentinel-2 data layer is much more detailed and better able to resolve the small-scale features in the area.

A part of this qualitative evaluation can be seen in the following two figures, where comparative transects across the data has been extracted from both datasets.

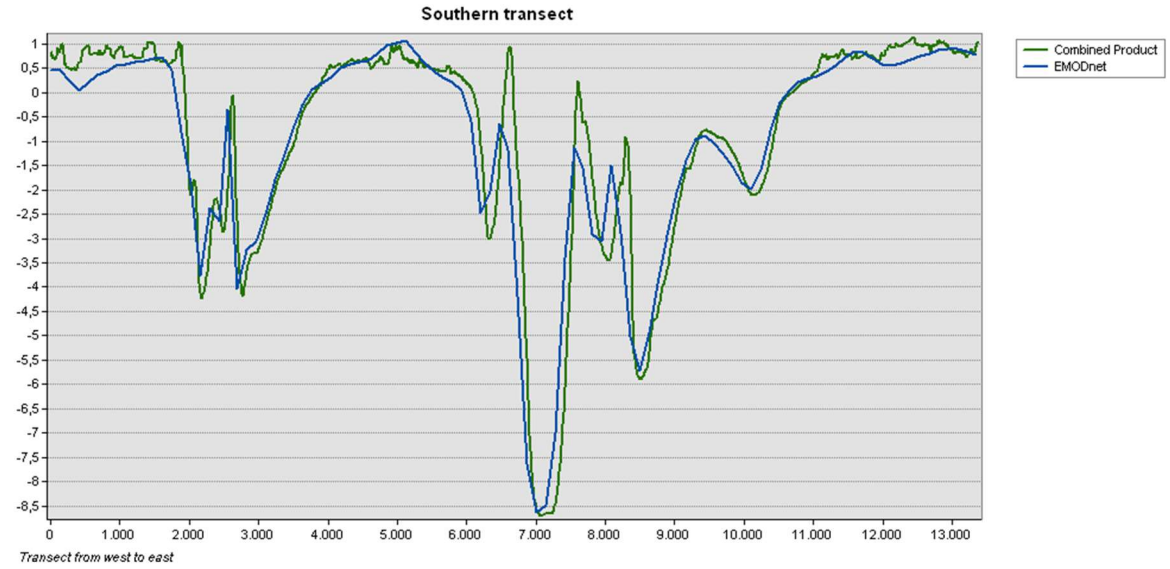

Figure 20: Transect across the waters south of Sylt. Shows a high degree of correlation between the two datasets as well as some of the smaller details in the Combined dataset.

In *Figure 20*, the high correlation between the datasets can be seen. However, in *Figure 21*, the shallow areas where EMODnet data struggles, due to the low density of information, the combined product maintains the level of detail.

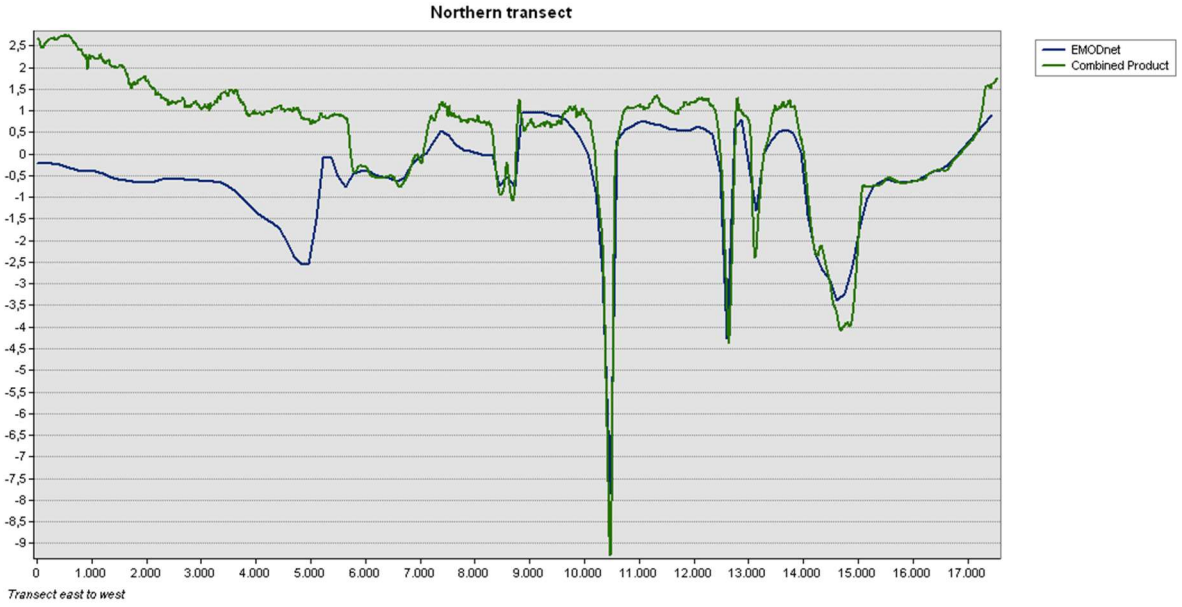

Figure 21: Transect across the waters north of Sylt. The area from 0-5000 is an example where the EMODnet data and the combined product disagree, due to inconsistencies within EMODnet.

The large differences seen in *Figure 21*, especially at 5000m of the transect likely relates issues with merging datasources in the EMODnet dataset, as the vertical jump in depths coincides with the

national border between Denmark and Germany. The positive values shown in Figure 20 and Figure 21 are related to the data being vertically referenced to lowest astronomical tide (LAT) .

3.4. VALIDATION OF COASTAL DYNAMICS

With Sentinel-2 we have an excellent source of information for monitoring coastal dynamics. The high spatial resolution combined with the high temporal frequency means we have good likelihood of cloud free conditions at any tidal period for any location globally. Similar to accounting for the bathymetry dynamics in the model setups, updated and detailed land/water boundary is important for high resolution modelling. Since bathymetry retrieval proved difficult in the Ebro Delta area, it was decided to look into the coastal dynamics of the area in detail instead.

The coastal dynamics is mapped based on Landsat and Sentinel-2 input data. Shoreline extraction procedures from optical data are quite well established, even though in certain situations (e.g. dark mudflats in tidal flat areas) separating water from land is still challenging. They can be grouped into two general categories: thresholding and classification (Gens 2010, Mitra et al. 2017). The thresholding methods usually first involve transforming the original reflectances into a specific set of indicators which allow easy separation of the features of interest, e.g. water and land or sand and vegetation. The indicator can be a spectral index (e.g. Normalised Difference Vegetation Index, Normalised Difference Water Index, Water Index) or a spectral transformation (e.g Tasselled Cap, Principal Component Analysis, Intensity Hue Saturation) and in certain studies a combination of multiple indices or transformations is used (Ouma 2006, Hagenaars 2017, Choung2016). The second step consists of actual separation of features through thresholding, with the threshold set as a constant value (e.g. 0 in case of Normalised Difference Vegetation Index when separating land and water), derived from the image (e.g. using Otsu's method) (Mitra 2017, Sekovski 2014) or determined by inspecting a histogram. The final step in the thresholding methods is the actual shoreline extraction through edge detection and raster to vector conversion.

For CEASELESS we have decided for a semi-automated approach following this overall flow:

1. manual selection of input images: manually selection allows optimal quality of the input data and a controlled handling of the tidal component.
2. Derive threshold used to separate land/water. Currently the NDWI is used
3. A K-Means unsupervised classification is made and from the bi-modal distribution two classes are derived and used to separate the land/water.

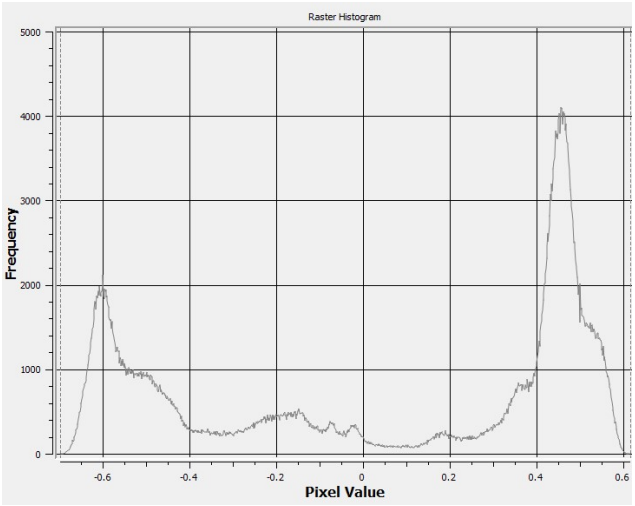

4. Postprocessing: calculate connected pixel count size (how many pixels of the same class are next to each other) from the K-Means classification.
    - Remap the class where patch size is below a certain threshold
    - Run a focal median kernel over any remaining patches below a minimum patch size.
5. Vectorise the results.

Step 4 in the process may be coastline dependent and require various settings. In some cases (simple coastlines) remapping may be sufficient, in other more complex cases focal median may be prioritized. The analysis can be carried out on image composites, or single date images of any sensor.

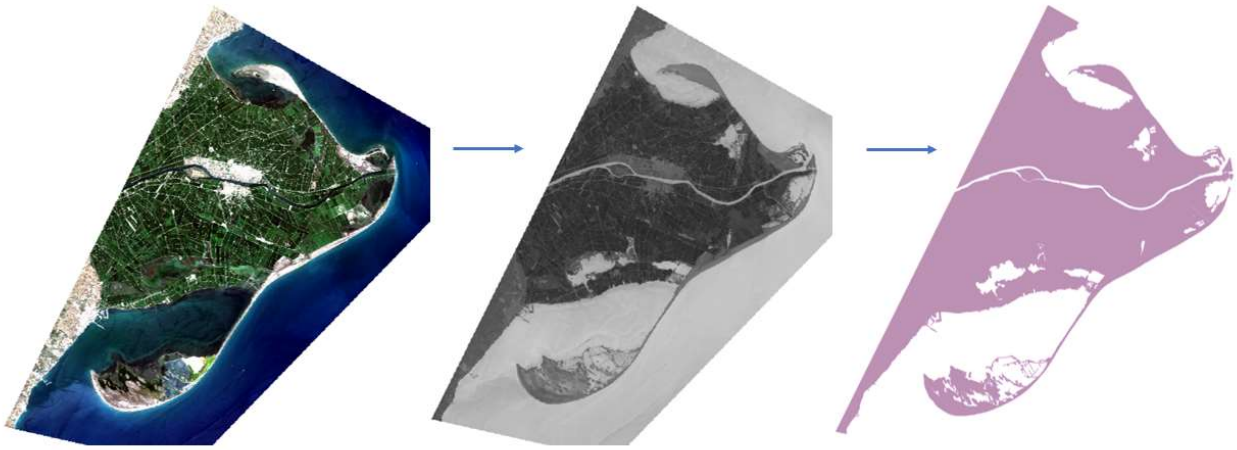

Figure 22. Illustration of the workflows from input imagery to derived index to a final vectorized coastline.

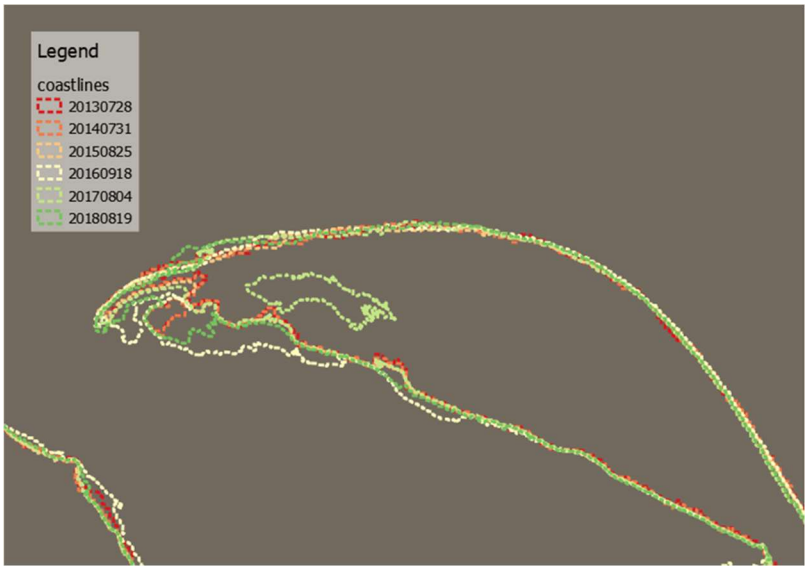

Figure 23. Example of time series of derived coastlines over a 5-year period of the northern part of the Ebro Delta. Based on Landsat 8 and Sentinel-2 imagery.

4. SENTINEL-3

4.1. OVERVIEW

Sentinel-3 is the Copernicus Medium Resolution Land and Ocean Mission with currently two satellites in operation. Sentinel-3A was launched on 18 February 2016 and Sentinel-3B on 25 April 2018. Both satellites are flying in an exact 27-days repeat cycle orbit.

There are five payloads onboard these satellites, including:

- Ocean and Land Colour Instrument (OLCI)
- Sea and Land Surface Temperature Radiometer (SLSTR)
- And three instruments in the Surface Topography mission, including:
    - SAR-mode Radar ALTimeter (SRAL), a dual-frequency Ku/C-band radar altimeter.
    - MicroWave Radiometer (MWR) to correct SRAL data for wet tropospheric delays.
    - Precise Orbit Determination (POD).

Further information about the Sentinel-3 mission and its payloads is available at https://sentinel.esa.int/web/sentinel/missions/sentinel-3.

4.2. VALIDATION OF SENTINEL-3 SRAL

4.2.1. Global validation of Sentinel-3 SRAL wind and wave products

Introduction

Surface wind speed (WS) and significant wave height (SWH), which are part of Seninel-3 (S3) Surface Topography Mission (STM) Level 2 Marine Ocean and Sea Ice Areas (SRAL-L2MA also known as SR_2_WAT), are validated using the procedure used successfully for the validation of the equivalent products from earlier altimeters. The procedure is described in Abdalla and Hersbach (2004). The procedure composed of a set of self-consistency checks and comparisons against other sources of data. Model equivalent products from the Integrated Forecasting System (IFS) of the European Centre for Medium-Range Weather Forecasts (ECMWF) and in-situ measurements available in NRT through the Global Telecommunication System (GTS) are used for the validation.

The validation is based on the NRT operational SRAL-L2MA from both Sentinel-3A and Sentinel-3B. For the time being, the product distributed by EUMETSAT in netCDF through their Online Data Access (ODA) system is used. The raw data product is split over 6-hourly time windows centred at synoptic times (00, 06, 12 and 18 UTC).

The data are then averaged along the track to form super-observations with scales compatible with the model scales of around 75 km. It is worthwhile mentioning that the model scale is typically several

(4~8) model grid spacing. This corresponds to 11 individual (1 Hz) Sentinel-3 observations (7 km each).

To achieve this, the stream of altimeter data is split into short observation sequences each consisting of 11 individual (1-Hz) observations. A quality control procedure is performed on each short sequence. Erratic and suspicious individual observations are removed and the remaining data in each sequence are averaged to form a representative super-observation, providing that the sequence has enough number of "good" individual observations (at least 7). The super-observations are collocated with the model and the in-situ (if applicable) data. The raw altimeter data that pass the quality control and the collocated model and in-situ data are then investigated to derive the conclusions regarding the data quality. The details of the method used for data processing is an extension to the method used for ERS-2 RA analysis and described in Abdalla and Hersbach (2004).

The results of wind and wave validation presented here focuses on the whole of year 2018. Both Sentinel-3A and Sentinel-3B products are assessed irrespective of the fact that Sentinel-3B SAR data temporal coverage is limited to the period from late June till end of December 2018 (i.e. about 6 months). It is worthwhile mentioning that Sentinel-3B was orbiting Earth in tandem with Sentinel-3A for more than four months until late October 2018. During this tandem phase, Sentinel-3B was ahead of Sentinel-3A by 30 seconds. Sentinel-3B was then moved to reach its nominal operational orbit (same as that of Sentinel-3A but separated by 140°) on 23 November 2018.

Sentinel-3 SRAL SAR wind speed

Figure 24 shows the global wind speed probability density function (PDF) of Sentinel-3A and Sentinel-3B SAR mode for the whole year 2018 (half a year in case of Sentinel-3B). The PDF's of the ECMWF Integrated Forecast System (IFS) model wind speed collocated with both altimeters during the same period are also shown. Although the PDF of Sentinel-3A wind speed is close to that of the model, there are some deviations especially around the peak of the PDF.

On the other hand, Sentinel-3B underestimates the wind speed for that period when compared to both Sentinel-3A and the ECMWF model. This is a consequence of overestimation of the normalised radar backscatter coefficient (backscatter, σ° or Sigma-0) by about 0.5 dB as can be seen in Figure 25. This issue was alleviated by ESA and EUMETSAT (Sentinel-3 operators on befalf of the EC) as part of Sentinel-3B Processing Baseline 1.13 introduced into operations on 6 December 2018.

The deviation between Sentinel-3A PDF and those of the other operational altimeters (Jason-3, Jason-2, CryoSat-2 and SARAL/AltiKa) are more pronounced as can be seen in the upper panel of Figure 26. The PDF's of model colocations with each satellite are shown in the lower panel of Figure 26. The deviation among the model PDF's as sampled along the ground track of each altimeter (i.e. the colocation with the altimeter super-observations) is not large. This suggests that the wind speed measurements from various altimeters show non-negligible deviations (at least in their PDF distributions).

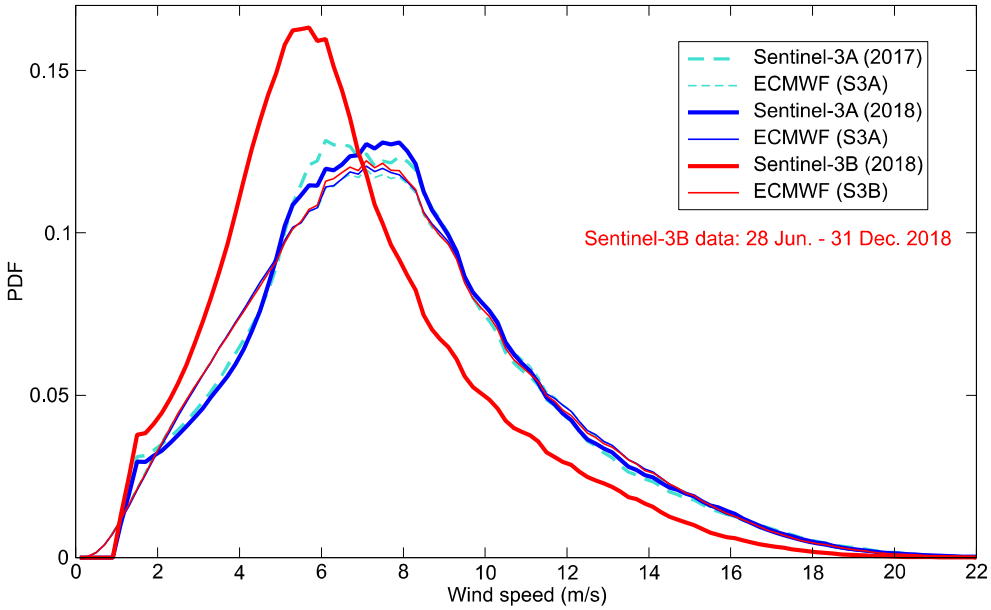

Figure 24. Sentinel-3A and Sentinel-3B SRAL surface wind speed PDF over the whole global ocean for year2018 (note that Sentinel-3B data have not covered 1 year yet). The corresponding ECMWF (collocated with Sentinel-3A and Sentinel-3B) PDF's are shown for comparison. The 2017 PDF's of Sentinel-3A and its model counterpart are also shown.

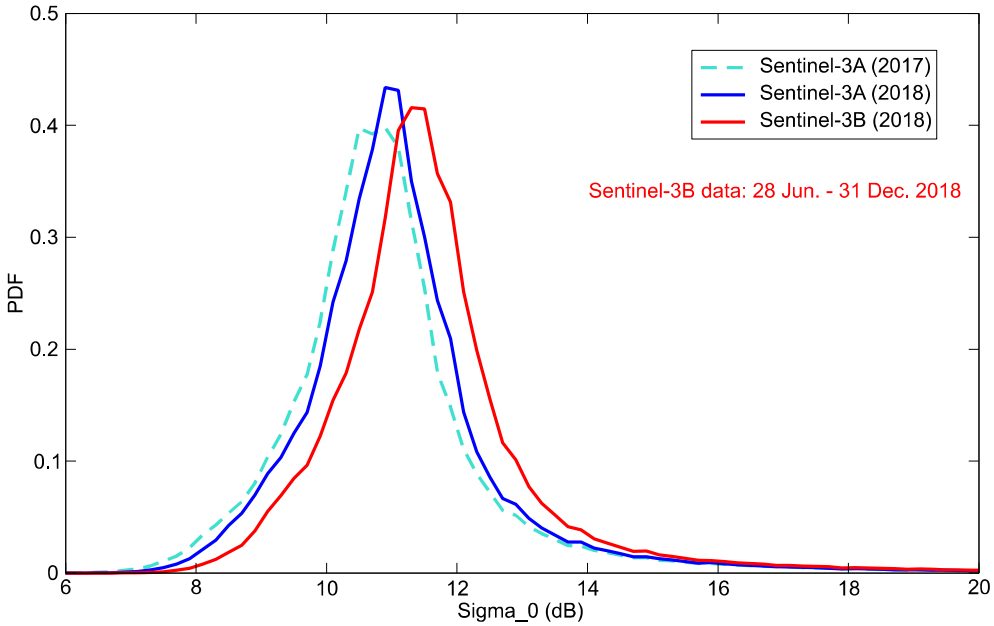

Figure 25. Sentinel-3A and Sentinel-3B SRAL backscatter coefficient PDF's over the whole global ocean for year 2018 (note that Sentinel-3B data have not covered 1 year yet). PDF of Sentinel-3A from 2017 is also shown.

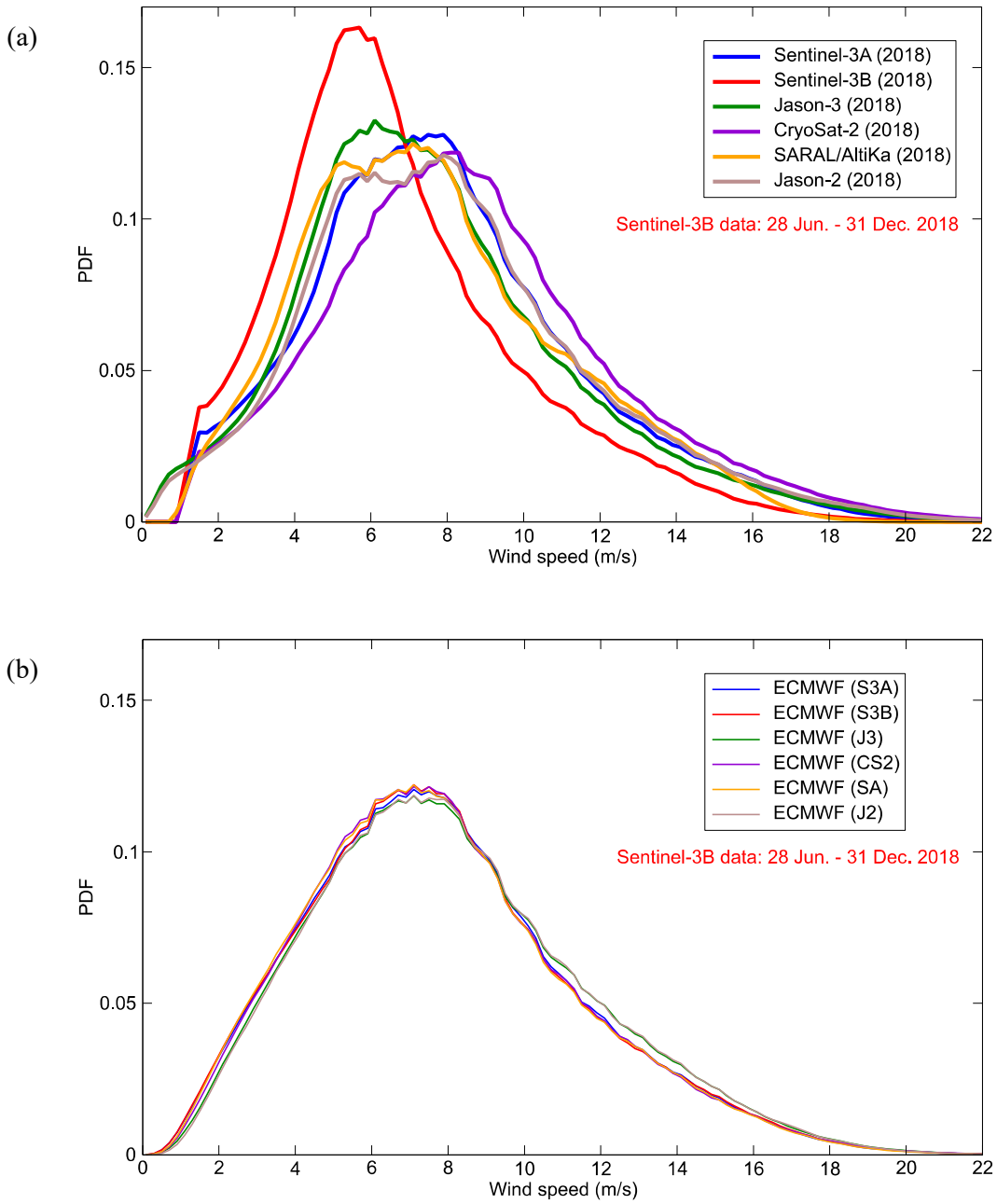

Figure 26. Panel (a): Comparison between wind speed PDF's of various altimeters for year2018 (note that Sentinel-3B data have not covered 1 year yet). PDF of Sentinel-3A from 2017 is also shown. Panel (b): The corresponding ECMWF model PDF's as collocated with the measurements. The abbreviations are as follows: S3A: Sentinel-3A, S3B: Sentinel-3B, J3: Jason-3, CS2: CryoSat-2, SA: SARAL/AltiKa and J2: Jason-2.

The time series of the global mean and standard deviation (SD) of the wind speed from both Sentinel-3 altimeters over a 7-day time window moving by 1 day at a time are shown in the upper and lower panels, respectively, of Figure 27. The corresponding time series of the model are also shown for comparison. The global mean of Sentinel-3A SAR wind speed is very close to that of the ECMWF model. However, Sentinel-3A altimeter shows lower wind speed variability (standard deviation) compared to the ECMWF model. The only exception is for a short period during July each year (i.e. 2017 and 2018) when the variance of Sentinel-3A and the model winds are almost identical. It is unusual for the instrumental measurements to show lower variability compared to the model. Note that at the scale of the super-observations (~75 km is used for this assessment) one would expect comparable SD values.

After early December 2018 when the backscatter bias was corrected, Sentinel-3B wind speed mean and SD are in very good agreement with those of Sentinel-3A and the model. Sentinel-3B mean is very close to the model mean. Both are slightly lower than Sentinel-3A mean (the difference is about 0.15 m/s).

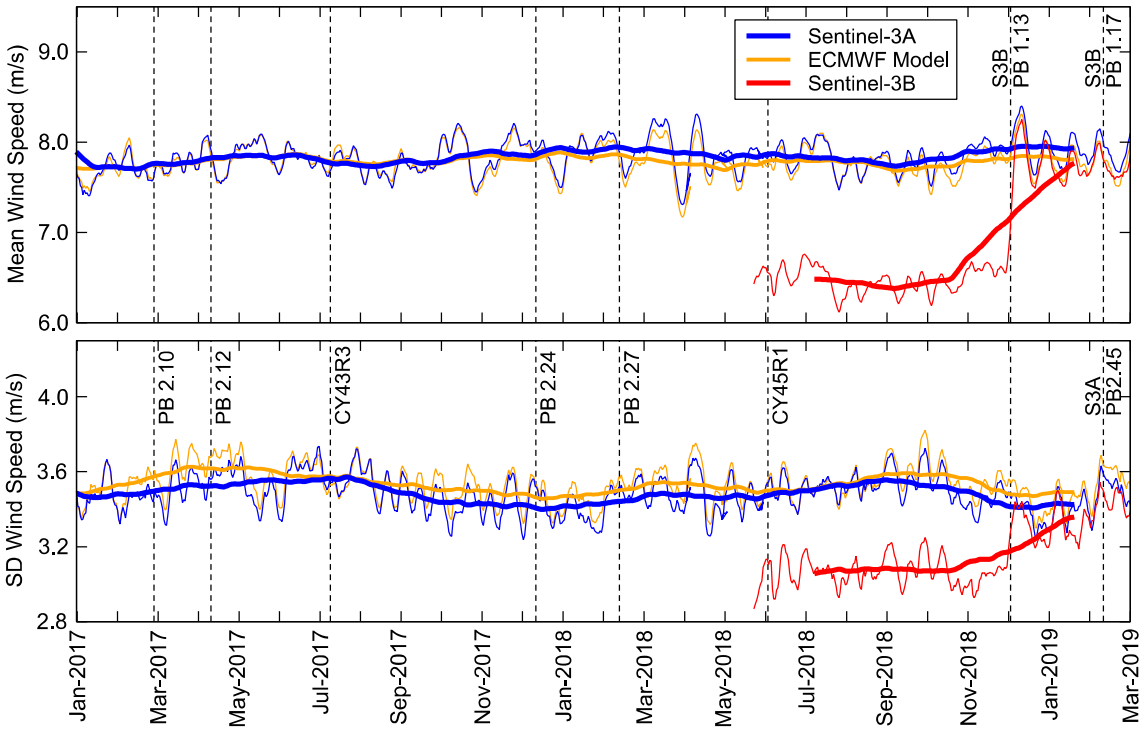

Figure 27. Time series of global mean (top) and standard deviation (bottom) of wind speed from SRAL Ku-band after quality control from both Sentinel-3A and 3B. The collocated model wind speed mean and SD are also shown. Mean and SD are computed over a moving time window of 7 days (shown as thin lines). The 92-day running means are shown as thick lines. Vertical dashed lines show events which may have impact on the comparison. This includes Sentinel-3 STM Instrument Processing Baseline (PB) changes as well as ECMWF IFS model changes like CY45R1.

Collocated pairs of altimeter super-observation and the analysed (AN) ECMWF model wind speeds are plotted in a form of a density scatter plot in Figure 28 for the whole globe over the whole year of 2018. Panel (a) is for Sentinel-3A while panel (b) is for Sentinel-3B (only for the second half of 2018). The scatter plots in Figure 28 and other similar wind speed scatter plots that appear hereafter represent two-dimensional (2-D) histograms showing the number of observations in each 2-D bin of 0.5 m/s × 0.5 m/s of wind speed.

According to Figure 28 (a) the agreement between Sentinel-3A winds and their model counterpart is very good with virtually no bias (except for slight bias at high wind speed values). The symmetric slope, which is another measure for the bias is about 1.0. The standard deviation of the difference (SDD) with respect to the model, which can be used as a proxy to the random error, is 1.08 m/s. The correlation coefficient is higher than 0.95. These values are better than the equivalent statistics from the other altimeters.

On the other hand, Sentinel-3B underestimates the wind speed by more than 1 m/s as can be seen from 28 (b). This is due to the higher backscatter values which prevailed the operational product for more than five months out of the period considered here for validation. The other statistics are within acceptable values. A simple correction to the backscatter coefficient by reducing it by 0.5 dB provided very good altimeter winds (not shown). In any case, Sentinel-3B PB 1.13 corrected this issue.

The comparison against in-situ (mainly buoy) observations for the same period is shown in panels (a) and (b) of Figure 29 for Sentinel-3A and Sentinel-3B, respectively. Sentinel-3A bias against in-situ observations for this period is rather small (about 0.1 m/s). The SDD is about 1.4 m/s which is about 17% of the mean. The correlation coefficient is higher than 0.92 and can be read from Figure 29 (a). These figures are similar to the same statistics emerging from the comparison of wind speeds from other altimeters against in-situ observations (not shown). Of course, the in-situ verification in Figure 29 (b) provides the same results as those provided by the verification against the model. It is important to state that most of in-situ observations are located in the Northern Hemisphere around the American and European coasts.

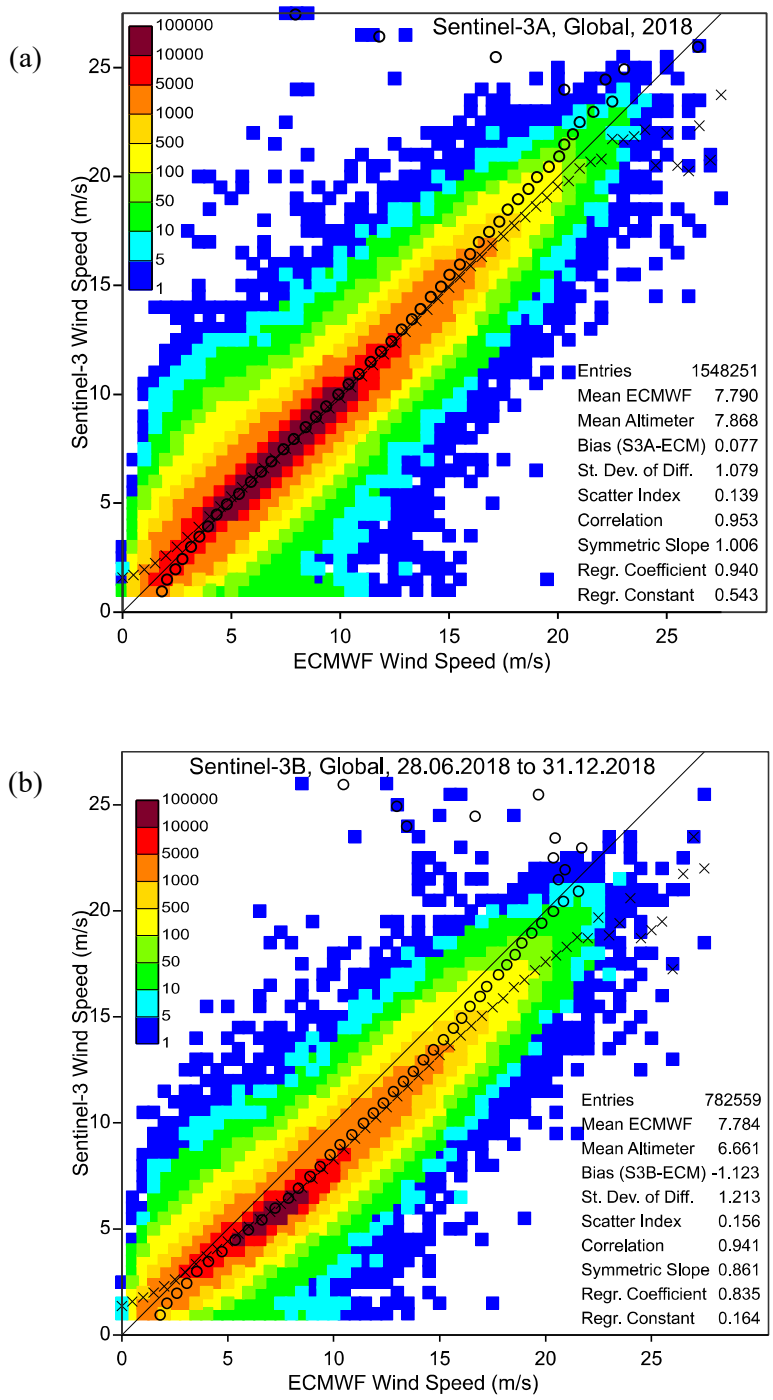

Figure 28. Global comparison of Sentinel-3A and Sentinel-3B, in panels (a) and (b), respectively, SAR surface wind speed against ECMWF model analysis for the year 2018 (Note that Sentinel-3B data have not covered 1 year yet). Number of colocations in each 0.5 m/s x 0.5 m/s 2D bin is color-coded as in the legend. The crosses are the means of the bins for given x-axis values (model) while the circles are the means for given y-axis values (Sentinel-3).

(a)

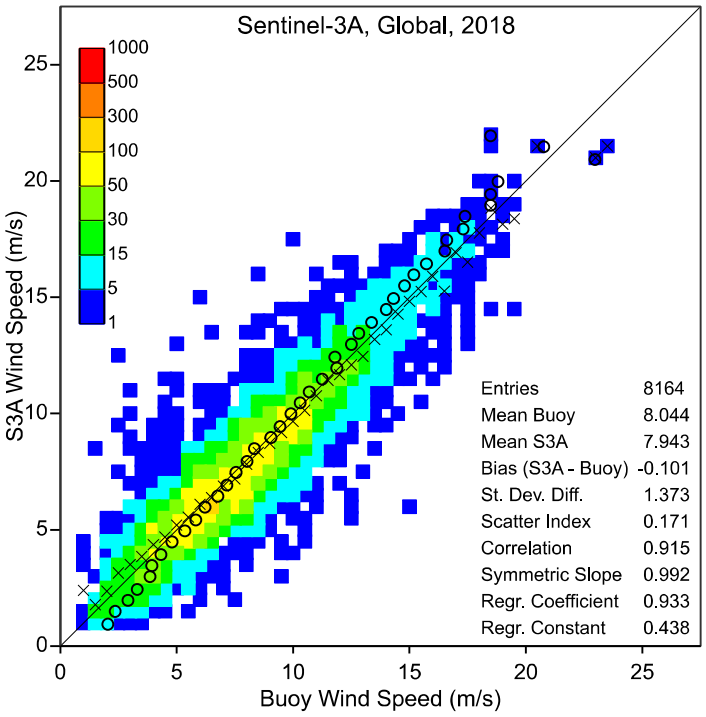

(b)

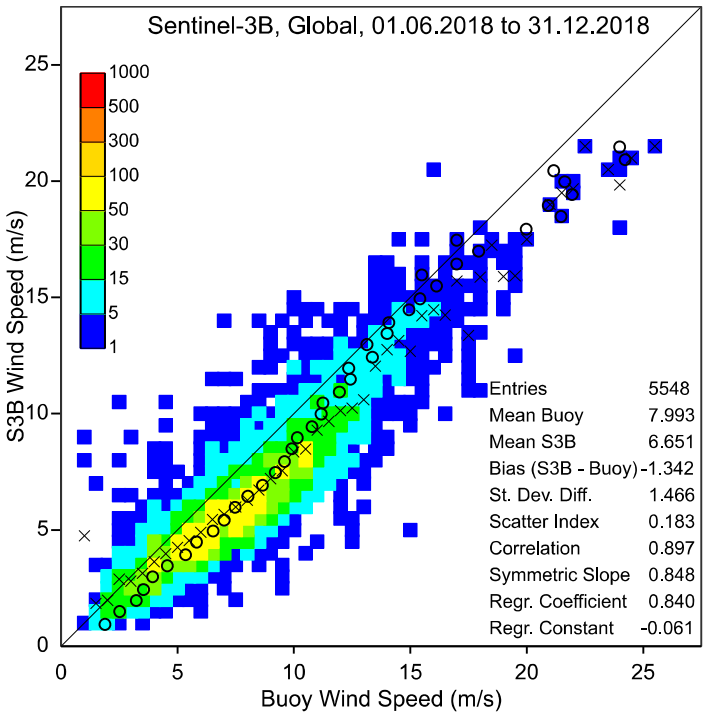

Figure 29. Same as Figure 28 but the comparison is done against in-situ observations (mainly in the NH).

The time series of the global wind speed weekly bias and SDD of 6 altimeters (including Sentinel-3A and Sentinel-3B) compared to the ECMWF model AN are shown in the upper and lower panels, respectively, of Figure 30. NRT data from all altimeters were used in Figure 30. The only exception is Sentinel-3A SRAL data before end of 2017. Instead the data reprocessed towards the end of 2017 were used to reflect the current quality of Sentinel-3A data.

It is clear that the wind speed from Sentinel-3A shows the best agreement with the ECMWF model winds. It has the lowest global bias (almost zero) and one of the lowest SDD values. However, there seems to be minor increase in the SDD (possible degradation) during the months of November and December. Sentinel-3B winds also compare very well after the implementation of Sentinel-3B PB 1.13 in early December 2018. It is expected that Sentinel-3B data will be reprocessed before mid 2019.

Keeping in mind that Jason-3, CryoSat-2, SARAL/AltiKa and Jason-2 are all conventional altimeters (the CryoSat-2 statistics in Figure 30 are for LRM only), it is possible to conclude that Sentinel-3A SAR wind speed is as good as (if not better than) its counterpart from the conventional altimeters. This statement extends comfortably to include Sentinel-3B after PB 1.13.

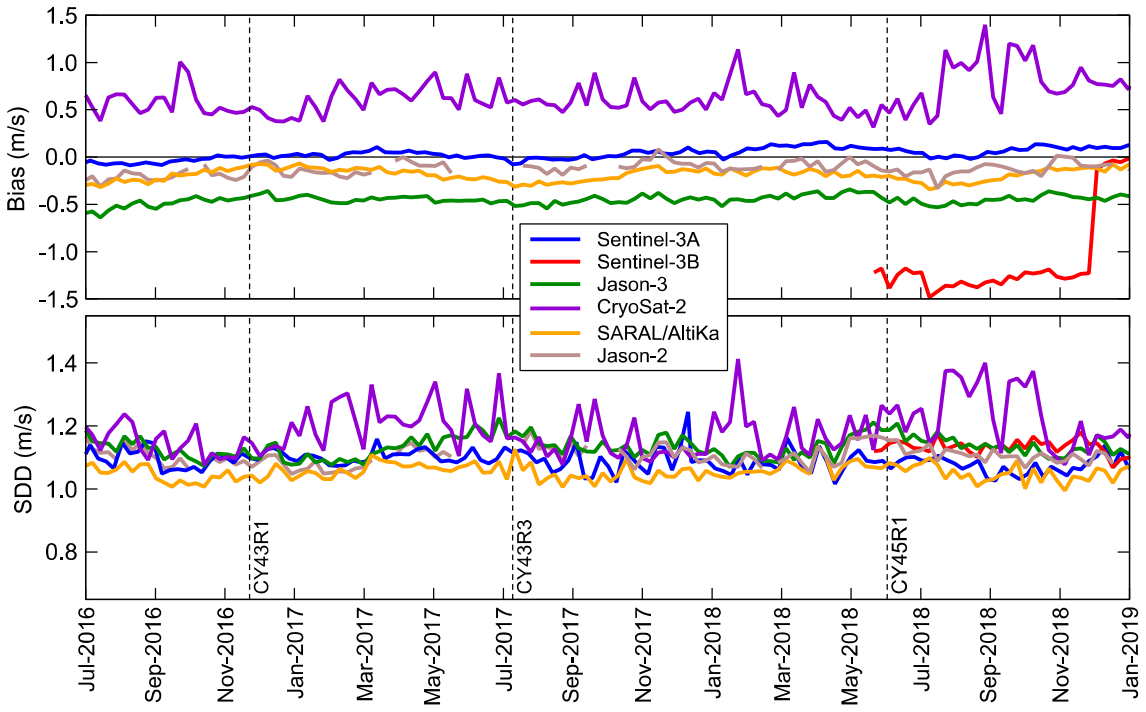

Figure 30. Time series of weekly global wind speed bias defined as altimeter - model (top) and standard deviation of the difference (bottom) between various altimeters (including Sentinel-3A and Sentinel-3B SRAL) from one side and ECMWF model analysis from the other. NRT data are used except for Sentinel-3A before end of 2017 when reprocessed data were used.

The geographical distribution of the mean Sentinel-3A and Sentinel-3B wind speed values and the wind speed bias, SDD and scatter index (SI, defined as the SDD divided by the model mean and expressed in percentage) with respect to the ECMWF model averaged over the whole year of 2018 are shown in Figure 31 for Sentinel-3A and in Figure 32 for Sentinel-3B. While the mean Sentinel-3A wind speed, the SDD and SI distributions all look similar to their counterparts from other altimeters (not shown), the bias in panel (b) is rather low almost everywhere. On the other hand, Sentinel-3B biases are rather high and that is a consequence to the high backscatter coefficient before 6 December 2018. It should be noted that Figure 32 does not represent the current quality of the current Sentinel-3B wind speed.

Sentinel-3 SRAL significant wave height

Since the wave model at ECMWF assimilates altimeter significant wave height (SWH) data, the practice is to the model first guess (FG) which is practically a short-term forecast. The analysis model fields, which represent the best available state of the atmosphere, are not suitable for assessing SWH. The use of the FG reduces the impact of error correlation between the model and Sentinel-3 SRAL SWH that may be conveyed through data assimilation.

Figure 33 shows the global SWH PDF of Sentinel-3A for the whole year of 2018 and Sentinel-3B for the six-month period from 28 June till 31 December 2018. For comparison, Figure 33 shows the PDF's of Sentinel-3A for 2017 and the ECMWF model FG SWH collocated with each altimeter (one year for Sentinel-3A collocations and 6 months for Sentinel-3B collocations). Irrespective of the fact that Sentinel-3A data cover a whole year while Sentinel-3B covers only half that period, the PDF's from both altimeters are very close to each other. Both PDF's compare very well with Sentinel-3A PDF of 2017 apart from the enhanced hump at SWH values of less than 1 m. The corresponding model PDF's agree well with their Sentinel-3 counterparts except around the peak of the PDF (at SWH of about 2 m) and at low SWH values (below 1 m).

The SWH PDF's from the altimeters on-board Jason-3, CryoSat-2 (only conventional altimetry data are used here), SARAL/AltiKa and Jason-2, which are all conventional altimeters or, in the case of CryoSat-2, operating in a conventional mode, are shown in upper panel of Figure 34 together with the corresponding Sentinel-3A and Sentinel-3B SAR SWH PDF's. The SWH PDF's for model colocations with each altimeter are shown in the lower panel of Figure 34. The data used to produce those PDF's cover the whole of 2018 except for Sentinel-3B and its corresponding model (only six months from late June till end of December 2018). The deviation among the model PDF's as sampled along the ground track of each altimeter (i.e. only the model points that are collocated with the altimeter super-observations) is not large as can be seen in the lower panel of Figure 34. However, the deviation between Sentinel-3A and Sentinel-3B SWH PDF's and those of the other altimeters is very clear (the upper panel of Figure 34). Except for that of CryoSat-2, SWH PDF's of the other altimeters are in better agreement with their corresponding model PDF's than those of both Sentinel-3 altimeters.

(a)

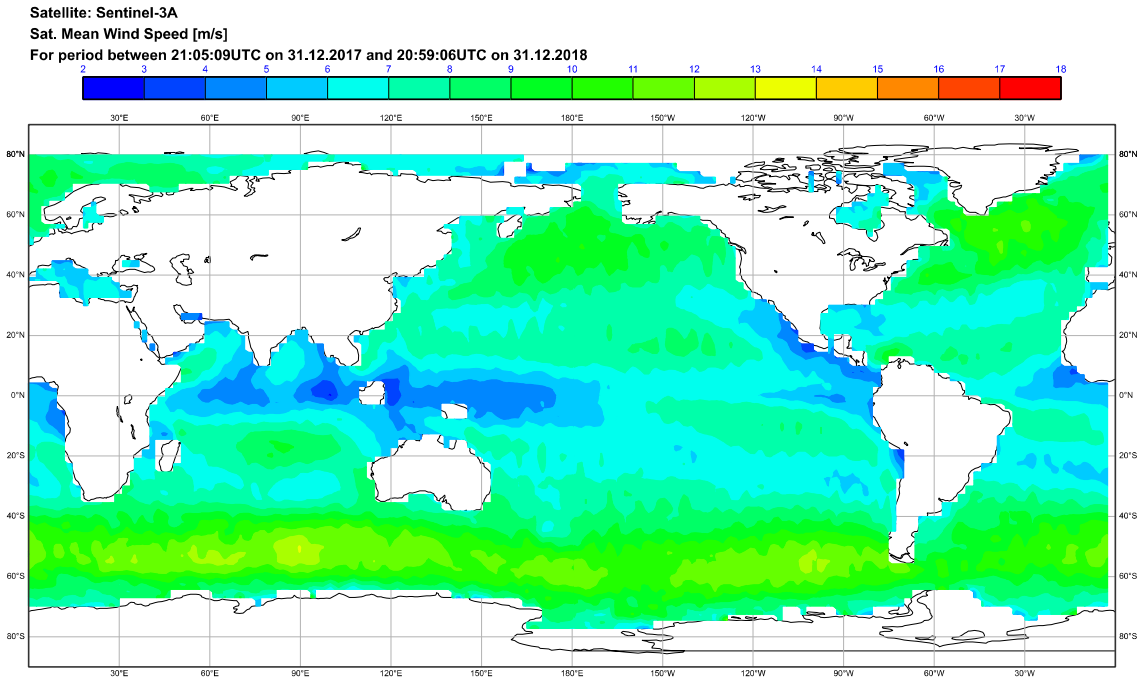

(b)

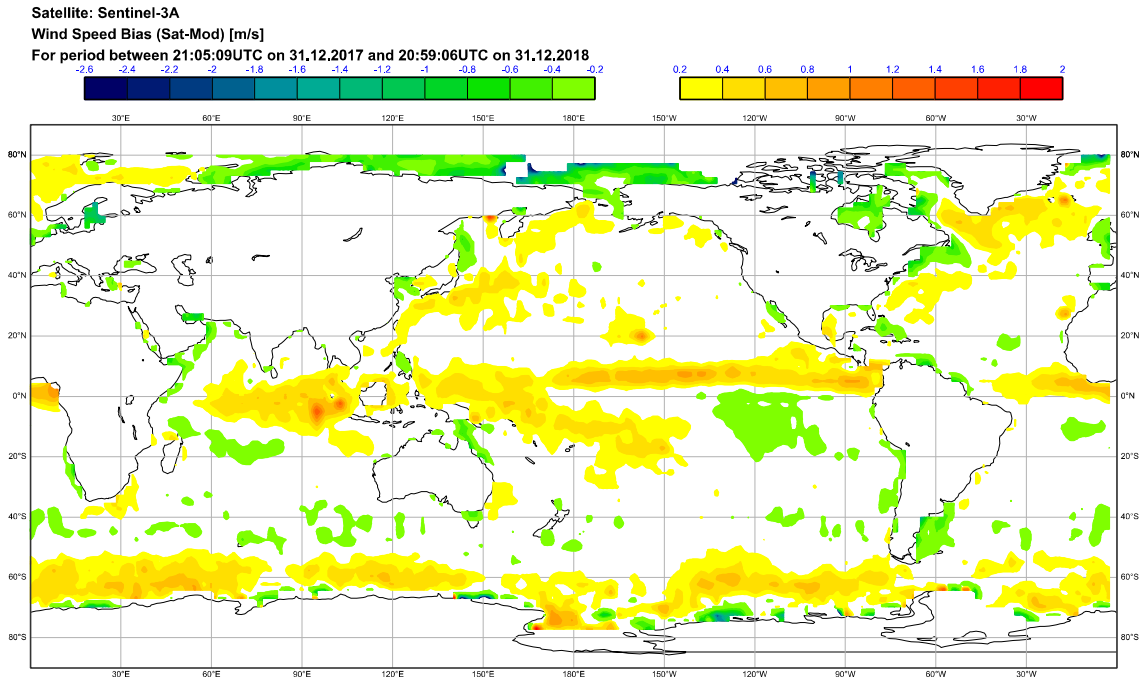

Figure 31. Geographical distribution of mean Sentinel-3 wind speed (a) as well as the bias (b); the SDD (c) and the SI (d) between Sentinel-3 and ECMWF model AN during the period from 13 December 2016 to 12 December 2017. Bias is defined as altimeter - model.

(c)

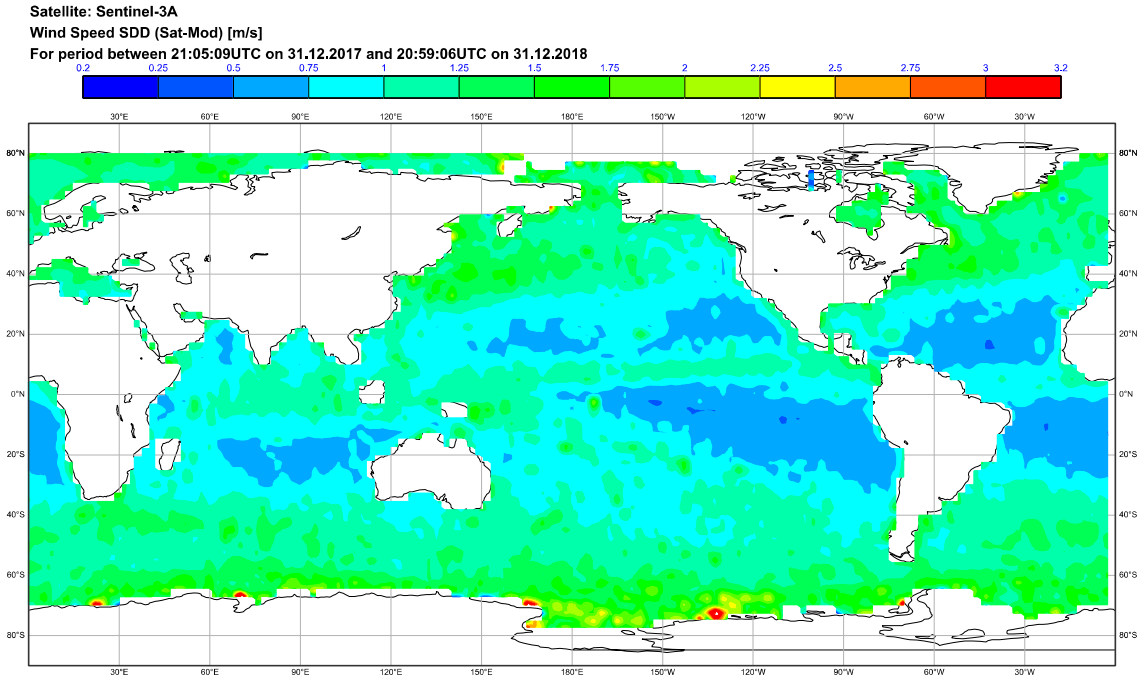

(d)

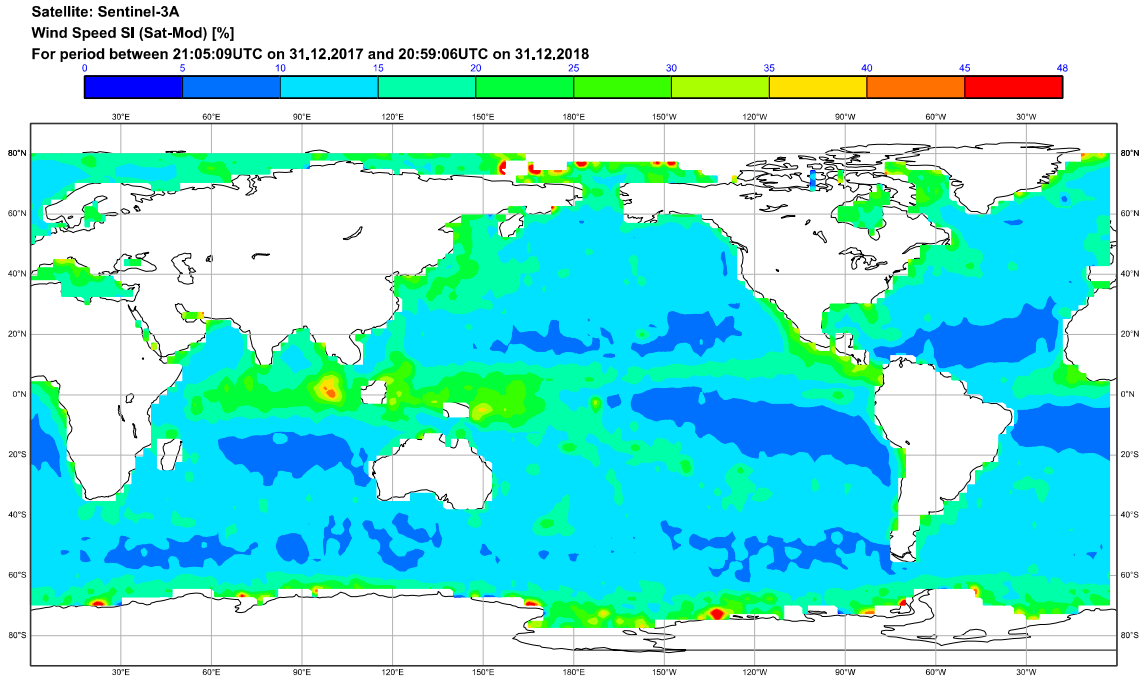

Figure 31: Continued.

(a)

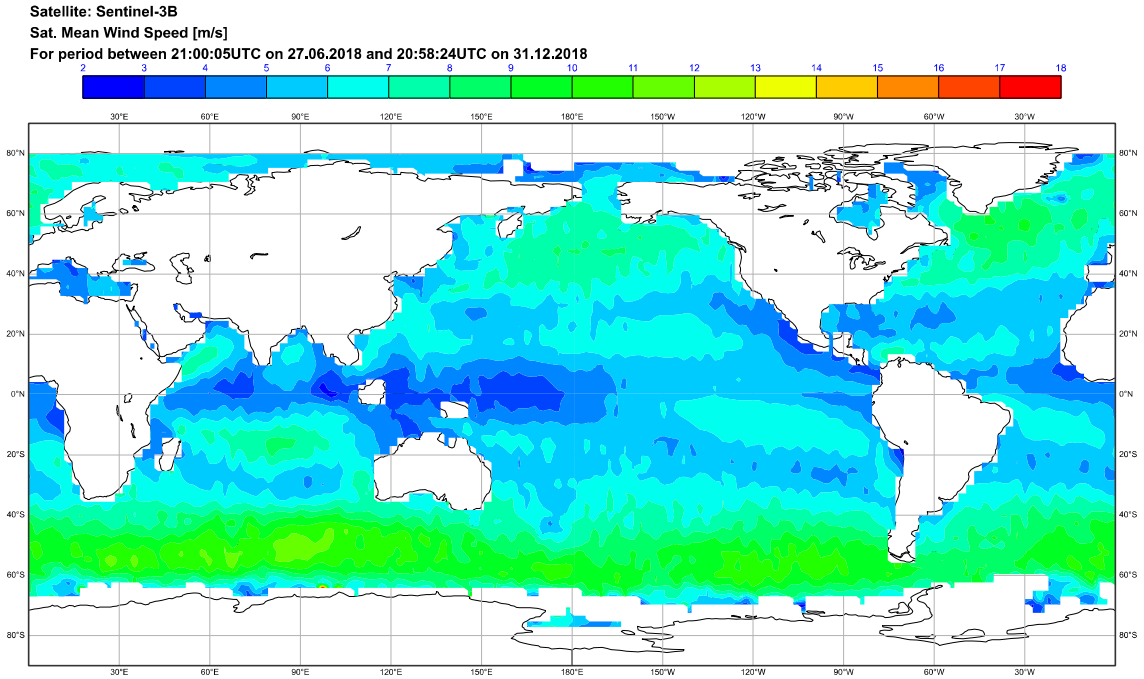

(b)

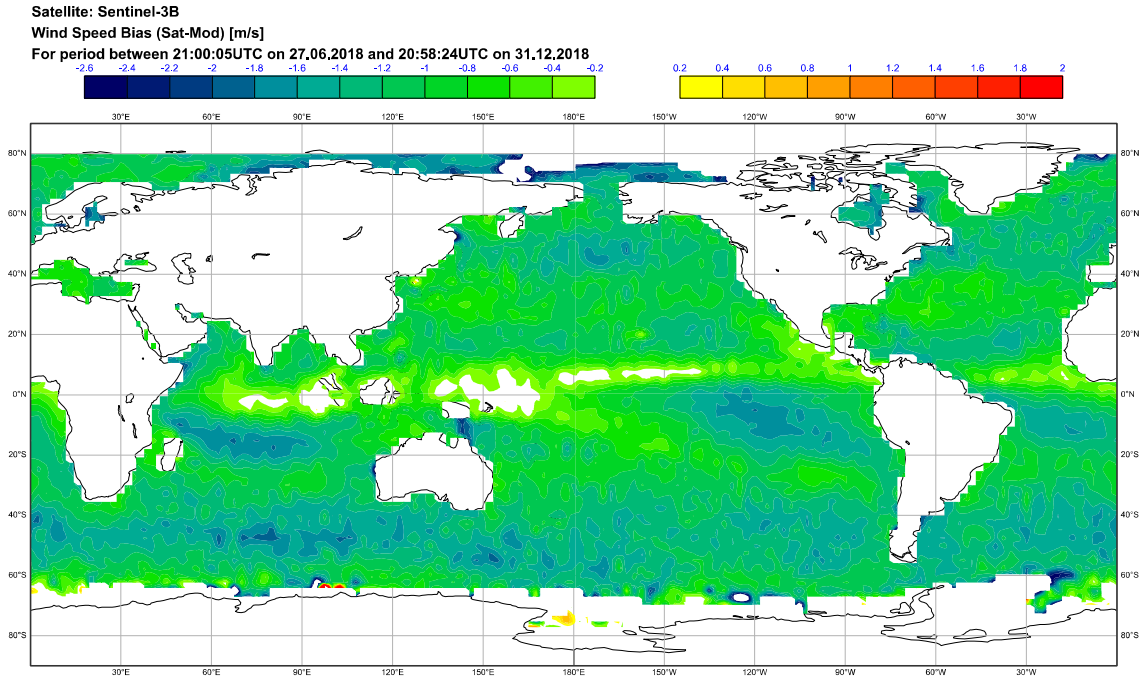

Figure 32: As in Figure 31 but for Sentinel-3B. Note that Sentinel-3B data temporal coverage is from 28 June 2018 till 31 December 2018 which is much less than 1 year yet.

(c)

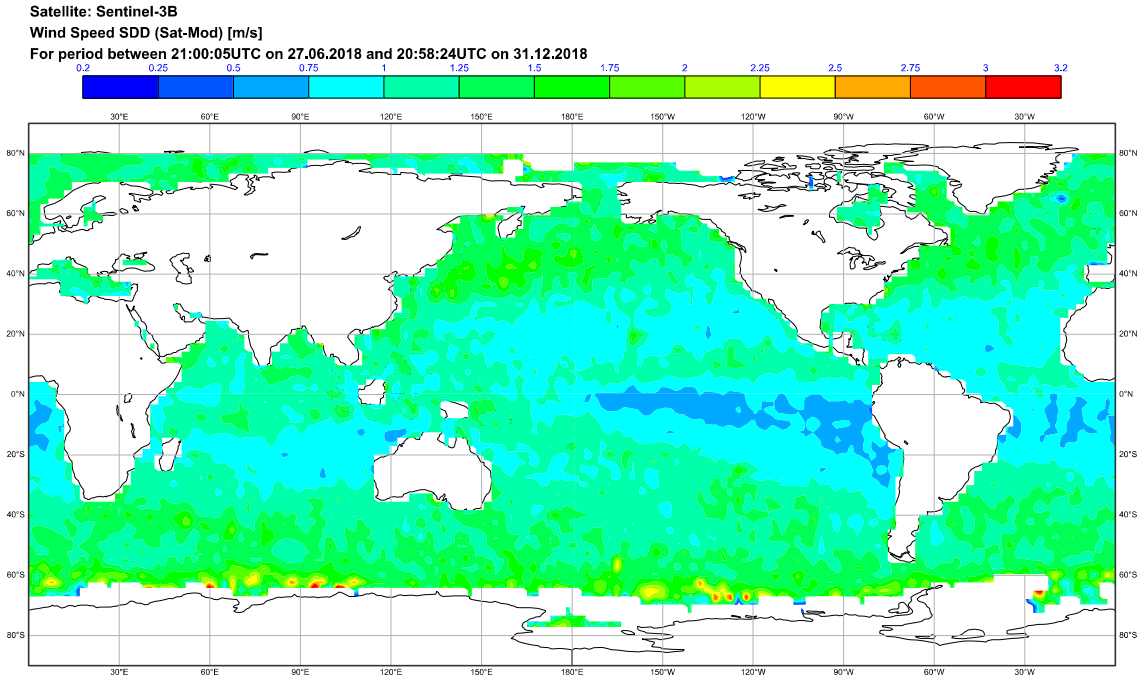

(d)

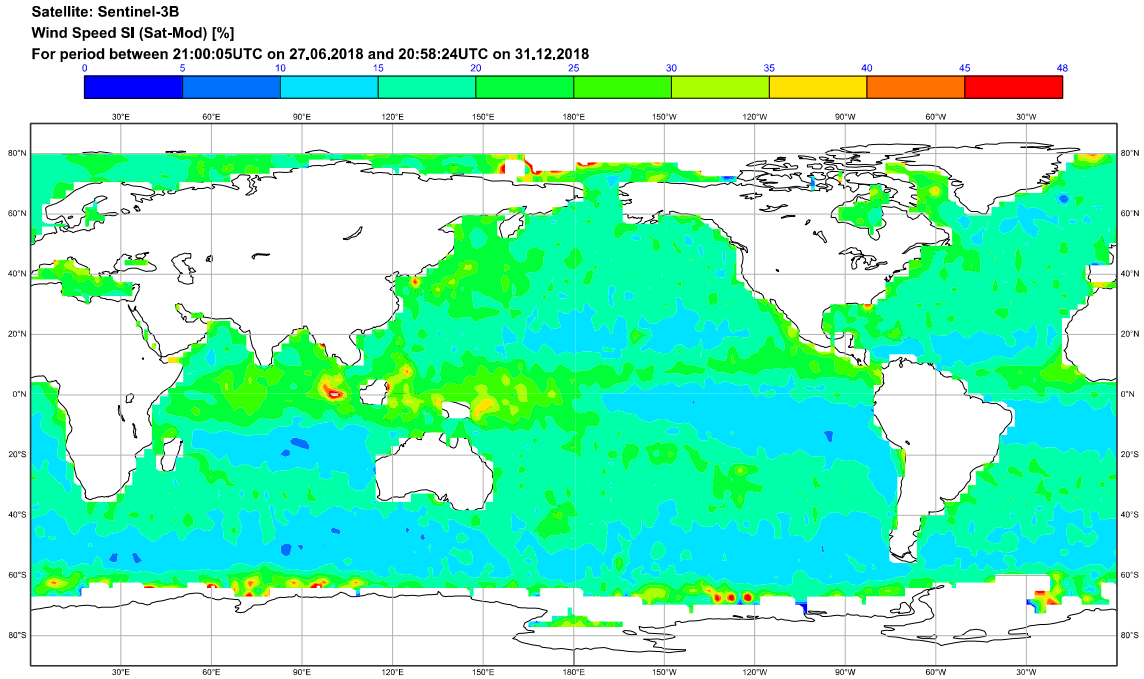

Figure 32: Continued.

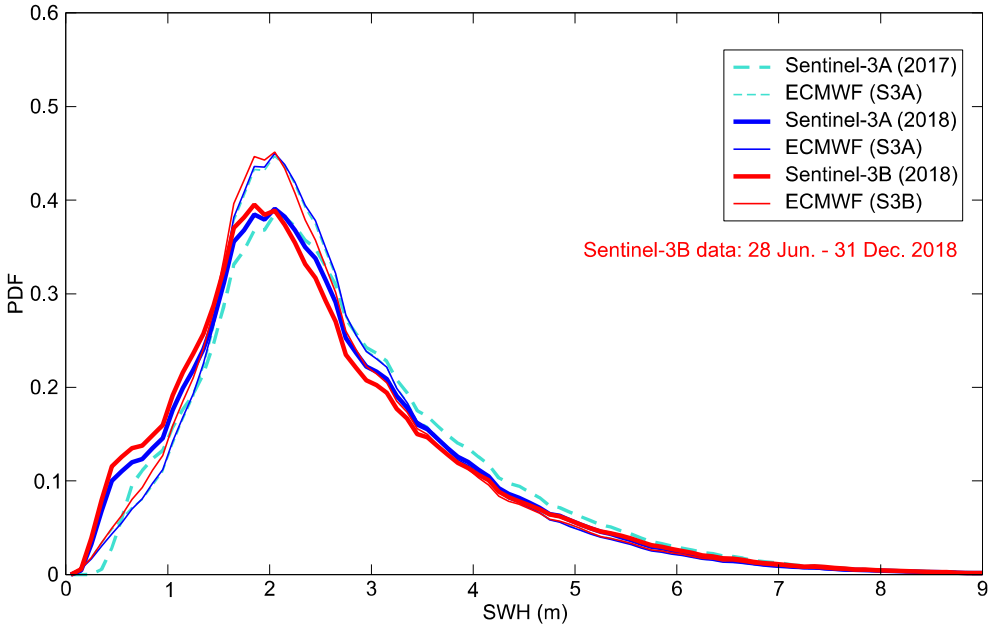

Figure 33: Sentinel-3A and Sentinel-3B SRAL SWH PDF's over the whole global ocean for the year 2018 (note that Sentinel-3B data have not covered 1 year yet). The corresponding ECMWF wave model (collocated with Sentinel-3A and Sentinel-3B) PDF's are shown for comparison. The 2017 PDF of Sentinel-3A and its model counterpart are also shown.

Based on the differences, the PDF's can be grouped into three groups: Sentinel-3A and Sentinel-3B as one group. Jason-2, Jason-3 and SARAL/AltiKa as a second group and CryoSata-2 on its own as the third. The corresponding model PDF's do not show that distictive groupness. Therefore, the differences among the three altimeter groups are not due to geophysical characteristics of regions sampled by the satellite orbits. Having Jasons and SARAL/AltiKa with totally different orbits in the same group affirms this conclusion. The enhanced number of Sentinel-3A and B wave height occurrences below 1 m is not supported by other altimeters and is not supported by the model. Therefore, it can be concluded that this is an artifact of the data rather than a genuine characteristic of the data.

The time series of the global mean and standard deviation (SD) of the SWH from Sentinel-3A and Sentinel-3B averaged over a 7-day time window moved by 1 day at a time are shown in the upper and lower panels, respectively, of Figure 35. The corresponding time series of the model as collocated with Sentinel-3 are also shown for comparison. Sentinel-3 mean and standard deviation are not much different from those of the model (and the other altimeters). The slightly higher Sentinel-3 SWH standard deviation compared to the model and the other altimeters (not shown) cannot be attributed to the fact that SAR mode has higher resolution compared to the conventional altimetry (LRM). The comparison is done at the scale of the super-observations (about 75 km) and, therefore, the impact of the high frequency variability in the SAR altimetry (below the 1-km scale) is eliminated. Therefore, this enhanced Sentinel-3 SWH variability and higher mean values indicate that fine tuning to SWH retrieval may be needed. Figure 35 suggests that since the implementation of Sentinel-3A PB 2.24 in December 2017, Sentinel-3A mean SWH has reduced and became similar to the model mean value.

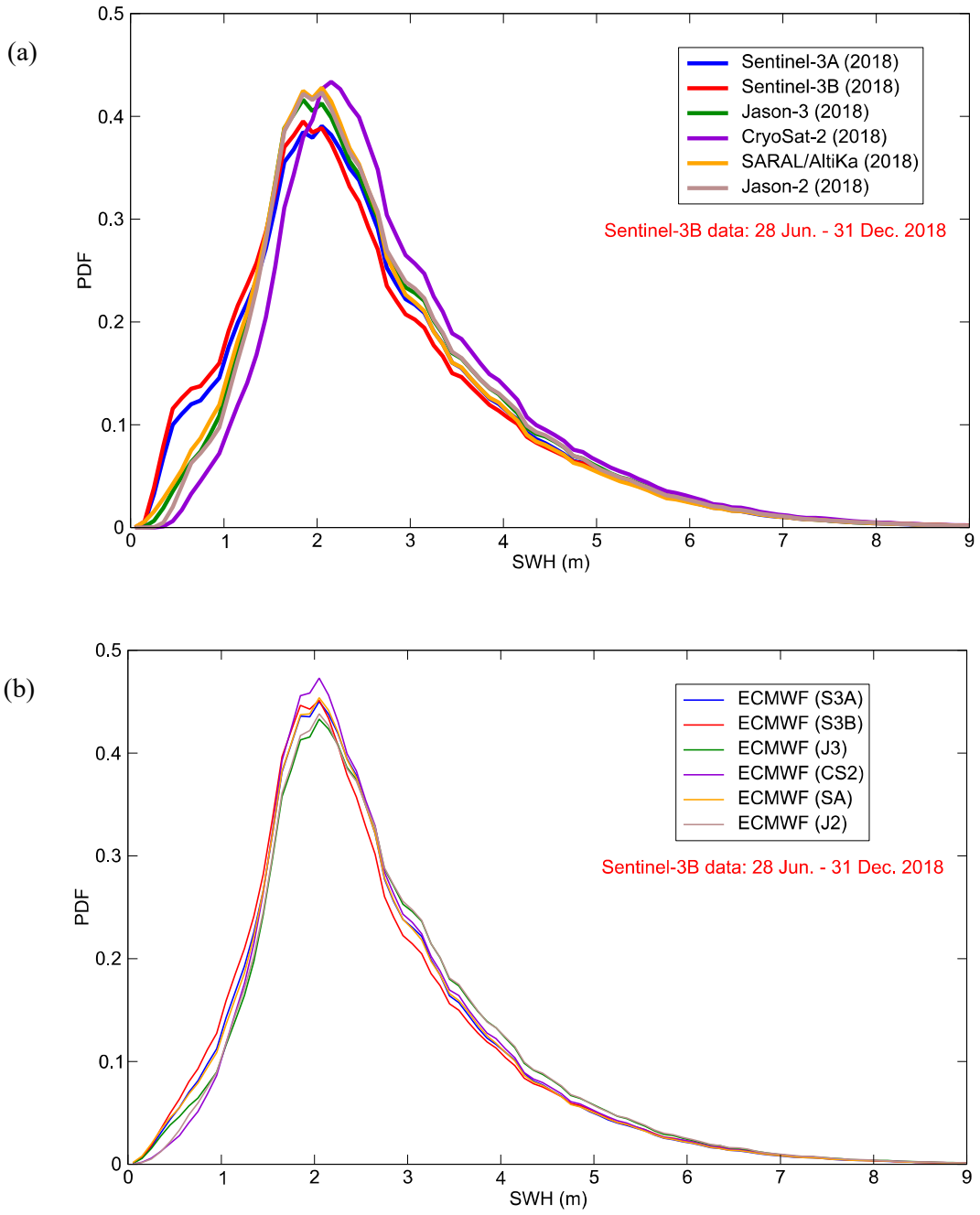

Figure 34: Panel (a): Global SWH PDF's from 6 altimeters, including Sentinel-3A and Sentinel-3B SRAL's, for the year 2018 (note that Sentinel-3B data have not covered 1 year yet). The corresponding ECMWF (collocated with each altimeter) PDF's are shown in panel (b) for comparison.

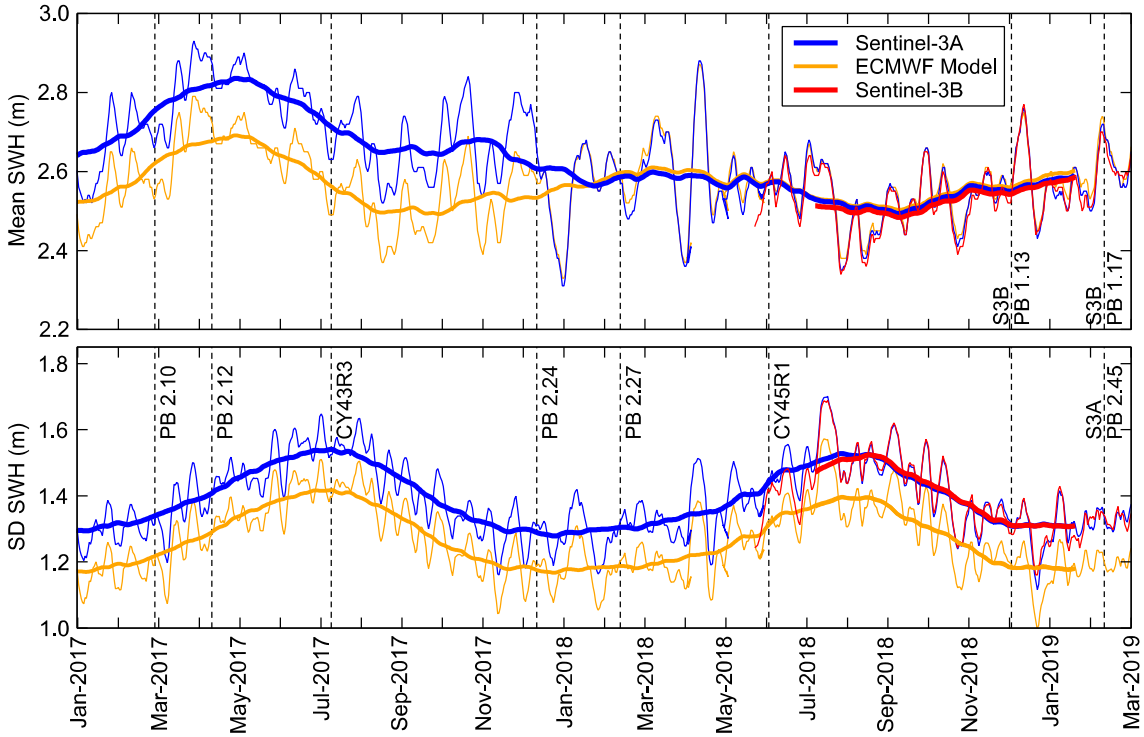

Figure 35: Time series of global mean (top) and standard deviation (bottom) of significant wave height from Sentinel-3A and Sentinel-3B SRAL Ku-band after quality control. The collocated ECMWF model SWH mean and SD are also shown. The mean and SD are computed over a moving time window of 7 days.

Figure 35 suggests that Sentinel-3B global mean and standard deviation is similar to those of Sentinel-3A. The only difference is Sentinel-3B mean SWH is consistently slightly lower than that of Sentinel-3A. As in the case of Sentinel-3A SWH, its global standard deviation is higher than that of the model.

Collocated pairs of Sentinel-3A and Sentinel-3B altimeter super-observation and the ECMWF model SWH FG are plotted as density scatter plots in Figure 36 for the whole globe over the whole year of 2018. Panel (a) is dedicated to Sentinel-3A (one year) while panel (b) is dedicated to Sentinel-3B (six months only). The SWH scatter plots (Figure 36 and other similar wave height scatter plots that appear hereafter) are plotted similar to those of the wind speed except for the size of the 2-D bin which is 0.25 m × 0.25 m in the case of SWH. It is clear from Figure 36 (a) that the agreement between SWH from both Sentinel-3 altimeters and their model counterpart is very good except for a slight underestimation at SWH values below ~ 2 m and an overestimation at moderate to high SWH's (above ~4 m). The underestimation at lower wave heights, although less noticeable, is not noticed in the case of other altimeters.

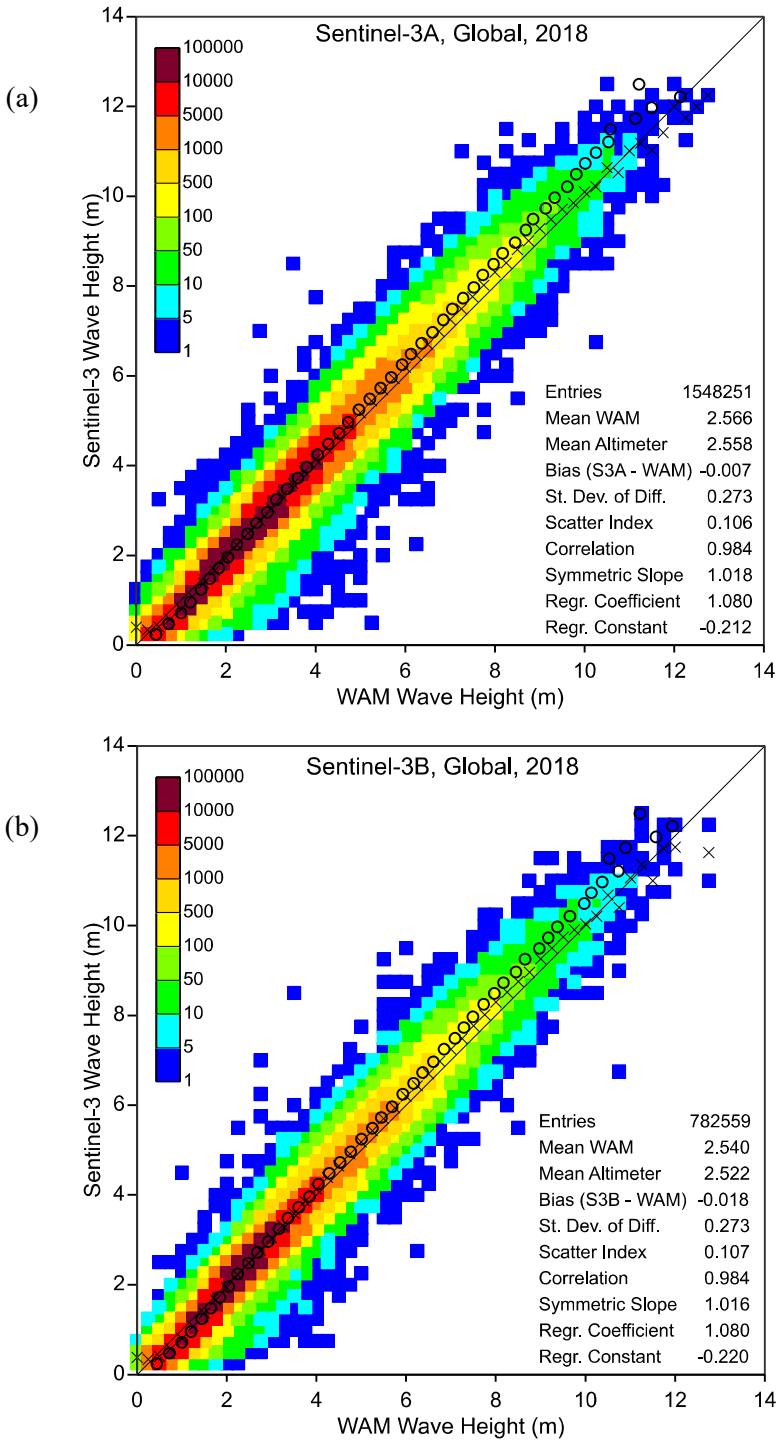

Figure 36: Global comparison of Sentinel-3A and Sentinel-3B, in panels (a) and (b), respectively, SAR SWH against ECMWF model first guess SWH values for the year 2018 (note that Sentinel-3B data have not covered 1 year yet). The number of colocations in each 0.25 m x 0.25 m 2D bin is colour coded as in the legend. Refer to Figure 28 for the meaning of crosses and the circles.

In general, compared to ECMWF model, SAR SWH from Sentinel-3A and Sentinel-3B is unbiased (global bias is less than 2 cm). The SDD between the altimeter and the model is about 0.27 m (or about 10.7 % of the mean value). The correlation coefficient is 0.983 which is quite high. These figures indicate that apart from the underestimation at low wave heights, the quality of Sentinel-3A and Sentinel-3B SAR SWH products is rather high.

The time series of the global SWH weekly bias and SDD of 6 altimeters (including Sentinel-3A and Sentinel-3B) compared to the ECMWF model FG are shown in the upper and lower panels, respectively, of Figure 37. NRT data were used for all altimeters except for Sentinel-3A where reprocessed data were used before mid December 2017. Bias in Sentinel-3A SAR SWH has been one of the lowest among the 6 operational altimeters. Sentinel-3B SWH bias is also very low but tends to be consistently negative and lower than (higher in absolute sense) that of Sentinel-3A. However, there is up to 0.10 m mean bias in the extra Tropics with negative bias in the summer (July-August in the Northern Hemisphere, NH, and January-December in the Southern Hemisphere, SH) and positive bias during the hemispheric winter (not shown). In the Tropics, negative bias of about 0.05 m dominates. The SDD follows a similar cycle especially in the NH (not shown).

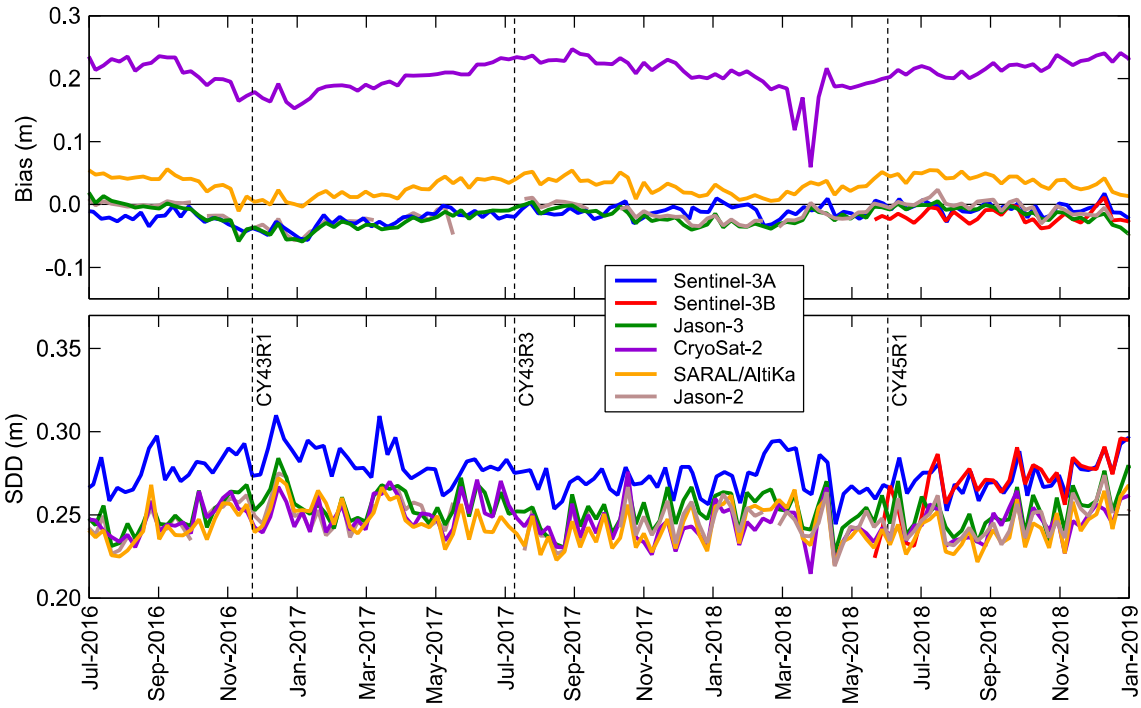

Figure 37: Time series of weekly global significant wave height bias defined as altimeter - model (top) and standard deviation of the difference (bottom) between 6 altimeters (including Sentinel-3A and Sentinel3B SRAL) from one side and the ECMWF model first-guess from the other. NRT data are used except for Sentinel-3A before end of 2017 when reprocessed data were used.

Sentinel-3A SAR SWH shows the highest SDD with respect to the model among all altimeters. During the last 6 months of 2018 it was joined by Sentinel-3B at this high SDD. It is worthwhile mentioning that during the single Sentinel-3B cycle when SRAL was configured to operate in conventional altimetry mode, the SDD of Sentinel-3B LRM SWH with respect to the model was one of the lowest. This can be seen in Figure 37. This suggests that the enhanced SDD of SWH at the scale of 75 km is due to the use of SAR altimetry.

The statistics from Sentinel-3B SWH verification are consistent with those of Sentinel-3A. However, since the length of time series is short, it is difficult to make any conclusions apart from the obvious fact that SWH from both altimeters show similar characteristics so far and the conventional altimtry mode of Sentinel-3B produced SWH with lower SDD as mentined above.

The wave height comparison against in-situ (mainly buoy) observations for the whole of 2018 in case of Sentinel-3A and the second half of 2018 for Sentinel-3B is shown in Figure 38. SWH from both altimeters is unbiased compared to available in-situ measurements for this period. The SDD (a proxy to the random error) is 0.30 m (~13.4% of the mean) and 0.28 m (~12.6% of the mean) for Sentinel-3A and Sentinel-3B, respectively. The correlation coefficient is about 0.98. These numbers indicate that Sentinel-3A and Sentinel-3B SAR SWH products are very close their counterparts from other altimeters (not shown). It is important to state that most of in-situ observations are located in the Northern Hemisphere around the American and European coasts.

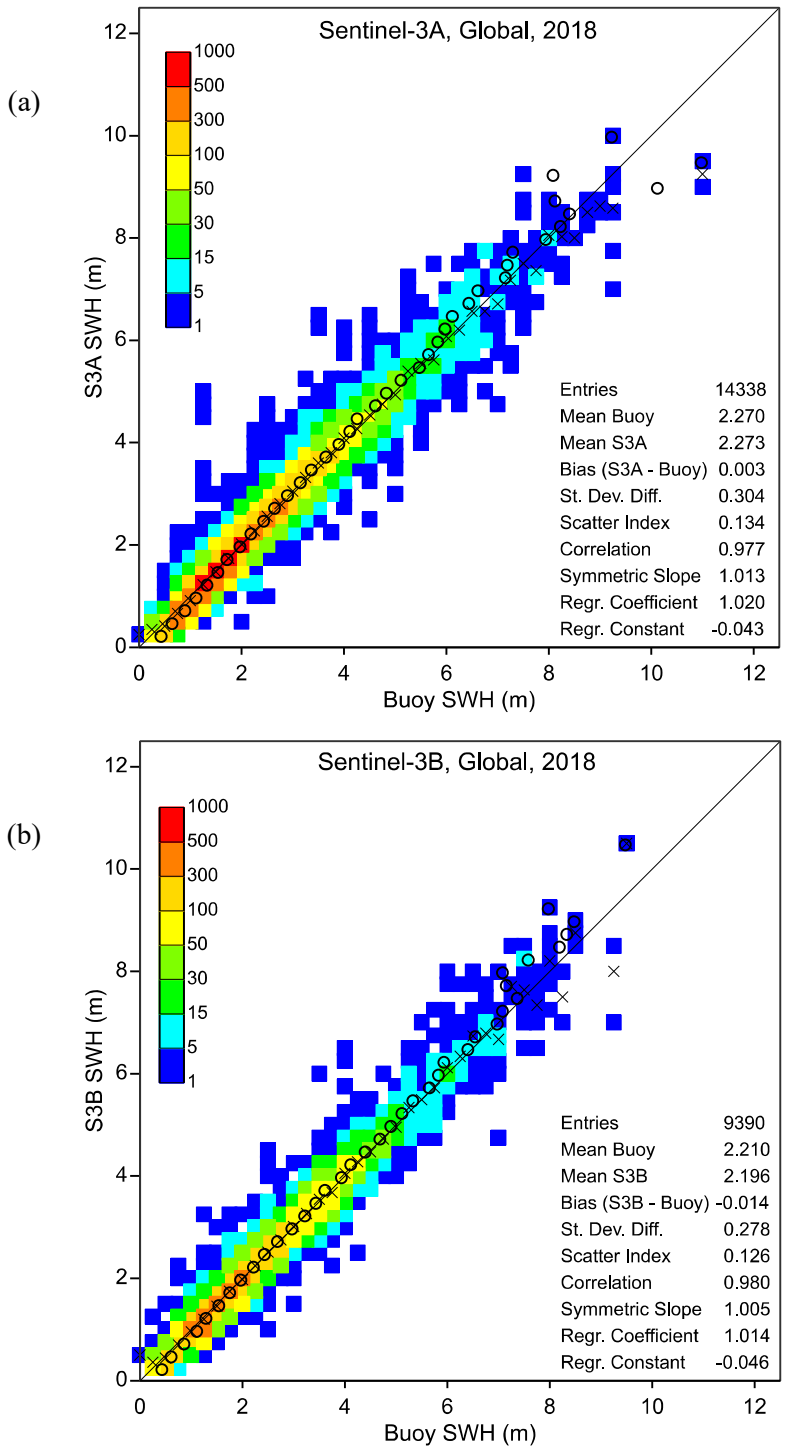

Figure 38: Same as Figure 36 but the comparison is done against in-situ observations (mainly in the NH).

(a)

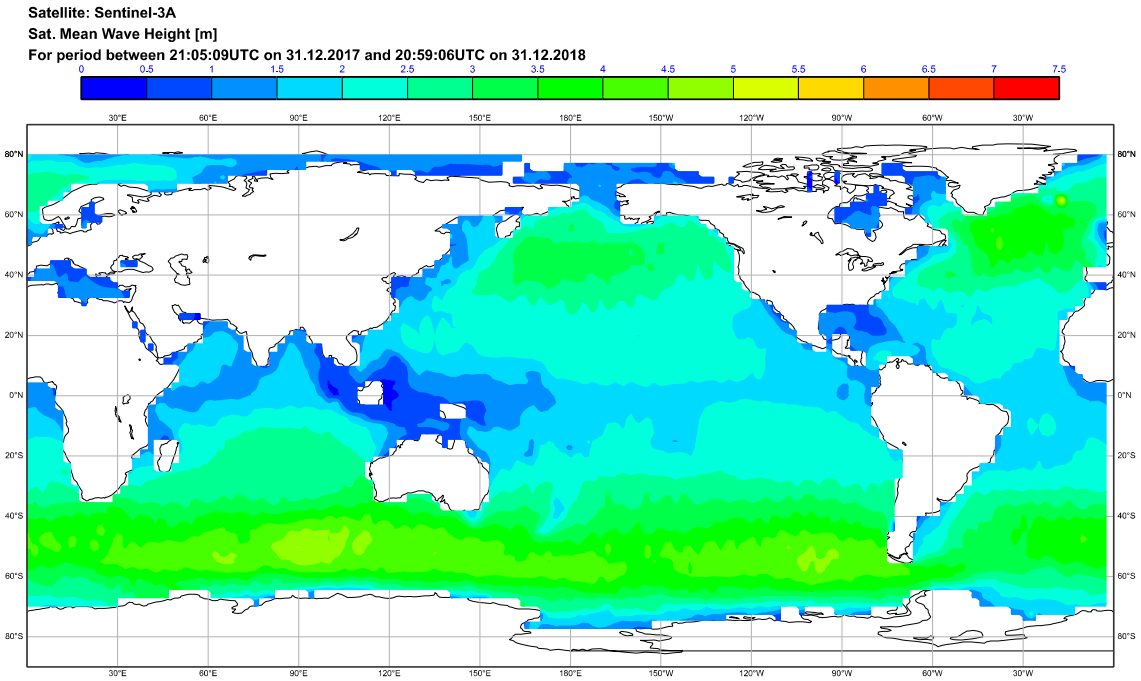

(b)

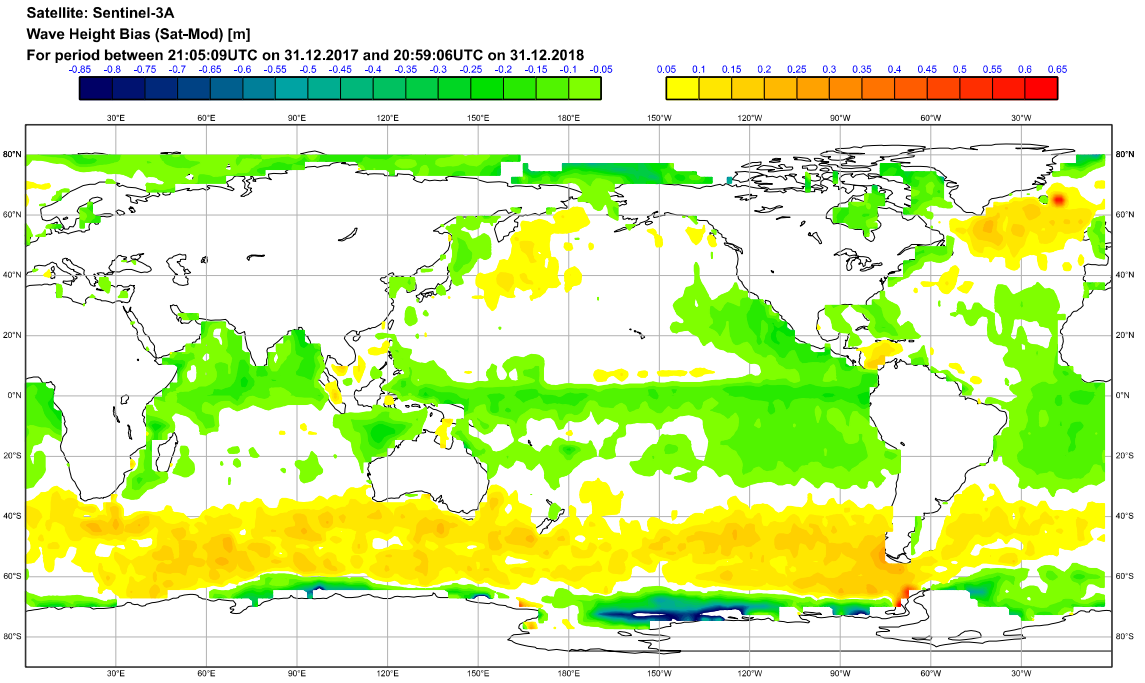

Figure 39: Geographical distribution of mean Sentinel-3A SWH (a) as well as the bias (b); the SDD (c) and the SI (d) between Sentinel-3A and ECMWF model FG during 2018. Bias is defined as altimeter - model.

(c)

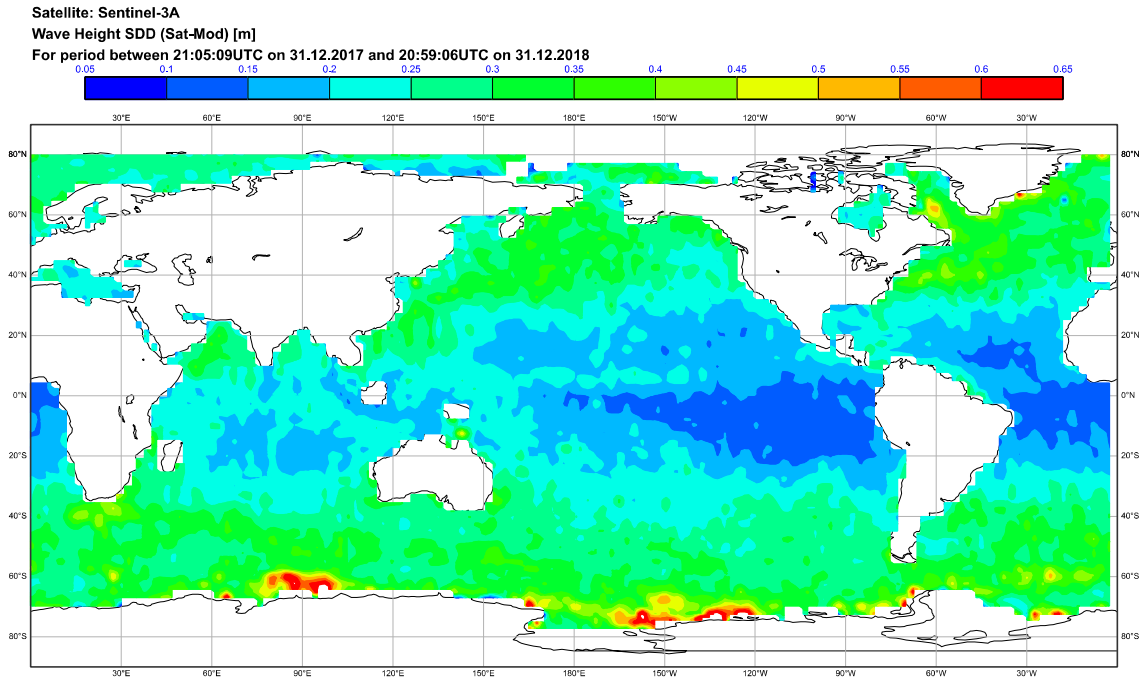

(d)

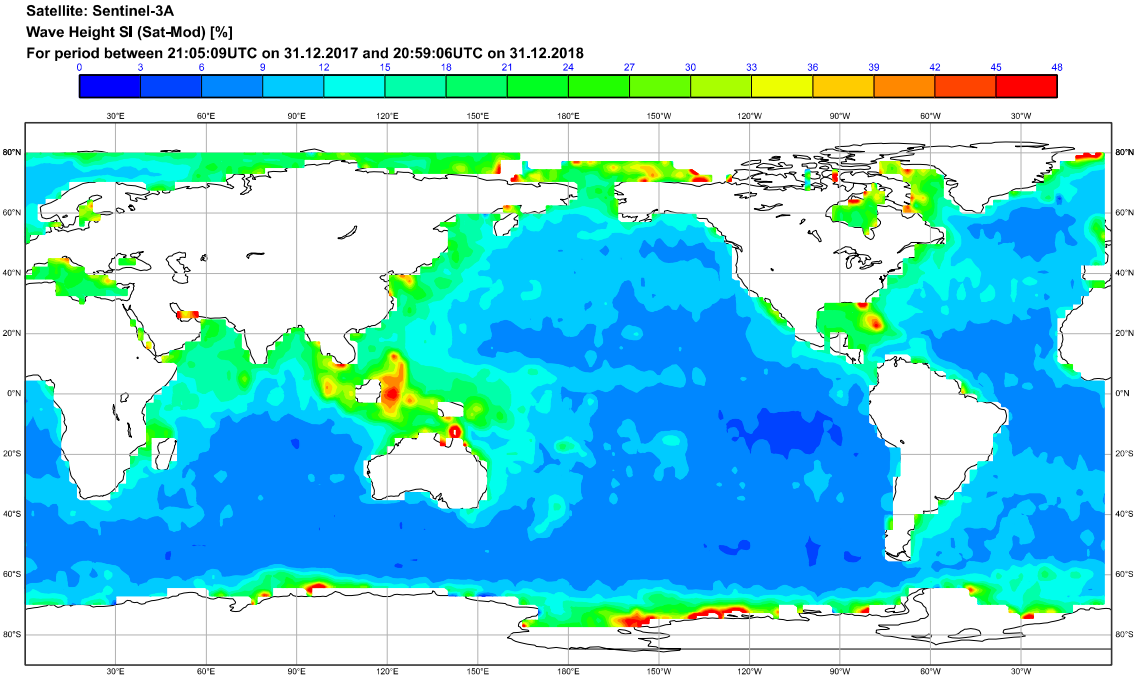

Figure 39: Continued.

(a)

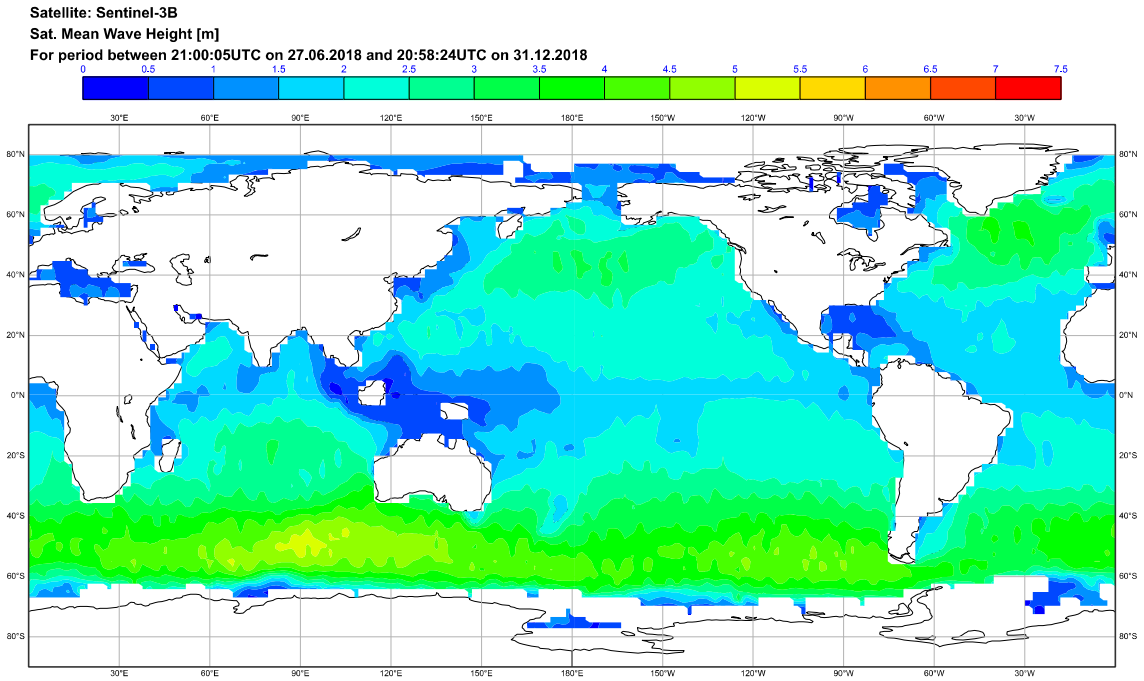

(b)

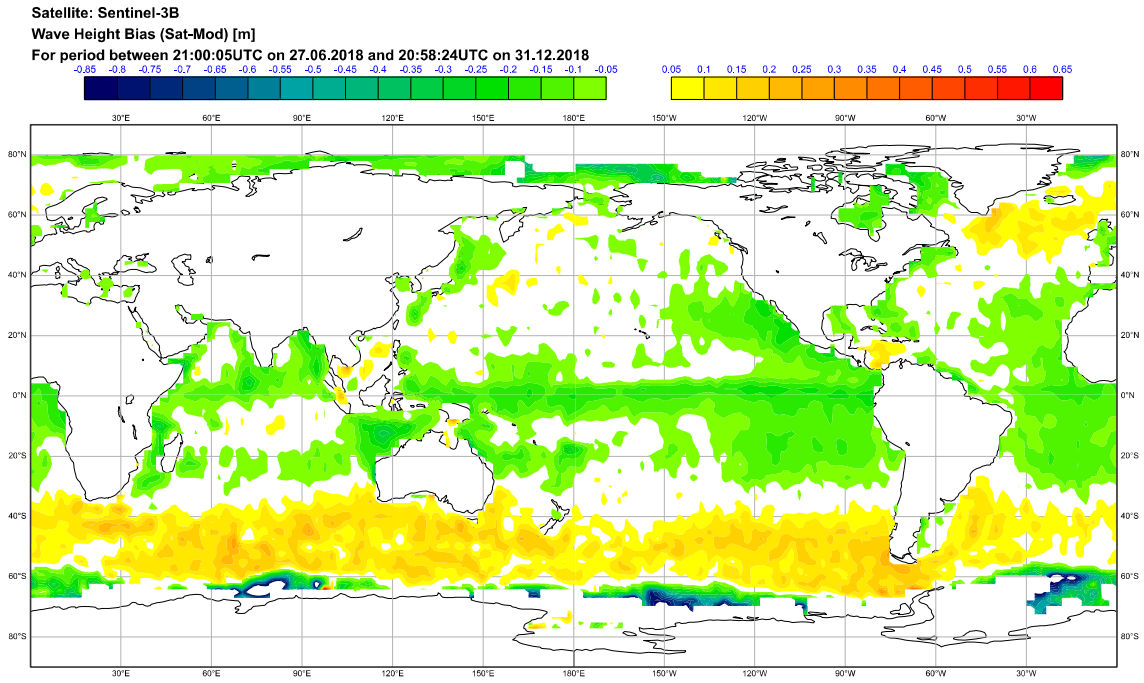

Figure 40: As in Figure 39 but for Sentinel-3B. Note that Sentinel-3B data temporal coverage is from 28 June 2018 till 31 December 2018 which is only half a year.

(c)

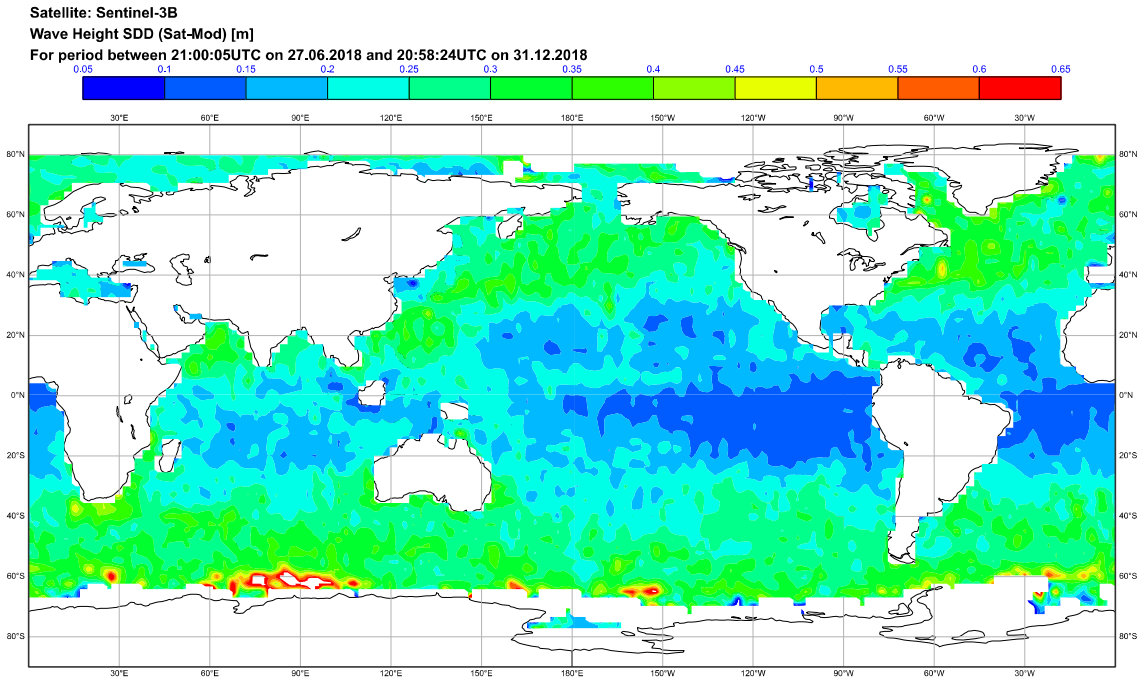

(d)

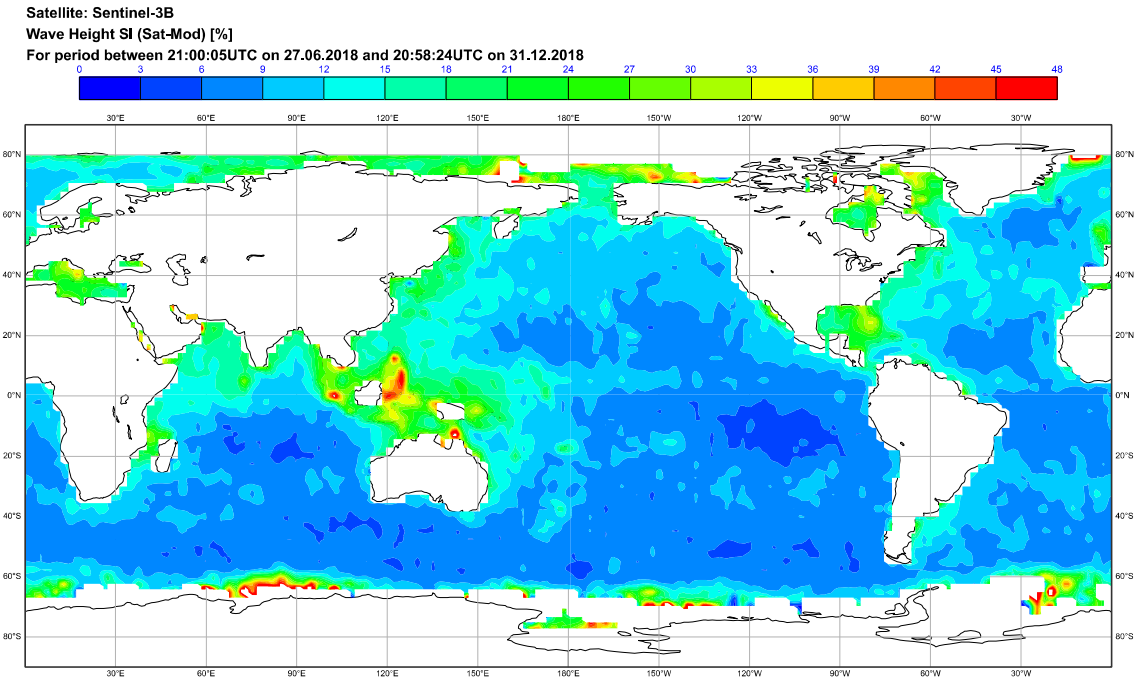

Figure 40: Continued.

Summary

Surface wind speed (WS) and significant wave height (SWH), which are part of Seninel-3 Surface Topography Mission Level 2 Marine Ocean and Sea Ice Areas (SRAL-L2MA) from Sentinel-3A have been very good since the start of the mission if the reprocessed data set produced in December 2017 is considered. Validation was carried out against the corresponding parameters from ECMWF Integrated Forecast System (IFS), in-situ measurements and other altimeters. The current quality of SAR wind speed and SWH from Sentinel-3A and Sentinel-3B SRAL can be summarized as being very good and they can be used for practical applications. However, some fine tuning of these products may still be needed to alleviate some of their imperfections:

Sentinel-3A SAR wind speed is globally unbiased compared the wind speeds from the model and the in-situ measurements. The standard deviation of the difference (SDD) between SRAL and model wind speeds is one of the lowest among all operational altimeters. The SAR wind speed is now globally unbiased compared the wind speeds from the model and the other altimeters. The standard deviation of the difference (SDD) between SAR and model wind speeds is as good as that of other altimeters. There is a seasonal cycle in both bias and the SDD between SAR wind and ECMWF model in Northern (minimum in July and maximum in January) and Southern (vice versa) Hemispheres.

Sentinel-3A SAR significant wave height is unbiased compared to the model and the in-situ measurements. However, SRAL overestimates high wave heights slightly according to the comparison with the ECMWF model. However, there is an enhanced number of Sentinel-3A small wave heights below ~ 1 m compared to the model, other altimeters and in-situ observations. Furthermore, the SDD against the model is one of the highest compared to other altimeters.

The characteristics of Sentinel-3B wind and wave data are similar to those of Sentinel-3A after the implementation of Sentinel-3B PB 1.13 on 6 December 2018 which eliminated the backscatter bias that degraded the wind speed products. The wave height SDD of Sentinel-3B wave height data was one of the lowest during the period when the altimeter was configured to measure in conventional altimetry.

4.2.2 Comparison of wind, wave and sea level products against Jason-3 at cross-over points in the four case studies area

In this section, we compare Sentinel-3A (S3A) and Jason-3 (J3) altimetric measurements of sea surface height anomaly (SSHA), significant wave height (SWH) and wind speed from March 2016 to January 2019. S3A is sun synchronous and has a repeat cycle of 27-days whereas Jason-3 is non-sun synchronous with a repeat cycle of around 10 days. The tracks and cross-overs of these two satellites for the four case studies are represented in *Figure 41*. Cross-overs between Sentinel-3A and Jason-3 happen at a range of time scales from 1-hour to 27-days. Satellite data are taken for the closest observation around the cross-over (always below 7km). During the defined time window (3-hour, 1-day, 7-day, 30-day) all observation pairs of S3A and J3 are taken for each cross-over. For this comparison, a balance is required between the number of pairs of observations with the observed geophysical phenomena we aim to consider. The number of pairs is a function of the collocation time window as the longer the time then the higher the number of pairs (Table 2). Typical time scales for wind speed is 1 hour, but a weather system can remain stable for three days or more. Here it has been decided to include all time scales (3-hours to 30-days) to have both the robustness implied by the number of observations and the precision linked to short collocation in time. Examples of these time series for the three regions are represented below (*Figure 42* to Figure 44): SSHA for Catalan Sea, Significant Wave Height for North Adriatic Sea and Wind speed for Denmark and German Bight area. Statistics for the three regions are summarised in Table 32.

Table 2: Number of cross-overs pairs for each regions and time window

Days	Spain	Italy	Denmark
30	2829	1404	7843
7	1041	489	2897
1	148	72	419
3h	23	13	46

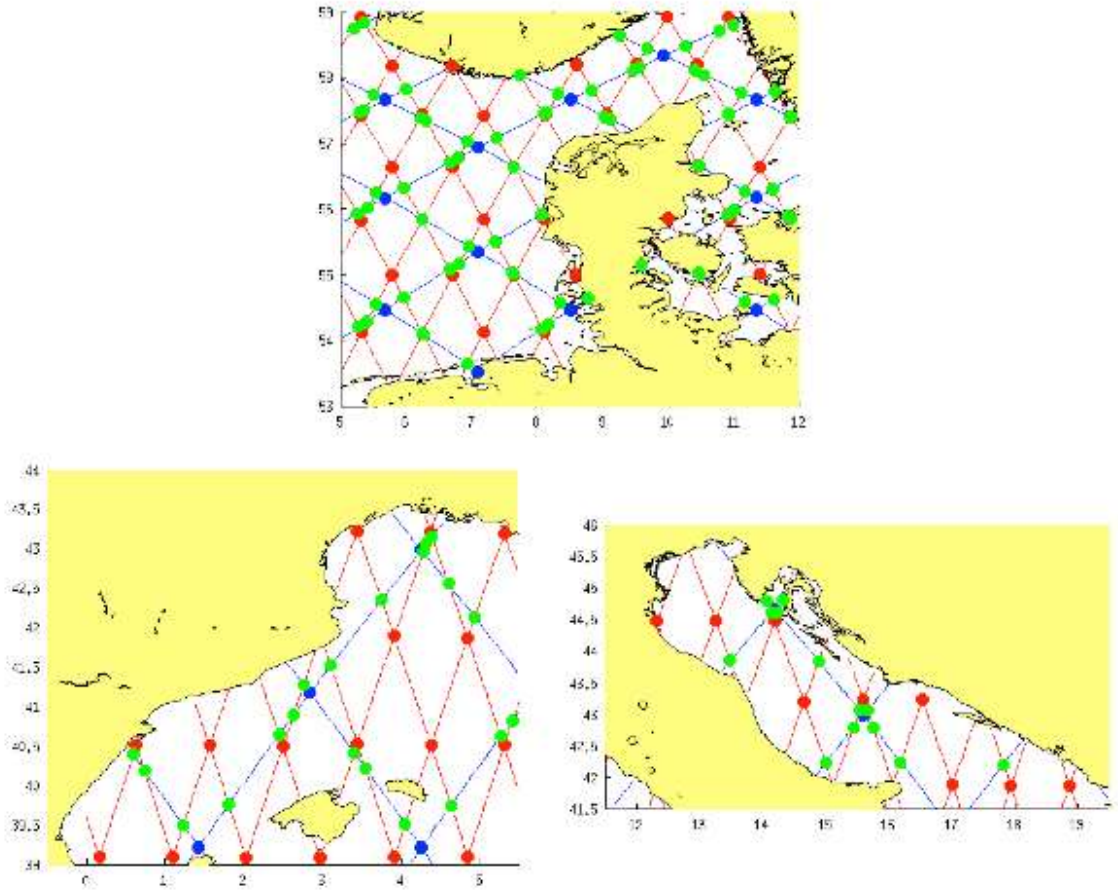

Figure 41: Satellite (line) tracks and (filled circle) cross-overs of (red) S3A and (blue) Jason-3. The green filled circles are the cross-overs between S3A and J3 for (top) Denmark and German Bight; (bottom left) Catalin sea; (bottom right) North Adriatic Sea.

There is good agreement between S3A and J3 for the three observables (SSHA, SWH and wind speed). Data from the two satellites characterises the annual SSHA cycle (*Figure 42*), the seasonal variability of both SWH and wind speed (top panels in Figure 43 and Figure 44). Indeed, for these latter two figures, there are higher values of wind speed and SWH during Winter than Summer for both J3 and S3A. There is not a pointwise agreement between S3A and J3 for a time window higher than 7 days, but the distributions are similar.

Statistics for S3A and J3 comparisons are represented in Table 3 for the three regions (Sp for Catalan Sea, It for North Adriatic Sea and Dk for Denmark Straigth and German Bight) and for the four different time windows (30 days, 7 days, 1 day, 3 hours). The number of pairs for each region and each time window are presented in Table 2. The statistics include: the bias which is the difference of S3A minus J3; the standard deviation of the differences between S3A and J3; and the correlation (pearson coefficient) between S3A and J3. All correlations are significant at 99% except for two values in North Adriatic Sea which is significant at 95%.

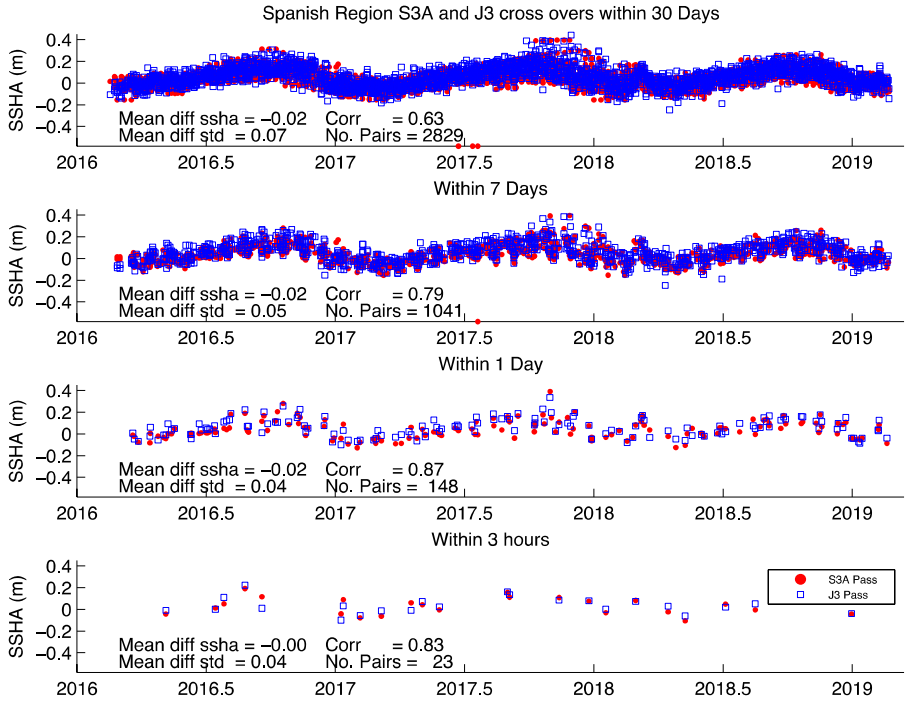

Figure 42. Time serie at all cross overs between S3A and J3 (Green filled circle in previous map) in the Catalin sea for sea Surface height anomaly (SSHA). Each panel from top to bottom correspond to the máximum time difference between each collocation: 30 days, 7 days, 1 day and 3 hours. Statistics for the mean difference, standard deviation of the differences, correlation and number of pairs are printed on the figure.

Comparisons between S3A and J3 for wind speed suggest an overestimation of wind speed for S3A between 0.3 and 0.8 m/s (Table 3). There is consistency amongst the three regions and the bias ranges from about 0.3 m/s for a collocation time window of 1 day or larger to over 0.6 m/s for a time window of 3-hours for which the standard deviation is the smallest (about 1 m/s for North Adriatic Sea and Denmark). The standard deviation of the wind speed differences between S3A and J3 increases with the collocation time window, as we would expect. The standard deviation is over 4 m/s for time windows higher than 7 days and generally lower than 3m/s when the time window is shorter than a day. Similar behaviour is found for correlation between S3A and J3. There is no significant correlation for 7-days and more. The correlation is high >0.9 for the shortest time window for North Adriatic Sea and Denmark region.

For the significant wave height, comparisons between S3A and J3 suggest an underestimation between 5cm to 20 cm of S3A SWH. This negative bias is consistent for the three regions but seems stronger in North Adriatic Sea and smaller around Denmark. S3A and J3 correlation of SWH is very high at 3h (0.94 to 0.998) and stay high at 1-day (0.75 to 0.87). The standard deviation of the difference of SWH between S3A and J3 increases with the collocation time window length: from 0.3m to 1.2m for Catalan Sea and around Denmark and from 0.3 to 0.8 to North Adriatic Sea. This lower dispersion for North Adriatic Sea is certainly due to smoother sea state compared to the two other sites (not shown).

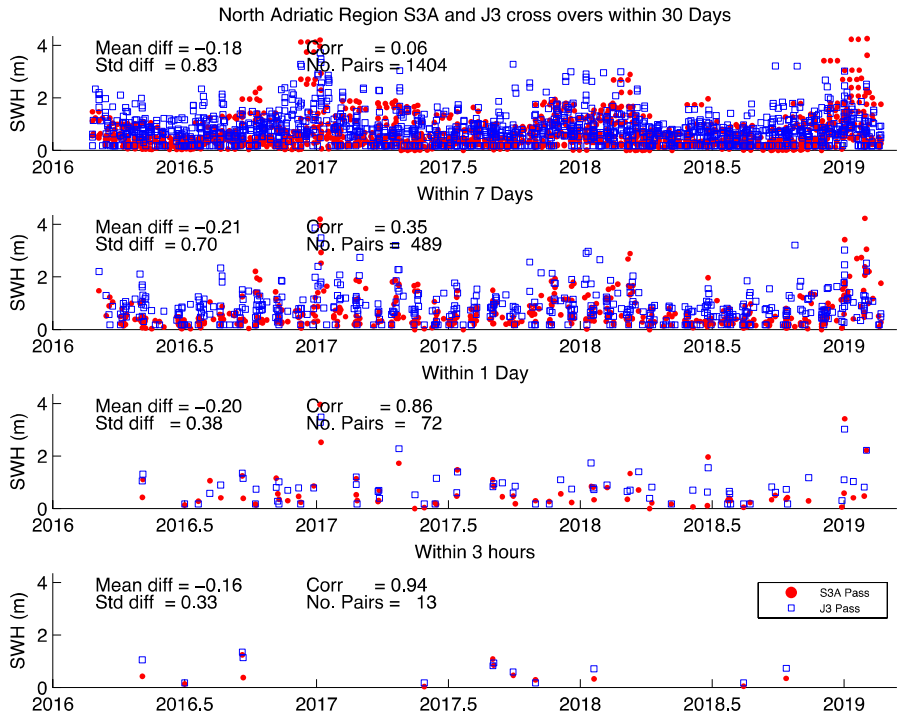

Figure 43: Same as above but in North Adriatic Sea and for significant wave height (SWH).

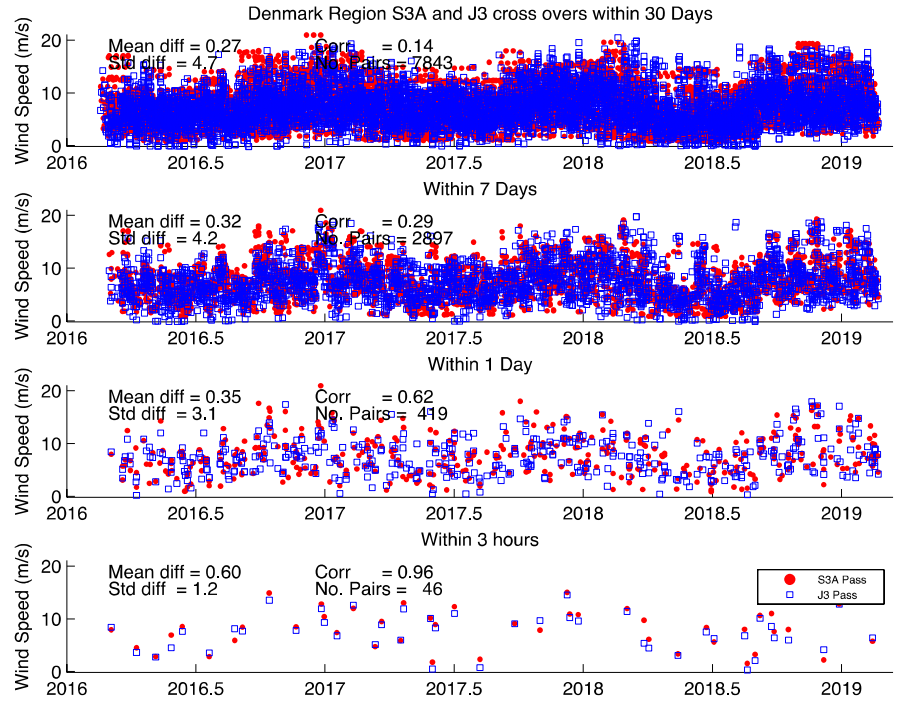

Figure 44: Same as above but over the Denmark and German Bight area for wind speed.

Table 3: Statistics of the Sentinel-3A and Jason-3 comparison

	Bias (S3A – J3)			Std of differences			Correlation		
	Wind speed								
Days	Sp	It	Dk	Sp	It	Dk	Sp	It	Dk
30	+0.30	+0.01	+0.27	4.9	4.5	4.7	0.25	0.09	0.14
7	+0.24	+0.00	+0.32	4.5	4.0	4.2	0.38	0.31	0.29
1	+0.32	+0.28	+0.35	2.8	2.8	3.1	0.74	0.70	0.62
3h	+0.79	+0.82	+0.60	2.5	0.9	1.2	0.86	0.96	0.96
	Signficant wave height (swh)								
30	-0.11	-0.18	-0.09	1.19	0.83	1.25	0.25	0.06	0.26
7	-0.11	-0.21	-0.07	1.10	0.70	1.11	0.39	0.35	0.41
1	-0.10	-0.20	-0.05	0.55	0.38	0.75	0.87	0.86	0.75
3h	-0.12	-0.16	-0.06	0.33	0.33	0.31	1.00	0.94	0.98
	Sea surface height anomalies (ssha)								
30	-0.02	-0.02	-0.00	0.07	0.09	0.15	0.63	0.33	0.36
7	-0.02	-0.02	-0.00	0.05	0.06	0.11	0.79	0.69	0.64
1	-0.02	-0.02	-0.00	0.04	0.05	0.10	0.87	0.80	0.76
3h	-0.00	-0.03	-0.00	0.04	0.05	0.09	0.83	0.61	0.84

The sea surface height anomaly (SSHA) estimates from S3A is better than 3cm in bias compared to J3. There is no bias consistency between the three regions. For North Adriatic Sea, S3A seems to have a consistent negative bias of 2-3cm whatever the collocation time window. For a collocation below 7-days, the discrepancies between S3A and J3 are generally (std) between 6cm with correlations better than 0.7. In the Catalan sea, the bias is 0 for 3h collocation but increase for increasing collocation time window. As there is a strong SSHA annual cycle in this region (see *Figure 42*), the correlation stays above 0.6 even for a time window of 30-days. Around Denmark, and over the German Bight bias for S3A is zero (Table 3). Discrepancy (std) between S3A and J3 is higher for this region (~10cm) than for the two Mediterranean sites (5cm) and this might be due to strong tidal signal in this region. Despites this, correlation are significant up to 7-days' time window.

To summarise, comparisons between Sentinel-3A and Jason-3 over the three regions including the four case studies, highlight a small bias against J3 in wind speed between 0.3m/s and 0.8m/s and in significant wave height between -5cm and -15cm. No consistent bias in sea level between the North Sea and the Mediterranean Sea has been observed.

4.2.3. Comparison against a coupled wave-ocean numerical model: Total Water Level

The total water level (TWL) is the effective water level above the mean sea surface, it includes tides and the inverse barometric height. Here, we validate S3A SRAL (altimeter) measurements of TWL against a regional coupled wave-ocean numerical model. The study region is defined as 20°W–-10°E in longitude and 46°N–62°N in latitude. S3A data are filtered using product flags indicating issues

with the quality of the ocean backscatter and/or altimeter range. TWL measured by S3A for June 2016 are shown in Figure 45. A first comparison with the model was carried out in order to remove satellite outliers when compared to the model *truth*. All data outside two standard deviations of the difference between S3A and the model have been removed.

The model used was the AMM15 which includes atmospheric forcing from ECMWF and is configured as a coupled wave-ocean currents model. AMM15 has been implemented to provide TWL by relying on the spectral wave model WaveWatch III (Tolman 2014), and the NEMO hydrodynamic model (Madec et al 2016). These model components are applied to the UK in a coupled configuration, with the atmosphere forcing the ocean (one-way), and the ocean and wave components coupled together (two-ways). The domain centre for the model was over the UK (cf Figure 46 below for the 20 June 2016 at 11h00). A detailed model configuration is described in Lewis et al. (2018).

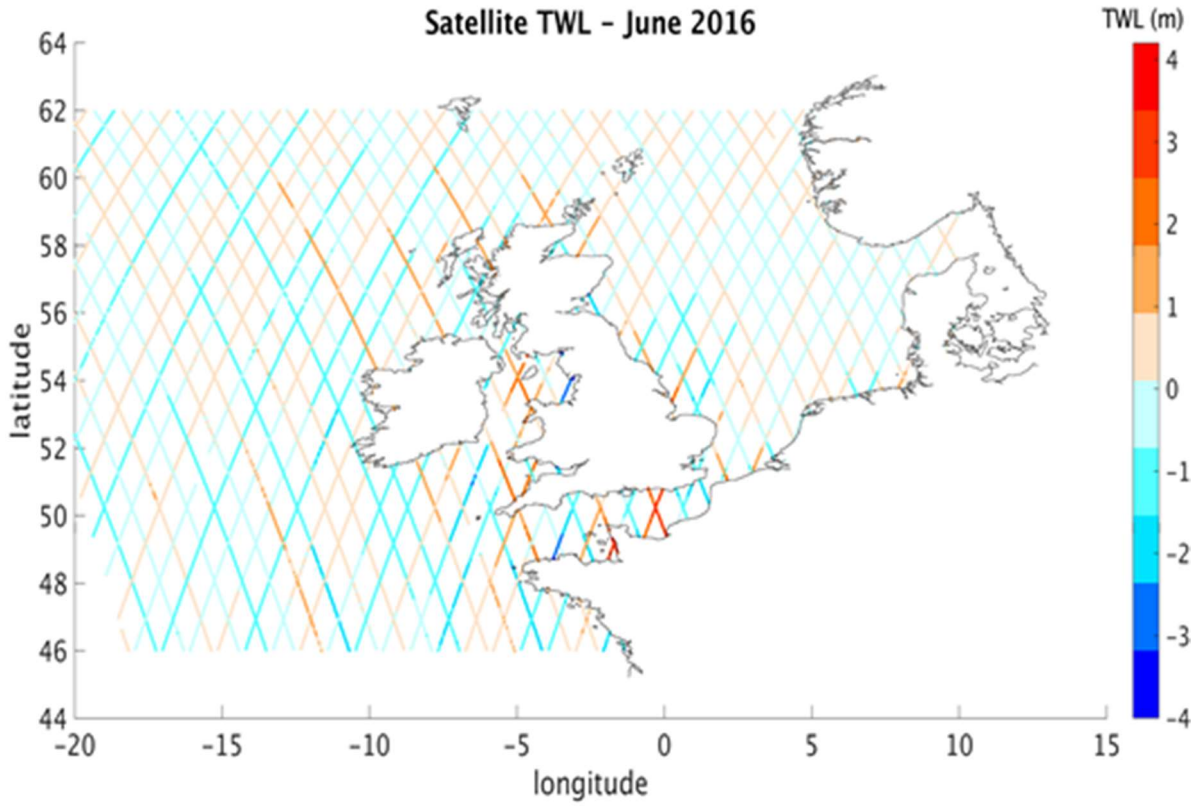

Figure 45: S3A TWL observations over the model domain area for June 2016.

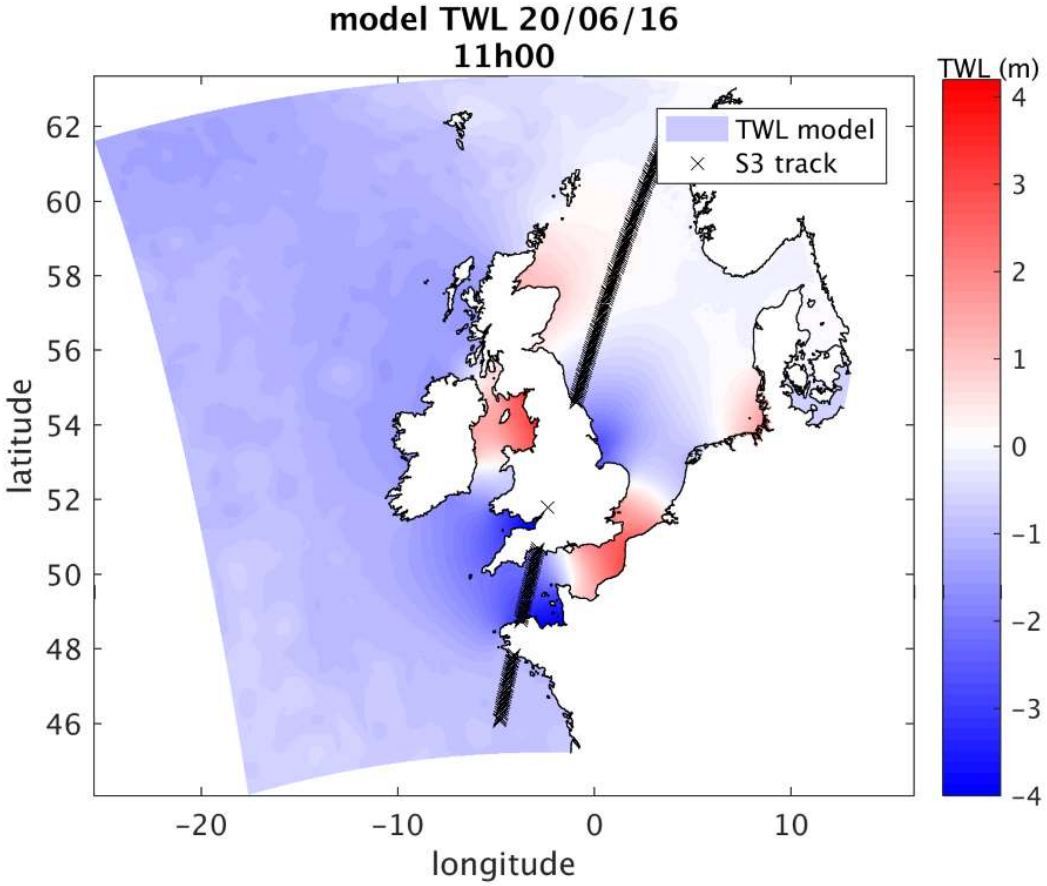

Figure 46: Full domain model simulation of the TWL for one-hour time step, at 11:00:00 on the 20th June 2016. The satellite track travelled over the domain this day between 10:50:45 and 10:55:22.

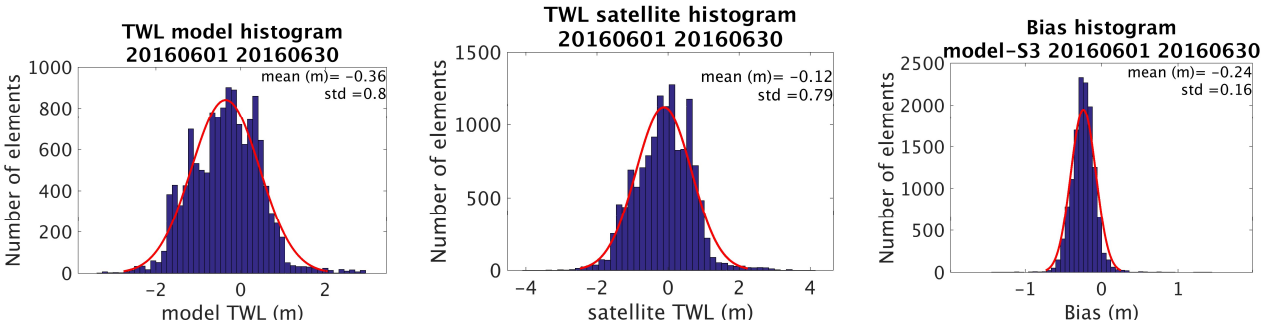

Figure 47: Histograms of TWL for June 2016 of the (left) model, (middle) S3A and (right) the difference between the model and S3A.

A comparison of Sentinel-3 against the model was undertaken for the period March 2016 to February 2017. Model data were collocated with S3A data within ±30 minutes (cf the model step of 1 hour) and spatially within 0.02° (approximatively 2km). The collocated TWL histograms for S3A and the model for June 2016 are given in Figure 47 along with the histogram of the differences. There is a mean bias between the two datasets of 0.24m in June 2016. The histograms have the same shape with a standard deviation of the distribution around the mean of 0.8m for both datasets. The histogram of the collocated differences between S3A and the model is represented in Figure 47-right and presents the same 0.24m bias with a standard deviation of 16cm.

The same differences between the model and S3A are shown geographically in Figure 48. We note there is good agreement between the model and S3A with typical differences ~±0.2m. As with the histograms, the spatial differences suggest S3A TWL tends to be slightly higher than the model values. Close to the coast, differences are higher and this is probably linked to the larger tidal signal at the coast and higher noise in S3A caused by land contamination in the satellite footprint. For consistency, the collocation of S3A/model data along individual S3A tracks is shown in Figure 49 for June 2016 (for readability zoomed between ±1m). S3A data (red) are generally above the model (blue) as expected by the positive bias of S3A against the model.

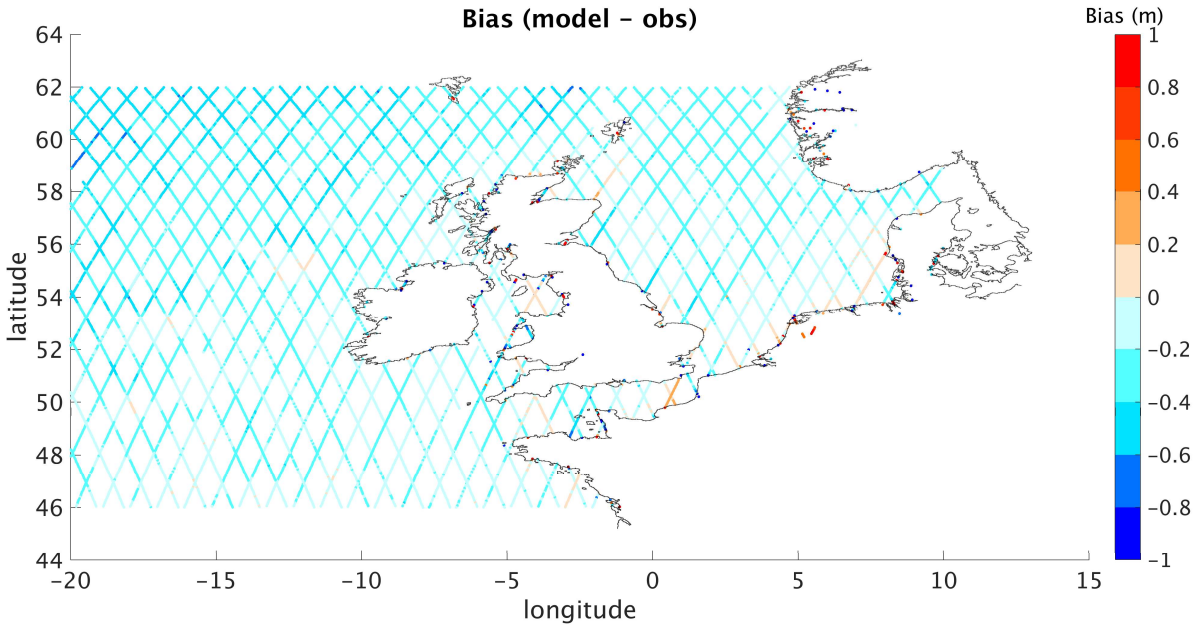

Figure 48: Map of total water level differences between the collocated model and S3A observations for June 2016

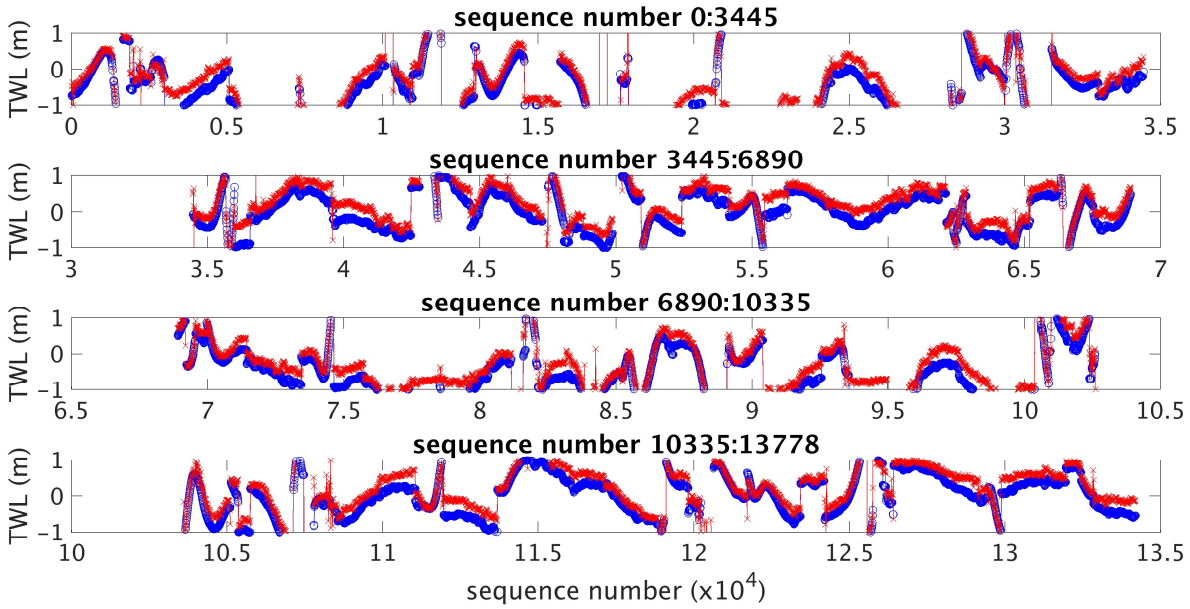

Figure 49: Sequence of pairwise (red) S3A and (blue) model TWL. Each track above the domain corresponds to a continuous curve. These tracks are represented for June 2016.

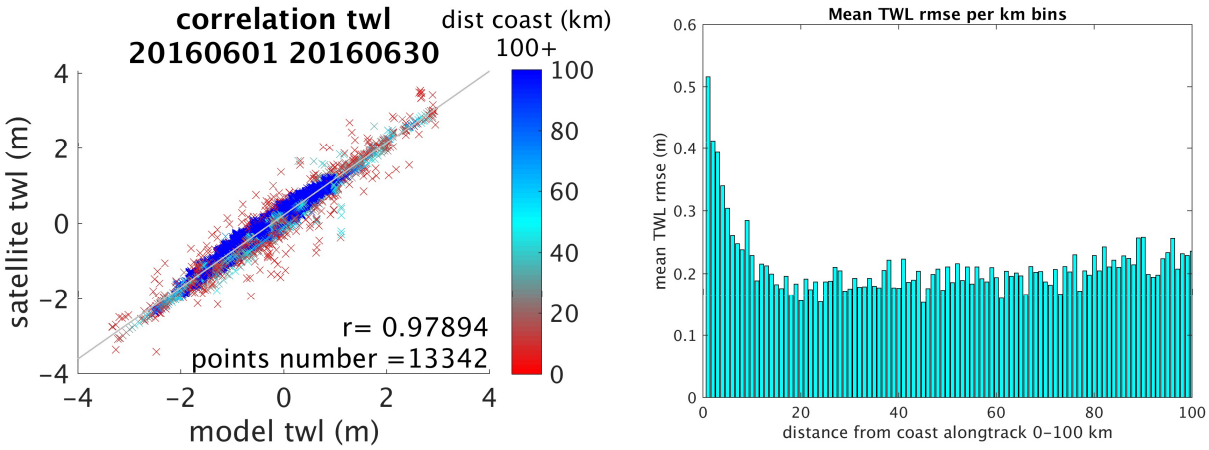

Figure 50: (left) Scatter of model TWL against S3A TWL for June 2016. The colour represents the distance from the coast. (right) Mean root-mean-square differences between S3A and the model as a function of distance from coast along-track for June 2016 from 0 to 100km.

Table 4: Statistics of model and S3A comparison for each month from March 2016 to February 2017. For the two latest column " >50" and "< 10" refer to km from coast.

month	mean model (m)	mean obs (m)	mean bias (m)	std bias	%bias	rmse (m)	cor coef	rmse (m) >50	rmse (m)<10
Mar-16	-0.46	-0.22	-0.24	0.17	13.86	0.29	0.98	0.29	0.43
Apr-16	-0.45	-0.20	-0.25	0.16	9.51	0.30	0.98	0.30	0.41
May-16	-0.40	-0.16	-0.24	0.16	8.94	0.29	0.98	0.29	0.38
Jun-16	-0.36	-0.12	-0.24	0.16	7.63	0.29	0.98	0.29	0.40
Jul-16	-0.33	-0.09	-0.25	0.15	4.75	0.29	0.98	0.29	0.34
Aug-16	-0.34	-0.11	-0.24	0.15	10.29	0.28	0.98	0.28	0.36
Sep-16	-0.28	-0.05	-0.23	0.16	-0.69	0.28	0.98	0.28	0.34
Oct-16	-0.39	-0.17	-0.22	0.16	7.80	0.28	0.98	0.27	0.37
Nov-16	-0.29	-0.08	-0.21	0.16	2.10	0.27	0.98	0.26	0.39
Dec-16	-0.27	-0.03	-0.23	0.18	-2.32	0.29	0.98	0.29	0.43
Jan-17	-0.33	-0.11	-0.22	0.17	6.19	0.27	0.98	0.27	0.41
Feb-17	-0.33	-0.10	-0.23	0.17	3.37	0.28	0.98	0.28	0.43

The mean difference (mean bias) shown above for June 2016 is consistent over time (within [-0.25;-0.21]: Table 4) and may be due to a different reference for the mean sea surface between the satellite and the model. The standard deviation of the bias for each month also does not vary much and is always between 0.15m – 0.18m with a minimum in July-August 2016 and a maximum in December 2016 (Table 4). The root-mean-square model/S3A differences (rmse in Table 4), which can be decomposed as the quadratic sum of the mean difference and standard deviation of the differences, is dominated by the mean difference for each month both in magnitude and variability: maximum in April at 0.30m and minimum in November and January at 0.27m. There is a strong correlation between S3A and the model at 0.98 for all months (Table 4 and, for June 2016, Figure 50). Figure 50 shows stronger discrepancies between the two datasets when the location approaches the coast (red). The mean root-mean-square differences between S3A and the model for June 2016 as function of the distance from coast is also given in Figure 50 and highlights stronger differences close to the coast than further offshore. At the coast, rmse is up to 0.5m and this decreases rapidly down to ~0.2m within 10km of the coast. On average, the rmse for the first 10km is about 0.4m with a minimum at 0.34 in July and September and a maximum at 0.43m in January, February and March.

To summarise, there is a very good agreement between S3A and the coupled wave-ocean numerical model of total water level with discrepancies below 20cm on a monthly average.

4.2.4. Comparison of wind and wave products over the North Sea-Baltic Sea

In this section, the quality of the newly available Sentinel-3A satellite data is assessed and compared to that of older satellite data. The focus in this study is on coastal areas, where the quality of both the satellite and the model data tends to deteriorate. Also, the quality of the Sentinel-3A data is analysed based on the relative orientation of the coastline and satellite heading, varying metocean conditions and the wind direction relative to the satellite flight direction.

General quality of measured significant wave height

To estimate the overall performance of the different satellite products from June till November 2016 and within the North Sea/Baltic Sea study area, scatter plots of the in situ measurements from the GTS data versus remote sensing measurements are analysed (Fig. 41). For these comparisons, the satellite data are allowed to have a maximum spatial distance of 20 km and a maximum time gap of 30 min with respect to the in situ measurements (Fenoglio-Marc et al., 2015). The general performance of all five satellite products is good and very similar. The correlation between all products varies by only 3 % with values ranging from 94 % to 97 %. The SI is the largest for the CryoSat-2 RDSAR product, being approximately 0.22. For the SAR products of Sentinel-3A and CryoSat-2 as well as for Jason-2, the SI is approximately 0.17. However, the satellites tend to overestimate the significant wave height of in situ measurements, especially Sentinel-3A SAR and both CryoSat-2 products, with biases of up to 26 cm. The smallest bias (only 6 cm) is found for the Jason-2 measurements (Wiesse et al, 2018).

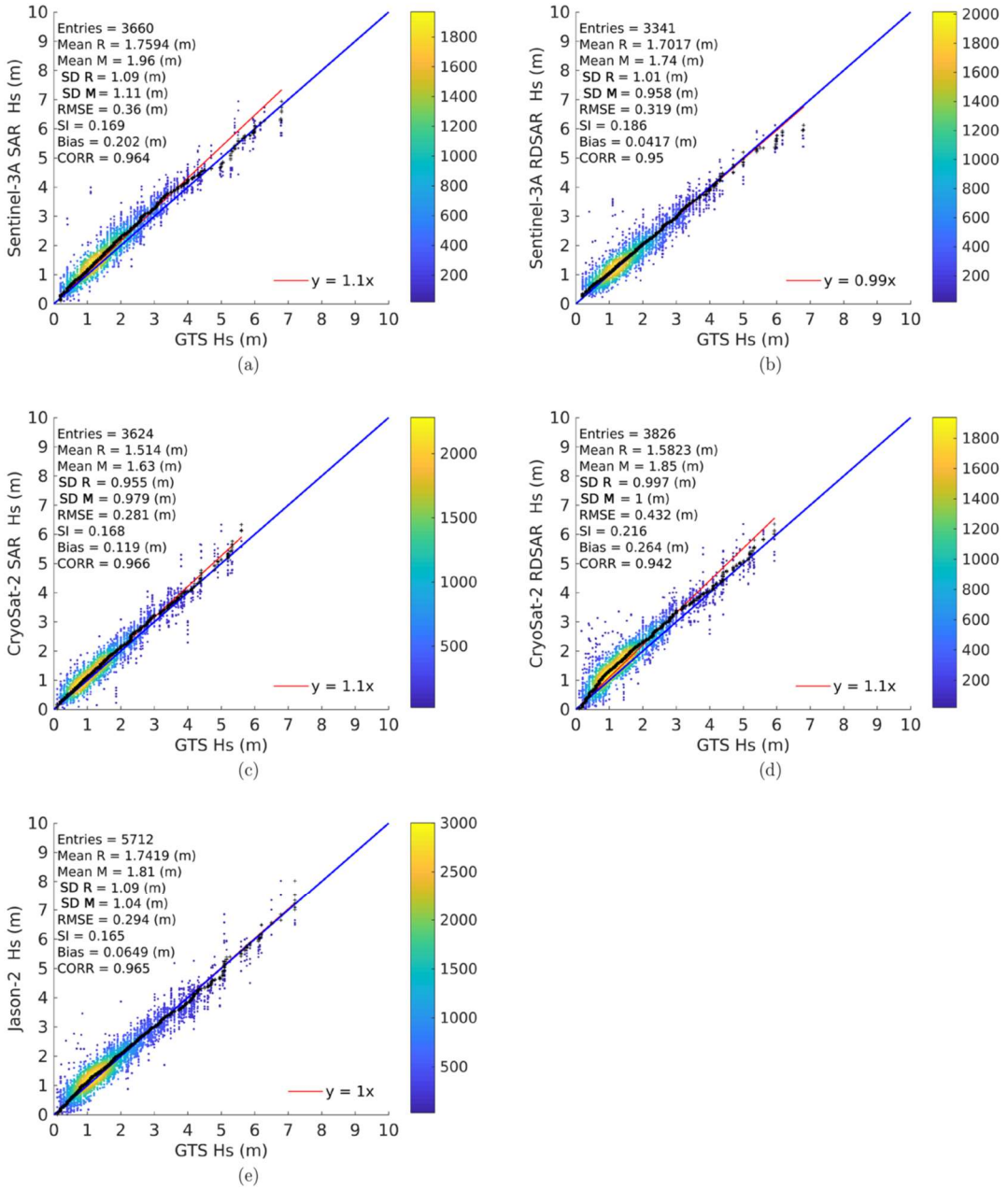

Figure 51. Q–Q scatter plots of measured significant wave height – in situ GTS (R) versus remote sensing data (M) of (a) Sentinel-3A SAR, (b) Sentinel-3A RDSAR, (c) CryoSat-2 SAR, (d) CryoSat-2 RDSAR and (e) Jason-2 from June to November 2016: Q–Q plot (black crosses), 45◦ reference line (blue line) and least-squares best-fit line (red line).

Scatter index along the satellite track

To analyse the spatial distribution of the quality of the satellite data, the SI between the modelled and measured significant wave heights along the satellite tracks within each grid box is calculated for Jason-2 and Sentinel-3A SAR (Fig. 42). Since very few data exist within each grid box during the study period, for this analysis, the study period is extended to the end of August 2017 to achieve a more robust SI result. For both satellites, the SI is small over the open ocean and becomes larger closer to the coast. Notably, in coastal areas, the SI for Sentinel-3A SAR is smaller than that for Jason-2. Especially in the northern part of the Baltic Sea, the Danish Straits and along the coastal areas of the southern North Sea, the SI is reduced for Sentinel-3A SAR compared to that for Jason-2. This clearly indicates that Sentinel-3A SAR performs better over coastal areas than Jason-2.

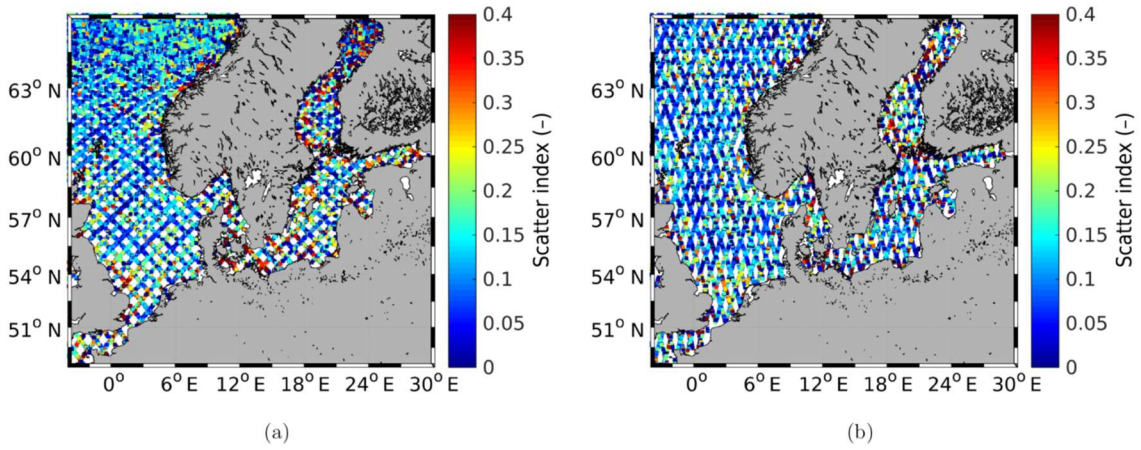

Figure 52 Scatter index between satellite and modelled significant wave heights along the satellite tracks for (a) Jason-2 and (b) Sentinel-3A SAR.

To quantify this, the statistical values within the first 10 km off the coast are calculated for all three different satellites (Table 5). In some earlier studies, this area was neglected due to the deteriorating quality of the satellite data (Fenoglio-Marc et al., 2015). For Sentinel-3A, the RMSE is reduced by approximately 0.1 m and the SI is reduced by 0.17 compared to the values for the other two satellites. The bias is reduced by 0.08 m compared to that for Jason-2 and 0.16 m compared to that for CryoSat-2. The correlation for Sentinel-3A is increased by 10 % compared to that for Jason-2 and 5 % compared to that for CryoSat-2. Furthermore, the statistics of Sentinel-3A within the first 10 km are closer to those over the whole study area, which is not the case for the other two satellites (Table 5; see Fig. 41). This indicates that the quality of the data of Sentinel-3A over coastal areas is closer to that over the open ocean compared to the data quality of CryoSat-2 and Jason-2.

Table 5. Comparison of the data quality within the first 10 km off the coast for all three satellites.

	Entries	RMSE (m)	SI	Bias (m)	Correlation
Jason-2	1076	0.5219	0.4977	0.2461	0.8075
CryoSat-2 RDSAR	1360	0.4860	0.4957	0.3334	0.8548
Sentinel-3A SAR	4192	0.3985	0.3324	0.1682	0.9138

Comparison of data quality for onshore and offshore flights

Due to the way satellite altimeter data are processed, the data quality can deteriorate in the vicinity of coastlines, particularly for passes from land to ocean. To test how much the satellite measurements over the study area are affected by this problem, the flights are separated into onshore and offshore flights, with onshore flights passing from the ocean to the shore and offshore flights passing from the shore to the ocean. For the analysis here, again, only measurements within the first 10 km off the coast are taken. When comparing the statistical values for Sentinel-3A SAR for both onshore and offshore flights, no substantial differences are found, and the statistical values are very similar (Table 6). Therefore, the transition from land to water does not influence the quality of the satellite observations over our study area.

Table 6 *Comparison of the data quality, organized by onshore and offshore flights, for Sentinel-3A SAR. Only measurements taken within the first 10 km off the coast are used.*

	Entries	RMSE (m)	SI	Bias (m)	Correlation
onshore	1694	0.3877	0.3244	0.1666	0.9151
offshore	2151	0.3981	0.3219	0.1695	0.9195

Comparison of data quality for long- and short-fetch conditions

Another assessment of the quality of the data measured by the satellites can be carried out by analysing their quality in terms of the fetch conditions. To test this, Sentinel-3A SAR data within the German Bight (53.23◦ N, 6◦ E to 55.62◦ N, 9.2◦ E) are split into two groups: that for long-fetch situations and that for short-fetch situations. Long-fetch situations within the German Bight are characterized by northwesterly winds, while short-fetch conditions occur for southeasterly winds. The analyses demonstrate that the data quality for both situations is very similar (Table 7). The SI and the correlation have better values for long-fetch situations. The correlation between modelled and

measured significant wave heights for long-fetch situations is 98 %, being 4 % larger than that for short-fetch situations. The SI for long-fetch situations is 0.09. The SI for short-fetch situations is approximately twice as large, i.e. 0.19. The RMSE and the bias, though, are better under short-fetch conditions. The RMSE, which is 21.6 cm for short-fetch situations, is approximately 16 cm smaller under short-fetch conditions than under long-fetch conditions. The bias under short-fetch conditions is only 0.7 cm. This is due to the over- and underestimation of the measured data essentially cancelling each other. Under long-fetch conditions, this is not the case, as the bias amounts to 33 cm. When analysing all directions, the statistical values lie between those under long- and short-fetch conditions. Hence, it can be concluded that the satellite measurements do not yield clearly better results for any of the conditions.

Table 7 Comparison of the data quality, organized by long- and short-fetch situations within the German Bight, for Sentinel-3A SAR.

	Entries	RMSE (m)	SI	Bias (m)	Correlation
Long fetch (NW)	143	0.3796	0.0943	0.3299	0.9809
Short fetch (SW)	86	0.2164	0.1854	0.0065	0.9411
All directions	993	0.2763	0.1658	0.1660	0.9524

Comparison of data quality for different relative wind and flight directions

In previous studies, e.g. Chelton and Freilich (2005), a dependency of the data quality on the wind and wave direction relative to the movement of a satellite was found, as satellites move while measuring the wind and wave conditions. Therefore, in this analysis, the measured significant wave height data are separated in terms of the wind direction relative to the satellite track. A slightly smaller RMSE, SI and bias can be found in situations where the wind comes from the direction opposite that of satellite motion (Table 8). The best correlation, though, is achieved under cross-wind conditions, having a value of 96.7 %. Since the differences between all situations are quite small, i.e. 1.3 % for the correlation, 6 cm for the bias, 0.009 for the SI and 6.6 cm for the RMSE, the difference in the statistical values for all three situations cannot be regarded as substantial. Therefore, it can be concluded that the quality of the Sentinel-3A measurements does not depend on the wind direction relative to the satellite flight direction (Wiesse et al., 2018).

Table 8 *Comparison of the data quality, organized by the wind direction relative to the satellite flight direction, for Sentinel-3A SAR.*

	Entries	RMSE (m)	SI	Bias (m)	Correlation
Along wind	7366	0.4396	0.1643	0.2794	0.9645
Opposing wind	6257	0.3757	0.1553	0.2254	0.9544
Cross wind	14940	0.4416	0.1625	0.2886	0.9673

The newly available Sentinel-3A data yield better results for coastal areas compared to the data quality of older satellites such as Jason-2 and CryoSat-2. Especially within the first 10 km from the coast, the statistical values of Sentinel-3A are substantially better then the ones for Jason-2 and CryoSat-2. Also, for Sentinel-3A, no substantial differences are found regardless whether the satellites pass from land to water, or vice versa. Furthermore, the quality of the Sentinel-3A data does not differ substantially under either long- or short-fetch conditions within the German Bight. When comparing the data quality based on the wind direction relative to the satellite flight direction, again, no substantial differences can be found. Therefore, the data quality is not affected by relative flight direction and the coastline or the wind direction, as well as different metocean conditions.

4.2.5. Comparison of wind and wave products over the Mediterranean Sea

A dedicated effort within the CEASELESS activities has been aimed at the intercomparison of Sentinel-3 altimeter data against the measurements provided by other EO sensors over the Mediterranean Sea. As described in CEASELESS Deliverable 4.2, in that study we considered data from Cryosat, Jason2, Jason3, and Sentinel-3 data (hereinafter referred to as Cy, J2, J3, S3), for the period from July 2016 to June 2017 in the Mediterranean Sea, compared among each other on the common benchmark of the wind and wave fields resulting from COSMO (see www.cosmo.model.org/content /model/default.htm) and WAM (Komen et al., 1994; Janssen et al., 2005) respectively. The results, recently published in Ocean Science Discussions (Cavaleri et al., 2018), showed that the four datasets had consistent performances as far as wind speed was concerned, but with significant differences in terms of estimated wave heights.

Following this analysis, we focused on the performance of Sentinel-3 data in coastal regions. The SRAL sensor can work either in low-resolution mode (LRM) or in the high-resolution SAR mode (https://sentinel.esa.int), combining 64 Ku-band and 2 C-band pulses. Operating in this mode, the SRAL can achieve an along-track resolution of approximately 300 m with a lateral swath up to 10 km: this in principle allows an improved capability of capturing the sharp spatial gradients that characterise coastal seas, but potentially at the price of a higher noise.

The scope of this study was thus to estimate the trade-off between spatial resolution and noise in the description of nearshore dynamics. The selected test case is a Sentinel-3 descending pass over the northern Adriatic Sea and Tyrrhenian Sea on 25 July 2017 (Figure 53), with relatively calm conditions

in the former (Figure 54) and a severe mistral storm in the latter, compared against operational wave model fields validated in turn, for the northern Adriatic Sea, on the data provided by the Acqua Alta Oceanographic Tower (Bertotti and Cavaleri, 2009, Figure 55: Detail of the Sentinel-3 pass shown in Figure over the northern Adriatic Sea, with SAR-mode significant wave height measurements. The sample is a Level-2 product provided by the Copernicus service containing 1 Hz and 20 Hz observations, both in SAR and pseudo-low resolution mode (plrm), a simulation obtained from Ku-band pulses of the classical altimeter LRM mode.

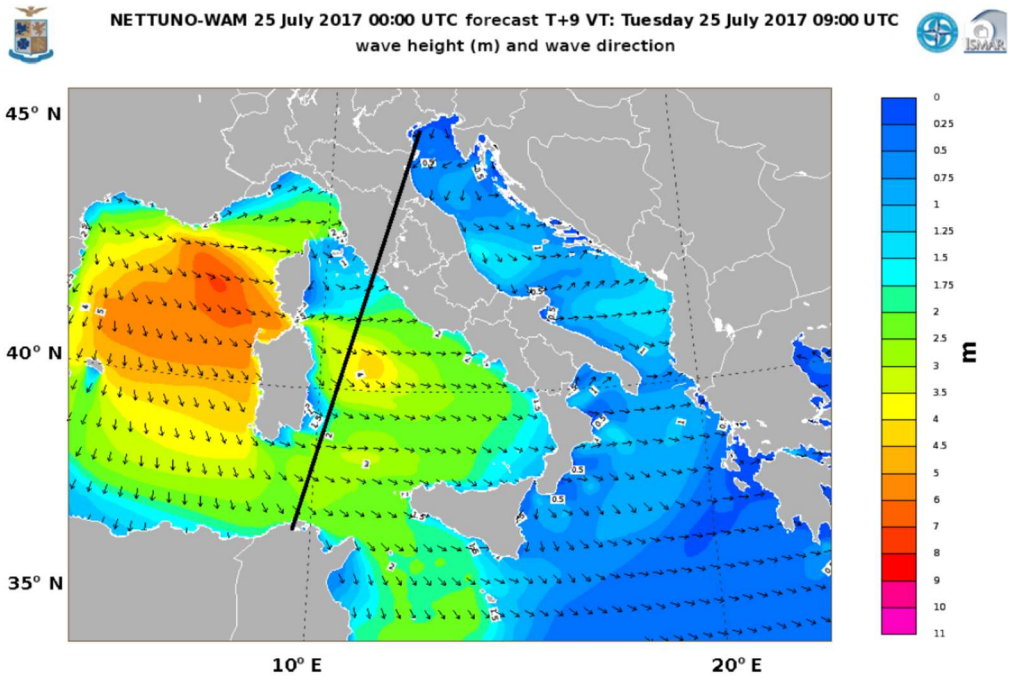

Figure 53: Track of Sentinel-3 pass altimeter on 25 July 2017 over modelled wave height (colour) and direction (arrows). Cavaleri et al., 2018.

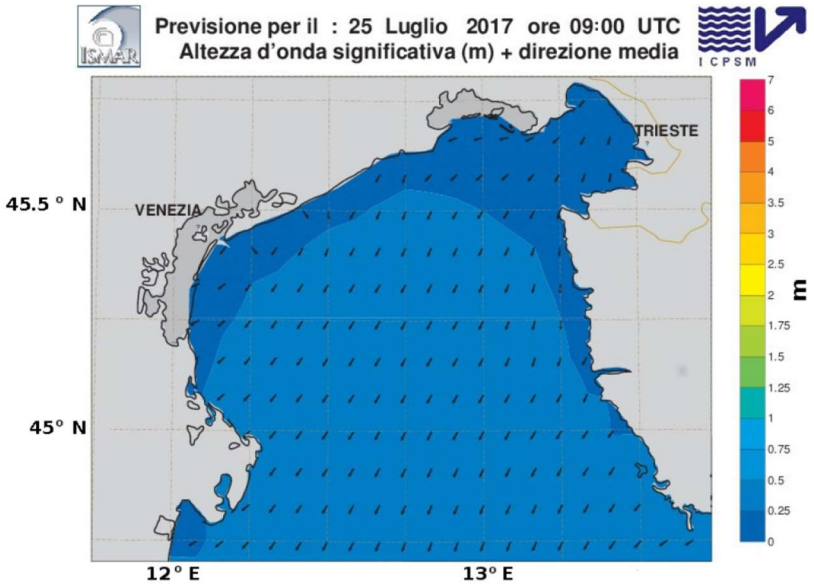

Figure 54: Detail of the modelled wave field in the northern Adriatic Sea at 09:00 UTC on 25 July 2017, with colour representing the significant wave height and arrows representing the wave direction (Cavaleri et al., 2018).

Concerning 1 Hz data, while in the Tyrrhenian Sea we find a good agreement between model results and the satellite-retrieved significant wave height (with the exception of some spikes in the proximity of the land), the Sentinel-3 data in the short northern Adriatic tract represent a physically inconsistent pattern (Figure 56). Figure 57 shows a detailed comparison of the three different (ku- and plrm-ku-) bands and model Hs values plus the distance (km) from the nearest coast. Values from Sentinel-3 exhibit unrealistic values in both signals, particularly in the plrm-ku band, for distances of less than 10km from the coast.

20 Hz data are explored in Figure 58, with panel (a) showing the whole pass, and panel (b) focusing on the Adriatic Sea. The signal appears evidently noisy also at a distance of more than 20 km from the coast, and also in the Tyrrhenian Sea where this can not be justified by a geophysical reason, suggesting that this is associated with the instrument and the sampling variability.

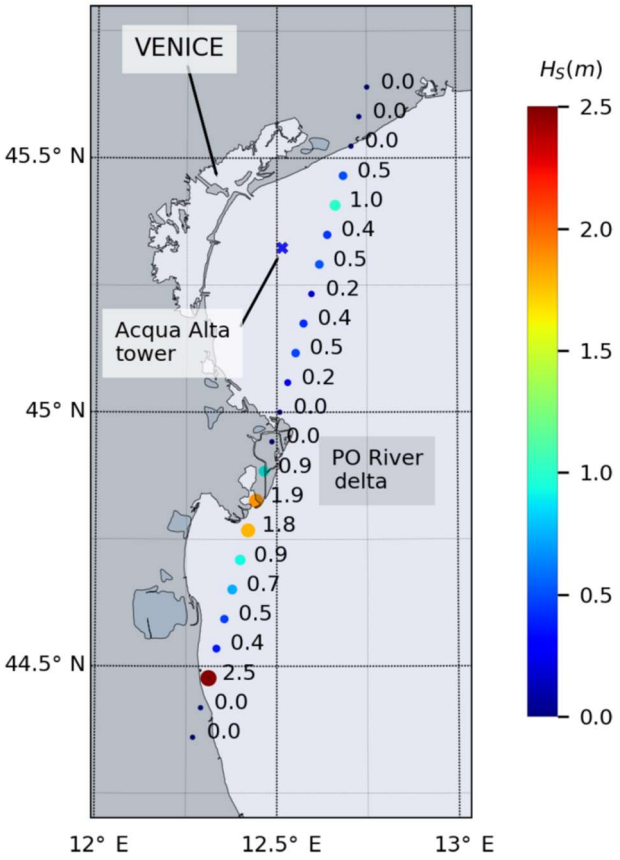

Figure 55: Detail of the Sentinel-3 pass shown in Figure over the northern Adriatic Sea, with SAR-mode significant wave height measurements.

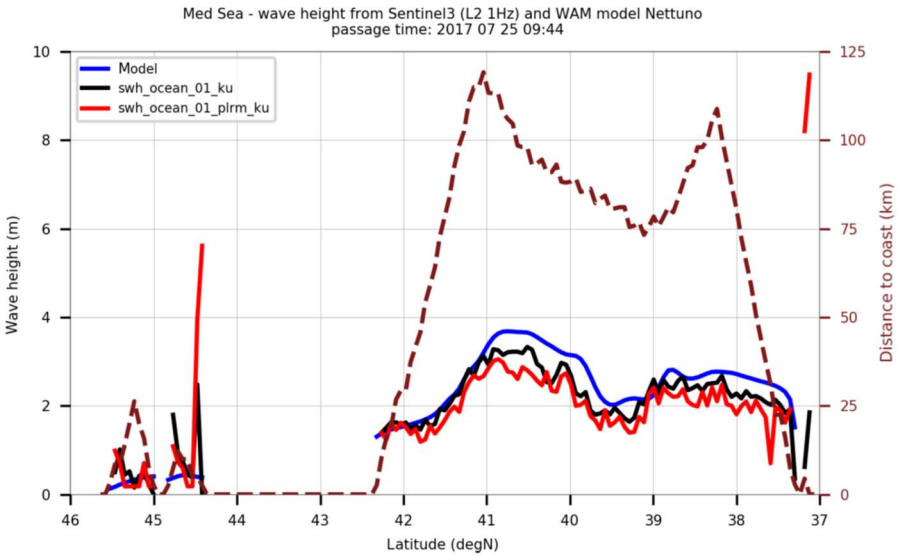

Figure 56: Intercomparison of modelled and satellite-retrieved significant wave height along the track shown in Figure . The dashed line represents the distance from the nearest coast (Cavaleri et al., 2018).

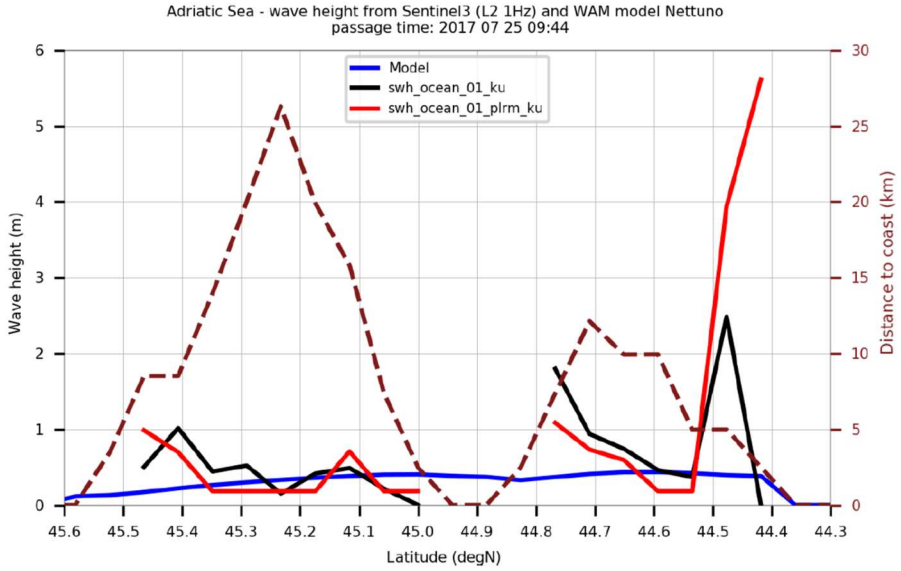

Figure 57: Intercomparison of the S3 ku- and plrm-ku- wave heights and the corresponding wave model results, with dashed line representing the distance from the nearest coast (Cavaleri et al., 2018).

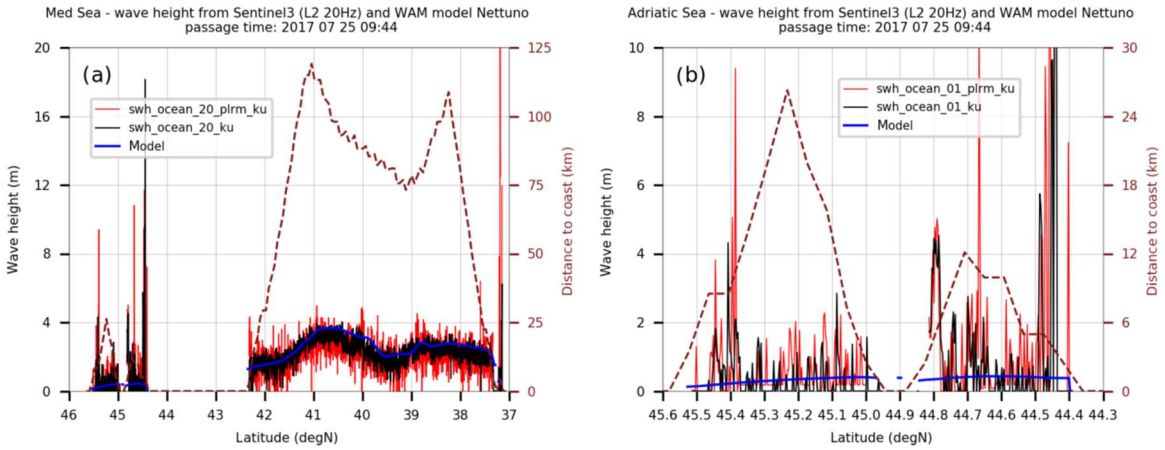

Figure 58: Intercomparison of the S3 20 Hz ku- and plrm-ku- wave heights and the corresponding wave model results, with dashed line representing the distance from the nearest coast (Cavaleri et al., 2018). Panel (a) represents the full pass and panel (b) represents the Adriatic Sea section.

4.2.6. Comparison of wave products over the Catalan Coast

In this contribution, the quality of wave data provided by the new Sentinel-3A satellite is evaluated for the Catalan Coast. We focus on coastal areas, where altimeter data are of lower quality than those for the open ocean. The satellite data of Sentinel-3A and Jason-3 are assessed in a comparison with in situ measurements.

In situ measurements

In this work, 5 deep-water buoys and 2 coastal-water buoys are used, which are summarized in Table 9 and which location can be seen in Figure .

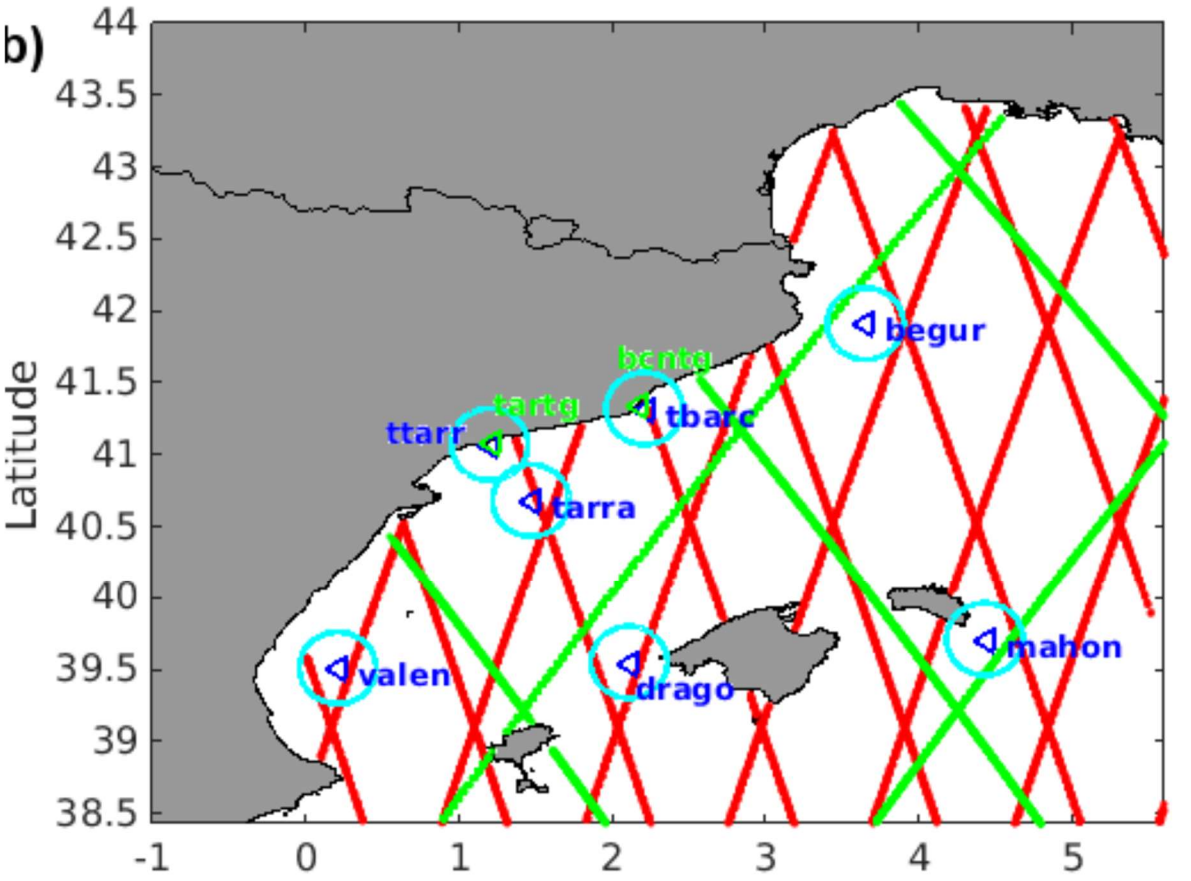

Figure 59. S3A and J3 satellite tracks for the Catalan Coast domain, buoy locations (blue triangles) with the corresponding collocation radius.

Table 9. Catalan Coast buoy characteristics.

	Code	Lon	Lat	Depth	Measured Parameters
Tarragona	tarra	1.47° E	40.68° N	688 m	Hs, Dir, Tm_{02}, Tp, $Wind$
Begur	begur	3.65° E	41.92° N	1200 m	Hs, Dir, Tm_{02}, Tp, $Wind$
Dragonera	drago	2.10° E	39.56° N	135 m	Hs, Dir, Tm_{02}, Tp, $Wind$
Mahon	mahon	4.42° E	39.72° N	300 m	Hs, Dir, Tm_{02}, Tp, $Wind$
Valencia	valen	0.21° E	39.52° N	260 m	Hs, Dir, Tm_{02}, Tp, $Wind$
Tarragona Coast	ttarr	1.19° E	41.07° N	15 m	Hs, Dir, Tm_{02}, Tp, sst
Barcelona Coast	tbarc	2.20° E	41.32° N	68 m	Hs, Dir, Tm_{02}, Tp, sst
Tarragona Tide Gauge	tartg	1.21° E	41.08° N	-	ssh, $Wind$
Barcelona Tide Gauge	bcntg	2.17° E	41.34° N	-	ssh, $Wind$

Satellite wave data

The Jason-3 (J3) and Sentinel-3A (S3A) altimeter missions data are used, which are available at the Copernicus catalogue (http://marine.copernicus.eu/). These are processed by the SLTAC multimission altimeter data processing system. To produce the near real time Hs data, the system acquires altimeter data for each mission and then performs an editing process that consist in selecting the valid data using a combination of criteria and thresholds on parameter values. Finally, the Hs values form the S3A mission are calibrated on the reference mission, the J3 mission, which is calibrated with buoys data. The measurements are available since July 2017 and have a 7 km along-track resolution. For J3 the latitude limits are 66º S and 66º N and for S3A the coverage is between 80º S and 80º N.

In order to be able to compare satellite measurements (along tracks) with buoy measurements (fixed points) the data need to be collocated in time and space. Regarding the time collocation, the satellite data is collocated to the nearest time step of the model/buoy data, which have an interval of 1 h. Thus, just the time steps where the difference between the two time stamps is less than 30 min are considered. And regarding the space collocation, a collocation radius of 0.25º is used to collocate the satellite data to the desired point. If there is more than one measure that satisfies the collocation condition, then a mean value of all of them is used. In Figure an example of the spatial collocation at a buoy location is presented. In this case, the point collocation of satellite data would be the mean value of the green points, which are inside the collocation radius.

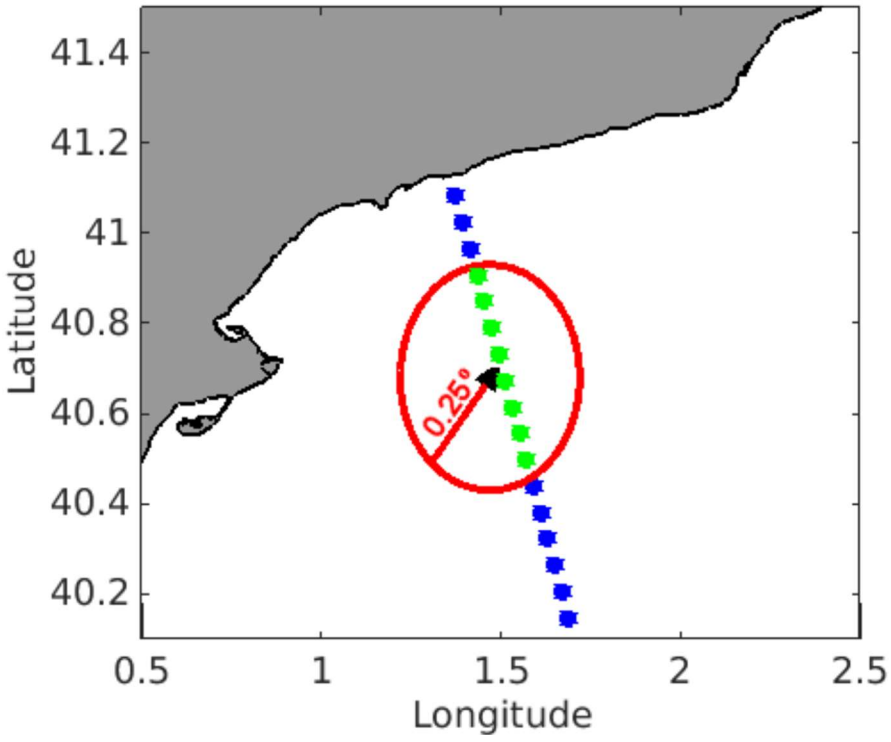

Figure 60. Example of satellite data collocation method. The black triangle is the buoy location, the red circle the collocation radius and the blue and green points the satellite data (being the green points the ones that are inside the collocation radius).

Finally, in order to filter spurious data, satellite data points where the Hs difference with respect to the Hs of the corresponding successive along-track point is greater than 0.5 m have been omitted.

Sentinel-3 wave product validation

Some statistics comparing the buoy measured data and the S3A satellite data are presented in Table 10 and 11, respectively. The period used to obtain these metrics is from 15 July 2017 to 15 March 2017 (8 months). First, it is important to notice the scarce number of samples, which limits the satellite data quality validation. From the obtained statistics, it is observed that S3A data is more biased from the observations than the J3 data. This is also observed in Figure (a), where the scatter plots of the collocated buoy-satellite pair of points are presented. Additionally, S3A data show worst RMSD values than J3 data but, in general, both satellite data sets show good agreement with the observations. Finally, in Figure (b) the time series of begur and mahon buoys are plotted together with the satellite collocated data. The visual inspection allows to see that the satellite data are able to capture the wave peaks.

Table 10. Bias, MAE and RMSD (in meters) comparing each buoy data with the collocated S3A data during the period 15 July 2017-15 March 2018.

	bias (m)	MAE (m)	RMSD (m)	N samples
begur	0.31	0.33	0.52	15
drago	0.26	0.27	0.33	18
mahon	0.43	0.43	0.57	9
tarra	0.16	0.17	0.20	18
tbarc	0.22	0.22	0.24	6
ttarr	0.33	0.34	0.44	8
valen	0.10	0.14	0.16	15

Table 11. Bias, MAE and RMSD (in meters) comparing each buoy data with the collocated J3 data during the period 15 July 2017 -15 March 2018.

	bias (m)	MAE (m)	RMSD (m)	N samples
begur	-0.04	0.19	0.24	23
mahon	0.09	0.20	0.33	23

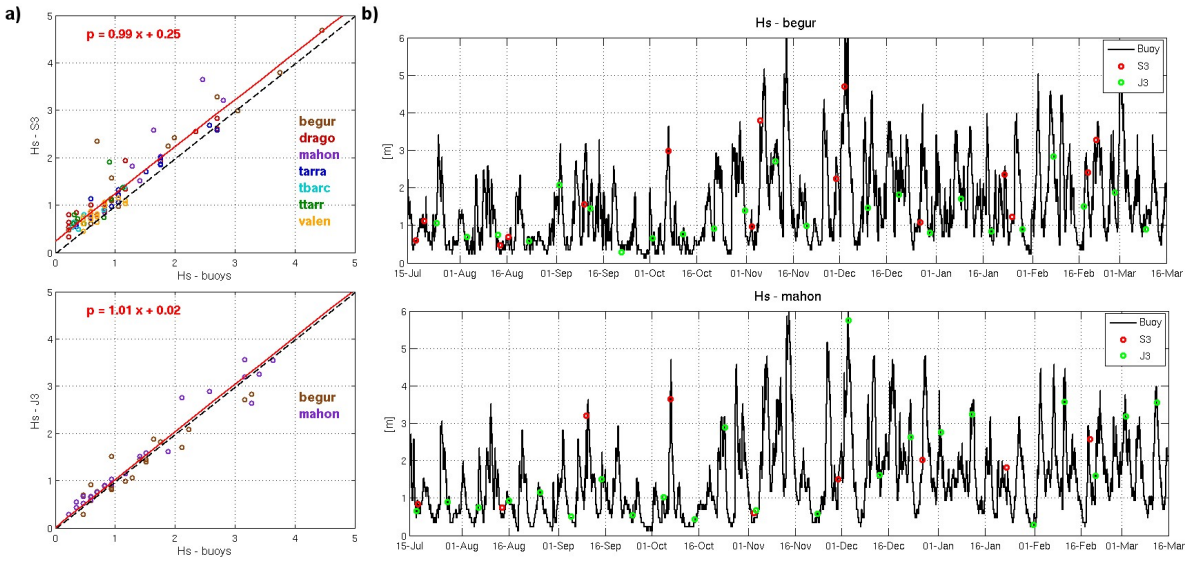

Figure 61. a) Scatter plots of the collocated buoy-satellite pair of points. b) Time series comparing buoy data and satellite data at begur and mahon buoy sites. The red line is the linear regression line (p=ax+b) and the black dashed line show the line that would correspond to a perfect agreement.

5. REFERENCES

Abdalla, S. and Hersbach, H., 2004. The technical support for global validation of ERS Wind and Wave Products at ECMWF. *Final Report for ESA contract 15988/02/I-LG*. ECMWF, Shinfield Park, Reading, RG2 9AX, UK. Available online at: http://www.ecmwf.int/en/research/publications.

Ahsbahs, T. et al., 2018. Applications of satellite winds for the offshore wind farm site Anholt. *Wind Energy Science*, 3, pp.573–588.

Ahsbahs, T. et al., 2017. Validation of Sentinel-1A SAR Coastal Wind Speeds Against Scanning LiDAR. *Remote Sensing*, 9(6), p.552.

Badger, M. et al., submitted. Inter-calibration of SAR data series for offshore wind resource assessment. *Remote Sensing of Environment*.

Bertotti, L. and Cavaleri, L., 2009. Wind and wave predictions in the Adriatic Sea, J. Marine Syst., 78, S227–S234, https://doi.org/10.1016/j.jmarsys.2009.01.018, 2009

Cavaleri, L., Bertotti, L., & Pezzutto, P., 2018. Accuracy of altimeter data in inner and coastal seas. Ocean Science Discussions, (July 2018), 1–13. https://doi.org/10.5194/os-2018-81

Chelton, D. B. and Freilich, M. H., 2005. Scatterometer-based assessment of 10-m wind analyses from the operational ECMWF and NCEP numerical weather prediction models, Mon. Weather Rev., 133, 409–429.

Choung, Y.-J. & Jo, M.-H., 2016. Shoreline change assessment for various types of coasts using multi-temporal Landsat imagery of the east coast of South Korea, *Remote Sens. Lett*., vol. 7, no. 1, pp. 91–100.

CLS, 2011. *Sentinel-1 Ocean Wind Fields (OWI) Algorithm Definition*, Available at: https://sentinel.esa.int/documents/247904/349449/S-1_L2_OWI_Detailed_Algorithm_Definition.pdf.

Gens, R., 2010, Remote sensing of coastlines: detection, extraction and monitoring, *Int. J. Remote Sens*., vol. 31, no. 7, pp. 1819–1836.

Grifoll, M. & Cerralbo, P. & Guillen, J. & Espino, M. & Hansen, L. B. & Sanchez-Arcilla, A., 2019. Characterization of bottom sediment resuspension events observed in a micro-tidal bay, Ocean Science, 15, pages 307--319, DOI 10.5194/os-15-307-2019

Grachev, A.A. & Fairall, C.W., 1996. Dependence of the Monin-Obukhov Stability Parameter on the Bulk Richardson Number over the Ocean. *Journal of Applied Meteorology*, 36(4), pp.406–414.

Hagenaars, G. & Luijendijk, A., 2017. LONG TERM COASTLINE MONITORING DERIVED FROM SATELLITE IMAGERY, *Coast. Dyn.*, no. 122, p. 13.

Hersbach, H., 2010. Comparison of C-Band Scatterometer CMOD5.N Equivalent Neutral Winds with ECMWF. *J. Atmos. and Ocean. Technol.*, 27(4), pp.721–736.

Fenoglio-Marc, L., Dinardo, S., Scharroo, R., Roland, A., Dutour Sikiric, M., Lucas, B., Becker, M., J., B., and Weiss, R., 2015. The GermanBight: A validation of CryoSat-2 altimeter data in SAR mode, Adv. Space Res., 55, 2641–2656.

Janssen, P.A.E.M., J.-R.Bidlot, S.Abdalla, and H.Herbach, 2005. Progress in ocean wave forecasting at ECMWF, *ECMWF Tech. Memo 478*, 27pp.

Komen, G. J., Cavaleri, L., and Donelan, M., 2018. Dynamics and modelling of ocean waves, Cambridge university press, 1994. Reinert, D., Prill, F., Frank, H., Denhard, M., and Zängl, G.: Database Reference Manual for ICON and ICON-EPS.

Martin, A. C. H., Gommenginger, C., Marquez, J.,Doody, S., Navarro, V, and C. Buck, 2016. Wind-Wave induced velocity in ATI SAR Ocean Surface Currents: First experimental evidence from an airborne campaign*, Journal of Geophysical Research: Oceans* , http://dx.doi.org/10.1002/2015JC011459.

Miranda, N., 2015. *S-1A TOPS Radiometric Calibration Refinement # 1*, Available at: https://sentinel.esa.int/documents/247904/2142675/Sentinel-1A_TOPS_Radiometric_Calibration_Refinement.

Mitra et al., 2017. Performance testing of selected automated coastline detection techniques applied on multispectral satellite imageries, *Earth Sci. Inform*., vol. 10, no. 3, pp. 321–330.

Mouche, A.A., Collard, F., Chapron, B., Dagestad, K., Guitton, G., Johannessen, J. A., Kerbaol, V., and Hansen, M. W., 2012: On the Use of Doppler Shift for Sea Surface Wind Retrieval From SAR*, Geoscience and Remote Sensing, IEEE Transactions on* , http://dx.doi.org/10.1109/TGRS.2011.2174998.

Ouma, Y. O. &Tateishi, R., 2006. A water index for rapid mapping of shoreline changes of five East African Rift Valley lakes: an empirical analysis using Landsat TM and ETM+ data, *Int. J. Remote Sens.*, vol. 27, no. 15, pp. 3153–3181.

Peña, A. et al., 2017. On wake modeling, wind-farm gradients and AEP predictions at the Anholt wind farm. *Wind Energy Science Discussions*, pp.1–18.

Sekovski et al., 2014. Image classification methods applied to shoreline extraction on very high-resolution multispectral imagery, *Int. J. Remote Sens*., vol. 35, no. 10, pp. 3556–3578.

Wiese A., Staneva J., Schultz-Stellenfleth J, Behrens A, Fenoglio-Marc L., and Bidlot JR, 2018. Synergy between satellite observations and model simulations during extreme events , Ocean Science, https://doi.org/10.5194/os-2018-87.